DISSERTATION

**Biophysikalische Eigenschaften und Biotransformation
metallbasierender Medikamente**

Diplom Chemikerin Anna Katharina Bytzek

angestrebter akademischer Grad
Doktorin der Naturwissenschaften (Dr. rer.nat.)

Wien, 2011

Studienkennzahl lt. Studienblatt: A 091 419

Dissertationsgebiet lt. Studienblatt: Chemie

Betreuerin / Betreuer: O. Univ.-Prof. Dr. Dr. Bernhard K. Keppler

Ph.D. – Thesis

Studies on the biophysical properties and biotransformation of metal-based drugs

Written by:

Anna Katharina Bytzek

Vienna, 2011

Für meine Eltern

"Der Zweifel ist der Beginn der Wissenschaft.

Wer nichts anzweifelt, prüft nichts.

Wer nichts prüft, entdeckt nichts.

Wer nichts entdeckt, ist blind und bleibt blind."

Teilhard de Chardin

Acknowledgment

I would like to thank

Prof. Dr. Dr. Bernhard Keppler for giving me the opportunity to perform my Ph.D. thesis in his multidisciplinary and excellently equipped group, the involvement in the drug development of KP1339 which motivated me a lot and of course for financial support.

Christian Hartinger for supervising me during my work, for his patience, motivation and creative ideas as well as for backing me all the way through. It was a pleasure to work in his group.

Caroline Bartel for her friendship, her help through difficult times, her entertainment and her enthusiasm for the postdoc project.

Eva A. Enyedy, Petra Heffeter and Ute Jungwirth for the good collaboration and valuable discussions.

All members of the working group for the friendly and funny but also scientifically productive atmosphere.

Elfriede Limberger for solving all administrative problems.

For financial support:

I want to express my deepest gratitude to my family for their encouragement. I thank my parents for their support throughout my life, optimism and love.

Special thanks go out to Prof. Dr. Dr. Keppler, Christian Hartinger, Caroline Bartel, Erwin and Veronika Masseli, Alexander Egger, Joanna Semkowicz, Silke Theison, Robert Trondl and Wolfgang Kandioller for supporting me during the illness of my mother and making my Ph.D. thesis in this time possible.

Abstract

Within this Ph.D. thesis, capillary electrophoresis (CE) and inductively coupled plasma mass spectrometry (ICP-MS) were applied to investigate the pharmacokinetic aspects of metal-based anticancer compounds with Ru or Pt as central atoms. Furthermore, both techniques were used for the first time to characterize the interaction between anti-diabetic complexes with serum proteins.

An important factor in antineoplastic chemotherapy is the cellular uptake of drugs. The more lipophilic a compound is, the easier it can pass the membrane by passive diffusion and accumulate in the cell. A higher accumulation of the anticancer drug in the tumor tissue normally results in higher antitumor activity. The lipophilicity of a set of Pt compounds was determined by the shake-flask method as well as indirectly by microemulsion electrokinetic chromatography (MEEKC). During these investigations the hybrid technique MEEKC-ICP-MS was established for the first time. This new method is characterized by a low detection limit and enables the determination of the capacity factor (log k) of UV/vis-silent compounds. A good correlation between log k obtained by MEEKC and MEEKC-ICP-MS and the corresponding octanol-water-partition coefficient (log P) was observable for complexes with minor structural differences. To confirm the structure-activity relationship, the log P and log k values were set in correlation with the accumulation of the Pt complexes in cancer cell lines and their cytotoxicity. It was found that the more lipophilic the compound is, the higher is the cellular uptake and the lower is the IC_{50} value.

The influence of the lipophilicity on the biodistribution of oxaliplatin and its methyl derivatives KP1537 and KP1691 was also studied in tumor-bearing mice. The analysis of the Pt content in different tissue samples indicated that KP1691 is quickly accumulated in the tumor but also the efflux is rather rapid. No differences in the tumor accumulation were seen for oxaliplatin and KP1537 in a time frame of 6 h.

A further focus of this thesis was the interaction of therapeutic metal complexes with serum proteins. The binding of drugs to serum proteins has a big impact on their biodistribution and modes of action. With the help of the hybrid technique CZE-ICP-MS, it was shown that albumin is the main binding partner for the Ru complex sodium *trans*-[tetrachloridobis-(1*H*-indazole)ruthenate(III)] (KP1339), currently undergoing clinical trials, as well as for Zn-based anti-diabetic compounds. The experimental data for the Zn complexes confirmed theoretical calculations based on stability constants. Additionally to the plasma distribution of KP1339, the accumulation in different tissues was investigated. High concentrations in lung and thymus make this compound interesting for the treatment of lung cancer and lymphoblastic leukemia.

Concluding, bioanalytical methods can significantly contribute to a better understanding of the properties and biological behavior of novel remedies. This enables the development of compounds with defined pharmacological mechanism, which could improve treatment efficacy and reduce side effects.

Zusammenfassung

Im Rahmen dieser Dissertation wurden Kapillarelektrophorese (CE) und induktiv gekoppeltes Plasma-Massenspektrometrie (ICP-MS) zur Untersuchung pharmakokinetischer Aspekte von metallbasierenden Krebsmedikamenten mit Ru und Pt als Zentralatom eingesetzt. Des Weiteren wurden beide Techniken zum ersten Mal zur Charakterisierung der Wechselwirkungen zwischen Antidiabetika und Serumproteinen verwendet.

Die zelluläre Aufnahme ist ein wichtiger Faktor in der antineoplastischen Chemotherapie. Je lipophiler eine Verbindung ist, desto leichter kann sie passiv die Membran passieren und in der Zelle angereichert werden. Eine höhere Akkumulation des Chemotherapeutikums im Tumorgewebe resultiert oft in einer verbesserten Antiproliferation. Die Lipophilie für verschiedene Pt Verbindungen wurde sowohl mit der Shake-Flask Methode als auch indirekt mit elektrokinetischer Chromatographie mit Mikroemulsionen (MEEKC) bestimmt. Im Zuge dieser Untersuchungen wurde die Hybridtechnik MEEKC-ICP-MS etabliert. Diese neuartige Technik zeichnet sich durch ein niedriges Detektionslimit aus und ermöglicht auch die Kapazitätsfaktor (log k) Bestimmung von UV/vis-inaktiven Verbindungen. Eine gute Korrelation zwischen den log k Werten, die mit MEEKC bzw. MEEKC-ICP-MS bestimmt wurden, und den dazugehörigen Oktanol-Wasser-Verteilungskoeffizienten (log P) wurde bei Komplexen mit geringen strukturellen Unterschieden beobachtet. Zur Bestätigung der Struktur-Wirkungs-Beziehung wurden die log P und log k Werte in Korrelation mit der Akkumulation der Pt-Komplexe in verschiedenen Zelllinien und deren Zytotoxizität gebracht. Es zeigte sich, dass je lipophiler der Komplex ist desto größer ist die zelluläre Aufnahme und umso kleiner der IC_{50} Wert.

Der Einfluss der Lipophilie auf die Verteilung von Oxaliplatin und dessen Methylderivaten KP1691 und KP1537 in tumortragenden Mäusen wurde ebenfalls untersucht. Die Analyse des Platingehaltes in verschiedenen Geweben zeigte, dass KP1691 zum einem sehr schnell im Tumor angereichert wird, aber auch sehr schnell wieder ausgeschieden wird. Zwischen Oxaliplatin und KP1537 wurden keine großen Unterschiede in der Tumorakkumulation im beobachteten Zeitraum festgestellt.

Ein weiterer Schwerpunkt dieser Doktorarbeit war die Untersuchung der Wechselwirkung von therapeutischen Metallkomplexen mit Serumproteinen. Die Anbindung an Serumproteine hat einen entscheidenen Einfluss auf die Bioverteilung und den Wirkmechanismus von Arzneimitteln. Mit Hilfe der Hybridtechnik CZE-ICP-MS konnte gezeigt werden, dass Albumin den Hauptbindungspartner im Blut für den zur Zeit in klinischen Studien getesteten Ru-Komplex Natrium *trans*-[tetrachloridobis-(1*H*-indazol)ruthenat(III)] (KP1339) wie auch für Antidiabetika auf Zinkbasis darstellt. Die experimentellen Daten für die Zn-Komplexe

bestätigten theoretische Berechnungen der Stabilitätskonstanten. Zusätzlich zu der Verteilung im Blut wurde für KP1339 die Akkumulation in diversen Mausorganen untersucht. Hohe Konzentrationen in Lunge und Thymus machen diese Verbindung möglicherweise interessant für die Behandlung von Lungenkrebs und lymphoblastischer Leukämie.

Zusammenfassend kann gesagt werden, dass bioanalytische Methoden signifikant zu einem besseren Verständnis des Verhaltens und der Eigenschaften von neuen Medikamenten beitragen können. Dies wiederum ermöglicht die Entwicklung von Verbindungen mit definierten pharmakologischen Wirkungsmustern, die die Effektivität von Therapien verbessern und Nebenwirkungen minimieren könnten.

Abbreviations

API	atmospheric pressure ionization
BGE	background electrolyte
CE	capillary electrophoresis
CEC	capillary electrochromatography
CGE	capillary gel electrophoresis
CI	chemical ionization
CIEF	capillary isoelectric focusing
CITP	capillary isotachophoresis
CTR1	copper transporter-1
CZE	capillary zone elctrophoresis
DNA	2'-deoxyribonucleic acid
e.g.	*exempli gratia* (for example)
EOF	electroosmotic flow
ESI	electrospray ionization
et al.	*et alii* (and others)
etc.	*et cetera* (and other things)
F_E	electrical force
F_F	frictional force
FDA	Food and Drug Administration
FOLFIRI	chemotherapy with 5-fluorouracil, leucovorin and irinotecan
FOLFOX4	chemotherapy with 5-fluorouracil, leucovorin and oxaliplatin
5-FU	5-fluorouracil
GC	gas chromatography
HPLC	high performance liquid chromatography
HSA	human serum albumin
ICP	inductively coupled plasma
KP1019	indazolium *trans*-[tetrachloridobis(1*H*-indazole)-ruthenate(III)]
KP1339	sodium *trans*-[tetrachloridobis(1*H*-indazole)ruthenate(III)]
KP1537	(*SP*-4-2)-[(*1R,2R,4R*)-4-Methyl-1,2-diaminecyclohexane-$\kappa^2 N,N'$][ethanedioato(2-)-$\kappa^2 O1,O2$]platinum(II)
KP1691	(*SP*-4-2)-[(*1R,2R,4S*)-4-Methyl-1,2-diaminecyclohexane-

	$\kappa^2 N,N'$][ethanedioato(2-)-$\kappa^2 O1,O2$]platinum(II)
LA	laser abalation
LADME	liberation, absorption, distribution, metabolism and excretion
log k	capacity factor
log P	octanol-water partition coefficient
LV	leucovorin
MALDI	matrix-assisted laser desorption ionization
MEEKC	microemulsion electrokinetic chromatography
MEKC	micellar electrokinetic chromatography
MS	mass spectrometry
MSA	mouse serum albumin
m/z	mass-to-charge ratio
NAMI-A	imidazolium *trans*-[tetrachlorido(*S*-dimethylsulfoxide)(1*H*-imidazole)ruthenate(III)]
RF	radio frequency
SDS	sodium dodecyl sulphate
Tf	transferrin
UV	ultra violet

TABLE OF CONTENTS

1. Introduction

1.1. Epidemiology

Worldwide 10.9 million people are diagnosed with cancer each year and there are approximately 6.7 million deaths due to this disease [1]. Malignant neoplasms are responsible for around 12% of deaths worldwide, but the percentage of all deaths due to cancer in the different regions of the world varies from only 4% in Africa to 23% in Northern America (Figure 1).
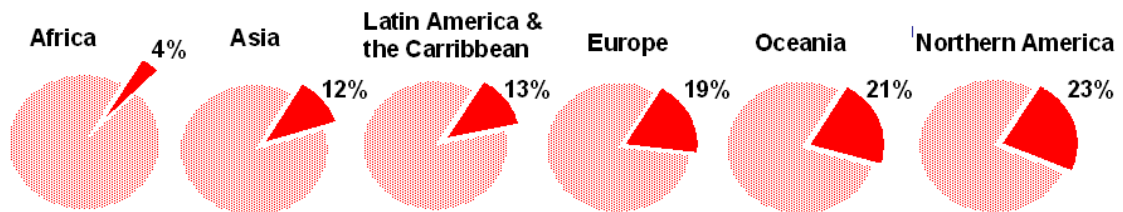

Figure 1. Proportion of all deaths caused by cancer in the world in 2008 [1].

This means that in industrial countries nearly one in four deaths is due to malignant neoplasms. In these countries, most deaths are still related to cardiovascular diseases. A closer look at age-adjusted mortality rates indicates that deaths related to the cardiovascular system have declined markedly since 1970 whereas cancer mortality shows only a slight, gradual downtrend (Figure 2) [2]. This will probably continue in the next years and in 15-20 years cancer will be the most frequent cause of death. When mortality of malignant neoplasms is more closely inspected, lung, colorectal and prostate cancer are the most frequent types responsible for death in the male population, while breast, colon and lung cancers are predominant for women [3]. Statistics for Europe indicate an increase in total cancer cases since 1975 but the death rates have fallen by 25% for males and 18% for females for all cancers since 1990 (Figure 3) [4]. This can be explained by the development of improved cancer therapeutics as well as by improved prevention and early diagnosis.
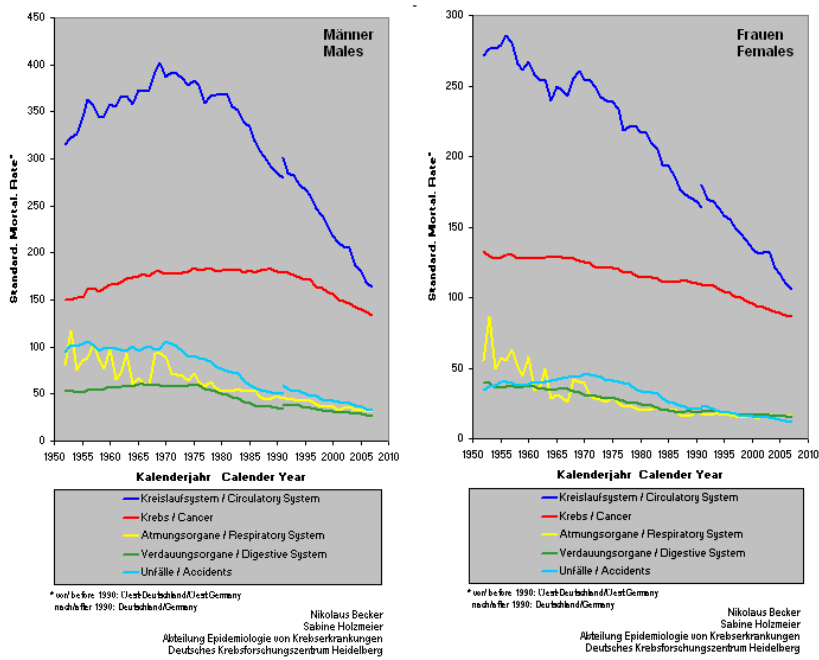
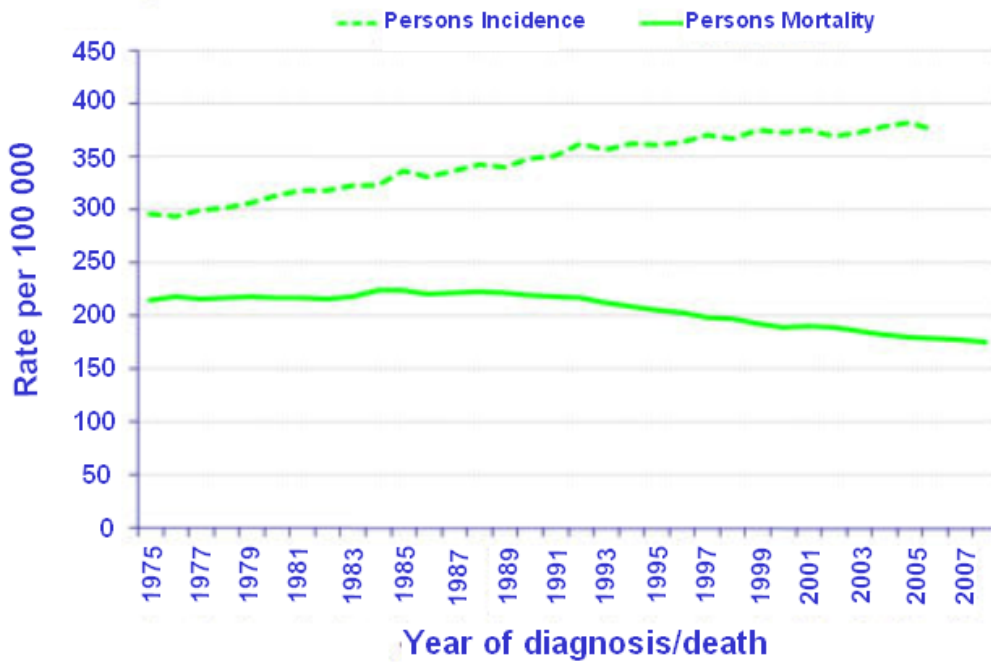**Figure 2.** The most common causes of death in Germany for men and women [2].

Figure 3. Age-standardized (European) incidence and mortality rates for all cancers [4].

1.2. Malignant transformation

The first reports of cancer are traceable to the time of the old Egyptians [5]. The term "cancer" was introduced by Hippocrates (ca. 460-370 BC) which also was searching for the cause of this illness. He suggested that an imbalance in the bodily fluids is the cause of cancer. This theory remained the conventional wisdom for generations, but with the improvements in medicine and clinical diagnostic his suggestion was rapidly discarded in favor of more evidence-based models [6, 7]. Nowadays cancer is recognized as a cell-based disease caused by sequential accumulation of mutations. In a lifetime, in any human individual being, 10^{10} DNA mutations occur, but a single mutation is not enough to lead to the development of cancer [8]. Analysis of the genome sequence in breast and colorectal cancers indicated that individual tumors accumulate an average of *circa* 90 mutant genes but only a subset of these contribute to the neoplastic process [9]. Especially alterations in genes called tumor suppressor genes and proto-oncogenes are critical [10]. Tumor suppressor genes like *p53*, *Rb* and *BRCA1* encode proteins that are responsible for control processes essential to limiting cell proliferation. They act upon pathways involved in growth control and cell cycle regulation. If *e.g. p53* detects DNA damage, it will stop cell cycle progression and allow time for DNA repair. If the repair mechanisms fail, it will activate the expression of several genes involved in apoptosis. 50% of all human cancers have a mutated *p53* gene [11]. Cancers with this mutation are generally aggressive and show resistance to radiation and chemotherapy which result in poor prognosis [12]. Oncogenes are genes which lead to modified proteins, which are unable to exert they function correctly and provide a selective growth advantage to the cell. They arise through the mutation of normal cellular genes with growth regulation called proto-oncogenes, such as growth factors (sis, hst-1, int-2), growth factor receptor tyrosine kinases (EGFR, Her2) or non-receptor tyrosine kinases (abl, src) [7].

The damage of the genetic material can arise spontaneously through mistakes in somatic recombination events or through endogenous factors like oxidative stress or DNA replication errors. Mutations can be induced also exogenously by physical (*e.g.*, ionizing radiation and UV light), chemical (*e.g.*, polycyclic hydrocarbons and heavy metal salts) and biological carcinogens (*e.g.*, bacteria, viruses and mycotoxins).

Tumorgenesis follows the Darwinian evolution theory, mutations which lead to selective growth advantages result in a progressive conversion of normal human cells into cancer cells [13]. Further mutations in the offspring of these already modified cells result then in even faster growth. Malignant cells are characterized by self-sufficiency in growth signals, insensitivity to growth-inhibitory signals, evasion of programmed cell death, limitless replicative potential, sustained angiogenesis, tissue invasion and metastasis [13].

Carcinogenesis is a multistage process and therefore the majority of incidences appears at an age > 65 because it takes decades for these multiple mutations to happen [14, 15].

1.3. Cancer treatment

There are five standard methods of treatment for cancer: surgery, chemotherapy, radiotherapy, immunotherapy and biological therapy. The choice of therapy depends of cancer state and type as well as patient's age, sex, physical and psychological conditions. Until 1960 surgical methods and radiotherapy dominated the field of cancer therapy but the cure rates also after even more radical local treatments just achieved 33% [16]. The reason for the low rate is that these two methods just can cure cancers that are confined to specific areas and have not spread, but often tumors are diagnosed when the patients already developed metastases. In these cases chemotherapy is required, which affects the entire body, not just a specific part. The use of chemotherapy to treat cancer began in the early 20th century and nowadays there are more than 50 chemotherapeutics available for the over 200 different types of cancer, which can be given in various ways (Figure 4) [17]. The major categories of chemotherapeutic agents are alkylating agents (*e.g.*, ifosfamide and cyclophoshamide), antimetabolites (*e.g.*, 5-fluorouracil and gemcitabine), anthracyclines (*e.g.*, epirubicin and mitoxantrone), plant alkaloids (*e.g.,* irinotecan and etoposide), antitumor antibiotics (*e.g.*, bleomycin), taxanes (*e.g.*, docetaxel), monoclonal antibodies (*e.g.*, cetuximab and herceptine) and Pt-based drugs. Despite of this variety of organic drugs, the three worldwide approved Pt drugs, cisplatin, carboplatin and oxaliplatin play a major role in contemporary medical oncology [18, 19].
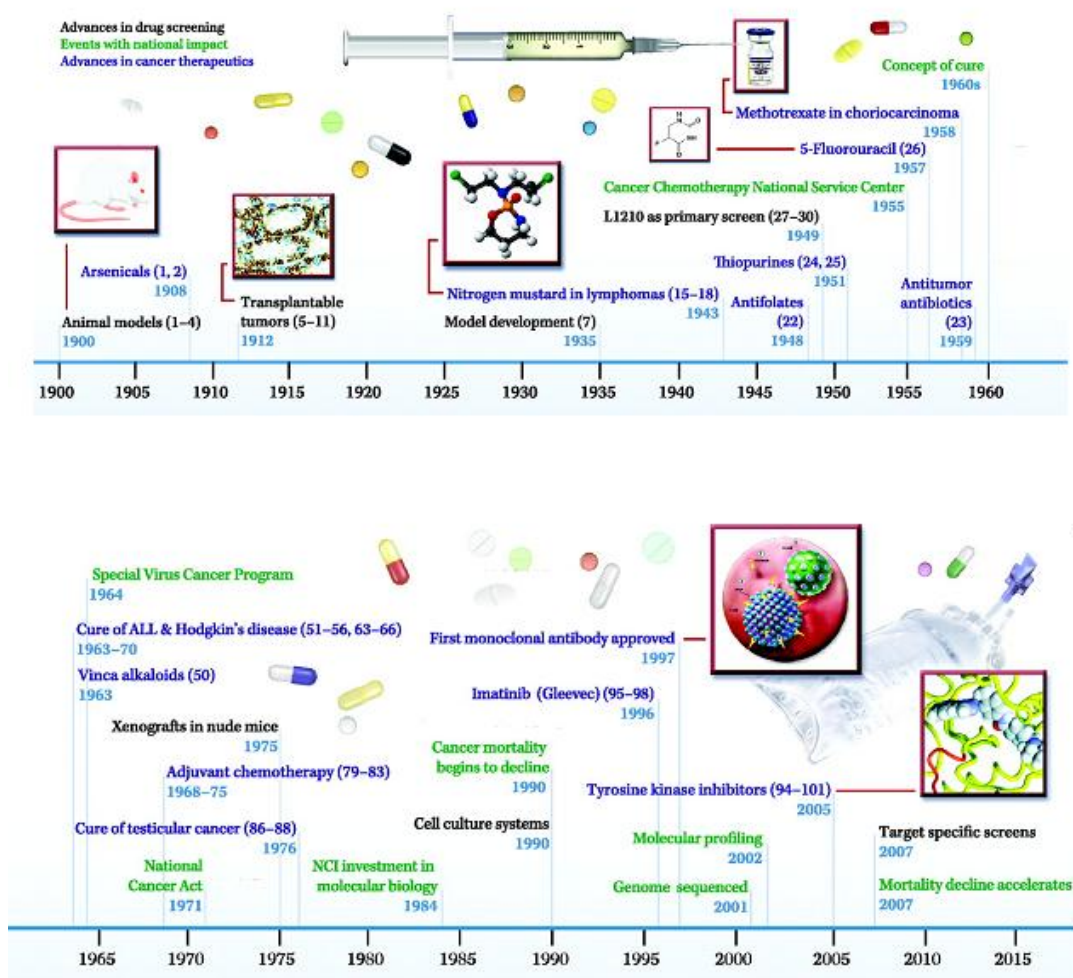
Figure 4. Key advances in the history of cancer chemotherapy [16].

1.3.1. Platinum-based anticancer compounds

A new era of chemotherapy started in the 1960ies with the accidental discovery of the anticancer properties of cisplatin (*cis*-[diamminedichloridoplatinum(II)]; Figure 5) [20-23]. Cisplatin is a very effective cancer drug which is used against epithelial malignancies of ovaries, testes, head and neck, esophageal and lung [24]. With the introduction of cisplatin-containing regimens the cure rate for men with metastatic testicular cancer rised from 5% to 80% [25]. The antineoplastic activity results primarily from the interaction of the drug with the DNA, leading to adducts which induce apoptosis in cells [26]. Despite the great success at treating certain kinds of cancer, cisplatin has some limitations. First of all, a number of severe

side effects such as nephrotoxicity, neurotoxicity, nausea, vomiting, ototoxicity and alopecia accompany the use of cisplatin [27, 28]. In addition to its toxic side effects, the major limitations of cisplatin chemotherapy are acquired and intrinsic resistance [19]. Acquired resistance results from the reduction in cisplatin accumulation inside cancer cells either by reduced drug uptake or enhanced efflux [29-31], the increased capability of cells to repair cisplatin adducts [32-36], the modulation of apoptotic pathways in various cells, the up-regulation in transcription factors, the loss of p53 and other protein functions and an increased detoxification by reaction with intracellular thiols [37-40].

To overcome these negative aspects, several thousands of new Pt complexes have been synthesized in the last 35 years in order to identify compounds with superior efficacy, reduced toxicity, lack of cross-resistance or improved pharmacological characteristics [41]. So far 35 complexes have entered clinical trials as anticancer agents but in addition to cisplatin only carboplatin and oxaliplatin were approved for worldwide clinical use (Figure 5) [42].
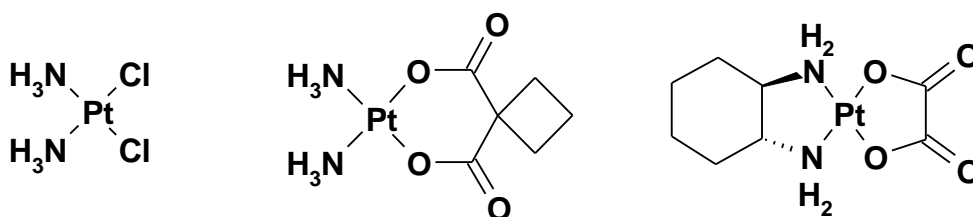

Figure 5. Pt-based drugs in worldwide clinical use: cisplatin (left), carboplatin (center) and oxaliplatin (right).

Carboplatin {(*SP*-4-2)-[diammine(1,1-cyclobutanedicarboxylato-κ*O*(2-))platinum(II)]; Figure 5} was introduced in 1981. Compared to the parent compound cisplatin, it has a lower reactivity and is therefore less toxic to the kidneys and the nervous system and causes less nausea and vomiting. However, myelosuppression is increased and was identified as the dose-limiting factor [43]. The mode of action is analogous to cisplatin with identical DNA lesions formed. Thus, it has not enlarged the spectrum of Pt-treatable cancers, nor has it proved active in cisplatin-resistant cancers [37].

Oxaliplatin {(*SP*-4-2)-[((*1R,2R*)-cyclohexanediamine-κ^2*N,N'*)(ethanedioato(2-)-κ^2*O1,O2*)-platinum(II)]; Figure 5} has a broad spectrum of antineoplastic activity and has demonstrated lack of cross-resistance with cisplatin and carboplatin [44]. The reasons for the different fields of application of cisplatin and carboplatin on the one side and oxaliplatin on the other are:

formation of different DNA adducts, mismatch repair recognition proteins do not recognize oxaliplatin-induced DNA adducts [32] and the cellular uptake of oxaliplatin seems to be less dependent on the copper transporter CTR1 [45]. Nowadays oxaliplatin is used in the clinic in combination with 5-fluorouracil (5-FU) and leucovorin (LV) (FOLFOX4) as first-line treatment against metastatic colorectal carcinoma [46-48]. The FOLFOX4 regimen improves the response rate and increases median time to progression as well as median survival times {} [49]. The limiting factor of dosage is chronic neurotoxicity and is usually seen in patients who have received total doses >780 mg/m^2 [50].

In order to find Pt-based drugs with better therapeutic properties than cisplatin, carboplatin and oxaliplatin, the focus of interest has moved to octahedral Pt(IV) compounds. Due to their increased inertness and consequently reduced toxicity and possibility of oral administration they could improve the living quality of cancer patients significantly [41, 42, 51]. Several examples of Pt(IV) complexes underwent clinical trials including satraplatin {(*OC*-6-43)-[bis(acetato)amminedichlorido(cyclohexylamine)]platinum(IV); Figure 6} and LA-12 {(*OC*-6-43)-[bis(acetato)(1-adamantylamine)amminedichlorido]platinum(IV); Figure 6} and show promising activity.
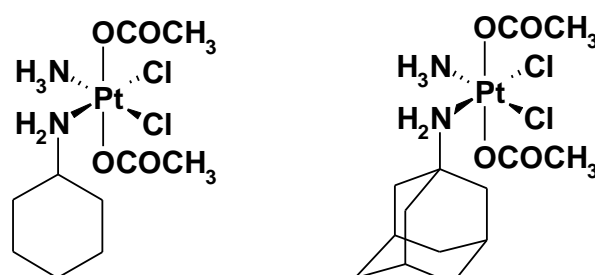
Figure 6. Chemical structures of satraplatin (left) and LA-12 (right).

Satraplatin was investigated in advanced phase III clinical trials in hormone refractory prostate cancer in combination with prednisone [52, 53], and is currently in a phase II trial against non-small cell lung carcinoma. The main *in vivo* metabolite of satraplatin is *cis*[amminedichlorido(cyclohexylamine)]platinum(II) [54]. This satraplatin metabolite binds in a similar manner to the DNA as cisplatin [55], but its cellular uptake is not dependent on CTR1 and shows therefore also activity in cisplatin resistant cancer cells [56, 57]. The satraplatin derivative LA-12 has finished phase I clinical trials and has shown promising *in vivo* activity in ADJ/PC6 plasmacytoma and A2780 ovarian carcinoma tumor mice models [53, 58, 59].

1.3.2. Ruthenium-based anticancer compounds

Although Pt complexes are now widely used as anticancer agents, the development of drug resistance, the toxic side effects and the lack of activity against several types of cancer are problems which need to be overcome. This has motivated the search for anticancer activity amongst complexes of other metals. In the last years many research groups focused on metal complexes of Fe, Ru, Ga, Ti and Rh [60-62].

Ru compounds appear well-suited for medicinal applications. They have been investigated as immunosuppressants (*e.g.*, *cis*-[Ru(NH$_3$)$_4$(Im)$_2$], Im is imidazole), nitric oxide scavengers (*e.g.*, Ru(III) polyaminocarboxylates such as AMD6245 and AMD1226), antibiotics (*e.g.*, Ru(III) derivative of thiosemicarbazone) and antimalarials ([RuCl$_2$(chloroquine)]$_2$) [63-65]. Clarke observed at first the anticancer properties of Ru compounds in 1980 [66, 67]. But the Ru(III) ammines (*e.g.*, [RuCl$_3$(NH$_3$)$_3$]) with which he was working, were too insoluble for clinical use. To date just two Ru(III) complexes, namely imidazolium *trans*-[tetrachlorido(*S*-dimethylsulfoxide)(1*H*-imidazole)ruthenate(III)], more commonly known as NAMI-A, and indazolium *trans*-[tetrachloridobis(1*H*-indazole)ruthenate(III)] (KP1019), have completed phase I clinical trials (Figure 7). Despite their structural and chemical similarities, these two complexes show distinctly different antitumor behaviors.
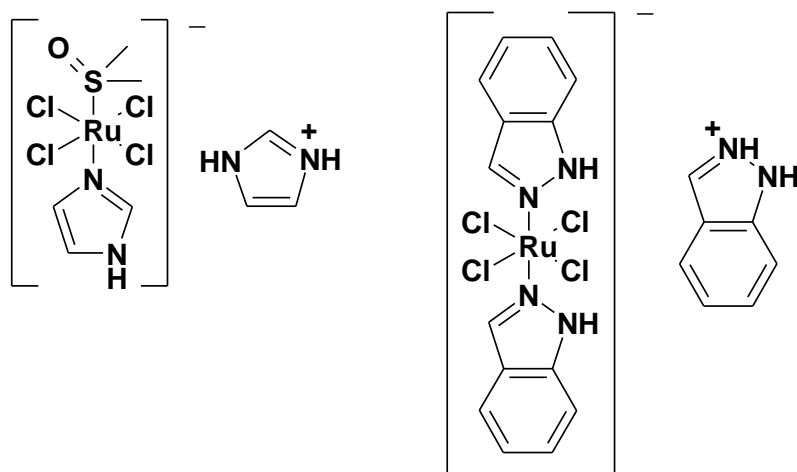
Figure 7. Chemical structures of NAMI-A (left) and KP1019 (right).

NAMI-A ("New anti-tumor metastasis inhibitor A") was the first Ru-based anticancer drug that entered clinical trials. Phase I clinical trials showed that the drug was well-tolerated in patients [68]. Dose-limiting toxicity was the formation of painful blisters on hands and feet which persisted for weeks and months [69]. Other side effects of NAMI-A were anemia, lymphopenia, fatigue, anorexia, stomatitis, peripheral edema, alopecia, nausea, diarrhea,

tinnitus, and infusion-site phlebitis. The NCI anticancer drug discovery screen as well as several other *in vitro* studies indicated the absence of the direct cytotoxicity of NAMI-A for tumor cells. But *in vivo* NAMI-A has shown selective activity against the development and growth of pulmonary metastases from a variety of primary tumors [70]. The mechanism of metastasis control seems to be attributable to combined anti-angiogenic and anti-invasive effects on tumor cells and blood vessels. The high activity of NAMI-A against lung metastasis results from its about eight times longer half-life of elimination in the lungs compared to other tissues, probably due to the high content of collagen to which NAMI-A binds efficiently [71].

KP1019 demonstrated exciting anticancer activity in a pilot clinical phase I study. It was well-tolerated, no dose-limiting toxicity was observed and five out of six patients treated achieved disease stabilization (duration of stable diseases reached up to 10 weeks). Due to its higher water solubility, the sodium salt of KP1019, sodium *trans*-[tetrachloridobis(1*H*-indazole)ruthenate(III)] (KP1339), has been selected as a lead candidate for further clinical development, and is currently in a phase I/IIa study. A comparison of the modes of action and activity pattern showed similar cytotoxic activity and drug accumulation profiles for KP1019 and KP1339 [72]. The mode of action of KP1019 is different to that of NAMI-A. It is significantly cytotoxic *in vitro* against colorectal cell lines (SW480, HT29) and is also highly effective in reducing tumor growth *in vivo.* Chemically induced colorectal tumors in rats treated with KP1019 showed a higher decrease in tumor volume than with 5-FU, the most effective drug in clinical use against colorectal cancer. Also complete remission of tumors was observed [73]. It appears that KP1019 induces caspase-mediated apoptosis *via* the mitochondrial pathway.

Besides NAMI-A, KP1019 and KP1339 a large number of other Ru complexes have been prepared and tested for antitumor activity. RAPTAs, a class of organometallic Ru(II) complexes, characterized by the presence of a 1,3,5-triaza-7-phosphatricyclo[3.3.1.1]decane (pta) ligand and a η^6-arene ligand, are very promising. As NAMI-A they show weak cytotoxicity against tumor cells *in vitro* and failed the NCI screening process [74]. But *in vivo* they selectively reduced the growth of lung metastases. A benefit of RAPTAs is that they are free of toxicity to healthy cells even with prolonged exposure at millimolar concentrations and this makes them highly attractive as drugs [71].

1.4. Pharmacokinetics

Pharmacology is the study of the interactions that occur between drugs and a living organism. It can be divided into the two main areas pharmacodynamics and pharmacokinetics [75]. Pharmacodynamics deals with the physiological effects of drugs on biological systems and involves receptor binding, postreceptor effects and chemical interactions [76]. Pharamacokinetics on the other hand describes the effects of biological systems on drugs. Pharmacokinetic processes are described by liberation, absorption, distribution, metabolism and excretion (LADME scheme) [76, 77], and are strongly dependent of individual physiology. Factors like genetic make up, sex, age, renal and hepatic failure, obesity, dehydration, etc. can change pharmacokinetics dramatically [78].

Liberation

Liberation is defined as the release of the drug from its dosage form. This process has a big influence on the pharmacokinetics of solid dosage forms (tablets, granules, capsules, *etc.*). Solid forms must be able to disintegrate in the respective desired environment before the drug can be absorbed.

Absorption

Absorption deals with the passage of a drug from its site of administration into the plasma. In all routes of administration, except intravenous injections, a drug must cross various semipermeable cell membranes before it reaches the systemic circulation (Figure 8) [79]. Membranes consist of phospholipid bilayers with embedded proteins. There are four ways by which drugs can cross these barriers: passive diffusion, facilitated passive diffusion, active uptake or endocytosis. Passive diffusion is based on the concentration gradient for a drug across the cell membrane and is mainly dependent of a molecule's lipophilicity, size and charge [80]. Lipid soluble drugs and small molecules penetrate cell membranes most rapidly. Weak acids or bases can cross the lipid matrix only in the uncharged form. Facilitated passive diffusion is important for compounds with low lipid solubility. Driven by the concentration gradient, trans-membrane proteins transport molecules across the membrane without consumption of energy. When energy (*e.g.*, ATP hydrolysis) is necessary for carrier-mediated passage, the process is called active transport. Active uptake is important for drugs with structures similar to endogenous substances like ions, vitamins, sugars and amino acids [79]. Endocytosis plays a minor role in drug uptake. It is an active transport in which molecules are enclosed in vesicles formed by an invagination of the cell membrane and released inside the cell.
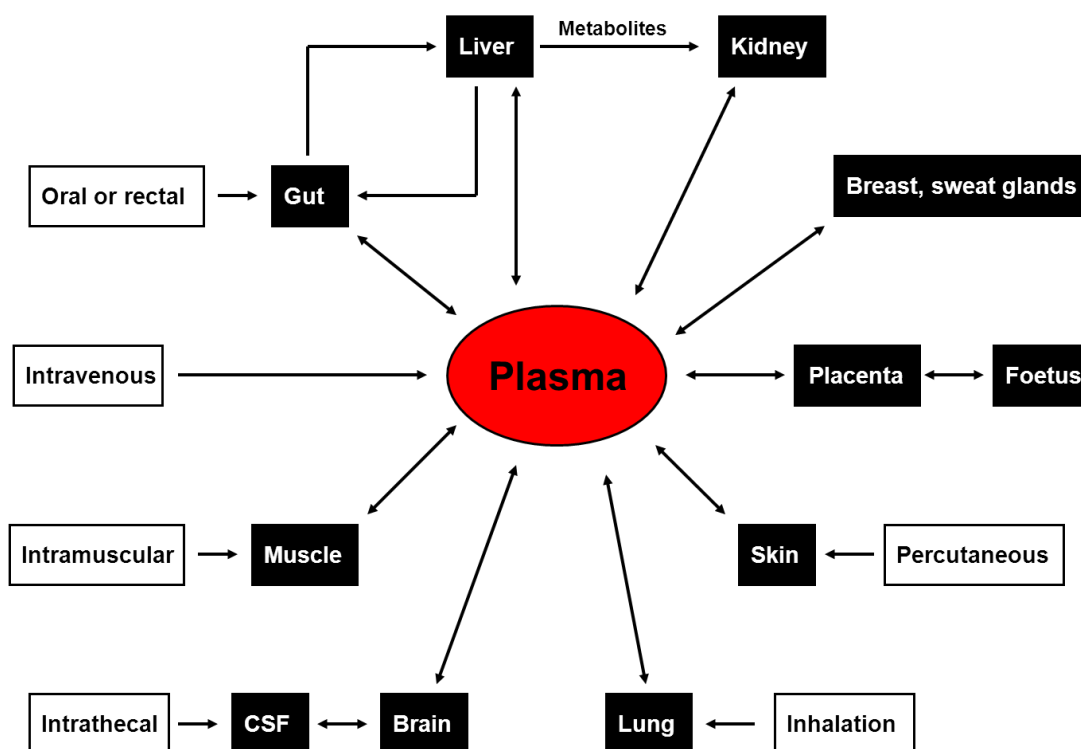
Figure 8. The main routes of drug administration and distribution, adapted from [81].

Distribution

Distribution deals with the transfer and diffusion of a drug from the intravascular to the extravascular space. The distribution of a drug in the body is not uniform, the accumulation of a molecule in a certain tissue depends on blood perfusion, binding within the tissue, regional pH and permeability of the membranes. An important role in the distribution of drugs plays the binding to serum proteins. Only unbound drugs are able to cross cell membranes by passive diffusion and therefore the effect of a drug is highly affected by the free concentration of the drug in plasma rather than total concentrations [82, 83]. Binding to serum proteins results mostly in an inactivation of the drug but on the other side if the binding is reversible drug-protein complexes in plasma could serve as drug reservoir for free drug concentration and prolong the duration of drug action. The interaction between drugs and serum proteins could also result in a selective accumulation of some chemotherapeutics in cancer cells. Neoplastic cells differ from normal cells by a high Fe requirement and an overexpression of transferrin receptors. Therefore, anticancer drugs with high affinity to transferrin (Tf) would selectively accumulate in tumor cells [84]. Albumin (HSA) is the main protein in plasma and is responsible for the transport of various molecules. Malignant tissue have an enhanced HSA uptake due to angiogenesis, hypervasucularization, a defective vascular architecture and an impaired lymphatic drainage [85]. Stehle *et al.* have supposed

that HSA is a major energy and nutrition source for tumor growth [86] and therefore therapeutic agents bound to HSA would be delivered specifically to cancer cells.

Metabolism

Metabolism is defined as the transformation of drugs into compounds which are easier to eliminate. Chemical reactions like oxidation, reduction, hydrolysis, hydration, condensation, and isomerization are involved in the metabolism of drugs [87]. Metabolism occurs mainly in the liver with the help of the cytochrome P450 system. Depending on the molecule, it can lead to an inactivation or activation of the drug.

Excretion

Under excretion the elimination of unchanged drug or metabolite from the body via renal, biliary or pulmonary processes is understood. The principal organ of extraction is the kidney. Elimination of drugs in this way is limited to water-soluble substances and therefore lipophilic molecules need to be metabolized to more polar products before they can be renally excreted. Lipophilic drugs can also be excreted by the hepatobiliary system. Elimination via the lungs is restricted to highly volatile compounds.

1.5. Drug Development

The development of a single new medicine from a research-based concept to a fully marketed product is lengthy, increasingly challenging and extremely costly (Figure 9). The entire process ranges from 12 to 20 years and costs approximately 800 million USD [88]. Before a drug can be tested in humans, laboratory and animal tests have to be performed to investigate the LADME properties, the mode of action and the side effects of a compound.

The steps between discovery and approval are known to be critical. A novel agent had only an 8% chance for clinical application in 2000, down from the historical success rate of 14% in 1985 [89]. The critical steps are the clinical phase I to III trials which are described in the following paragraphs according to the U. S. Food and Drug Administration (FDA) [90].
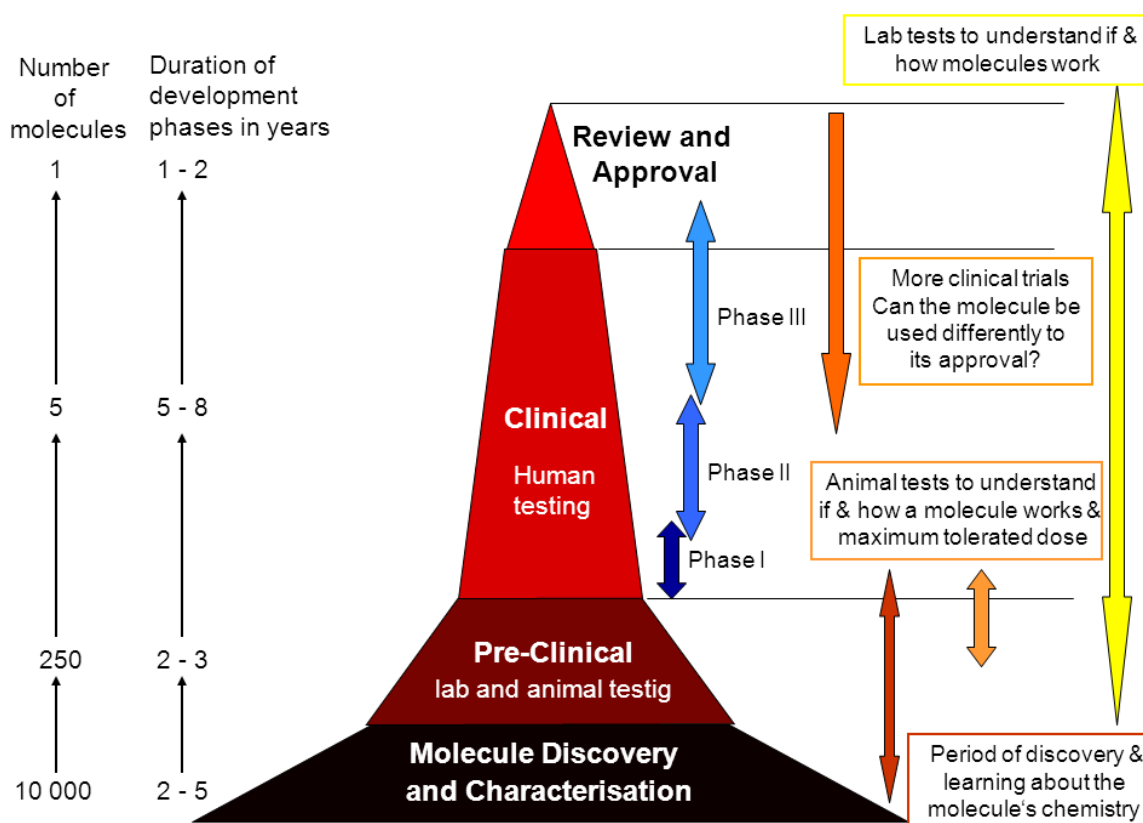
Figure 9. The drug development process [91].

Phase I Clinical Trials

In phase I trials the drug is tested in humans for the first time. This initial phase of testing is designed to determine the effects of the drug candidate on humans including pharmacokinetics and pharmacodynamics as well as side effects that occur as dosage levels are increased. This phase of testing takes several months and is conducted with 20 to 100 volunteers.

Phase II Clinical Trials

The second phase of testing is designed to confirm safety, determine efficacy and side effects over a short time and to find the optimal dose and administrations schemes for phase III study. It can last from several months to two years and involves about 100 to 500 patients. Most phase II studies are placebo-controlled and double-blinded. Only a third of the clinically tested compounds successfully complete phase I and II trials.

Phase III Clinical Trials

This part of the clinical trials is very expensive and lengthy. Phase III studies are typically double-blinded and placebo-controlled, and involve 1000-5000 patients over many months usually years. Safety profiles and adverse effects are studied to determine the benefit-risk relationship. Due to the large test group researchers and physicians have the opportunity to identify rare side effects of treatment. Phase III trials are the principle criterion for FDA approval. Nowadays, 50% of the experimental drugs that make it through phase I and II of clinical studies fail in phase III, compared to a 20% failure rate 10 years ago.

Drug development and sponsors of clinical trials are nowadays under increasing pressure. The investment required for one successful therapeutic launch rised more than 55% in less than a decade [89]. Many of the scientific tools used to predict and estimate safety and effectiveness are outdated. They are time-consuming and imprecise, and fail often in prediction of safety problems in the early state of the critical path [92]. There is a large economical interest to develop new *in vitro* methods and techniques which aid in the prediction of the activity of a compound *in vivo.* The earlier a product can be brought to market, the longer a company may sell the product without any competition.

2. Bioanalytical Techniques

2.1. Capillary Electrophoresis

Electrophoresis as a separation technique was introduced by Tiselius in 1937 (1948 Nobel Prize) and is defined as the movement of charged colloidal particles or polyelectrolytes, immersed in a liquid, under the influence of an external electric field [93, 94]. Tiselius' separation technique in free solution was limited by thermal diffusion and convection. The modern era of capillary electrophoresis (CE), which led to current instrumentation, was developed over the years and the theory was first described in 1981 by Jorgenson and Lukas [95, 96]. They demonstrated that the use of fused silica capillaries produced highly efficient electrophoretic separations. CE has now become a mature analytical technique with advantages like short analysis time, high separation efficiency, easy and predictable selectivity, low sample and electrolyte consumption, low waste generation, automation and reproducibility. These remarkable advances have benefits in application fields like food analysis, pharmaceutical analysis, bioanalysis and environmental pollutant analysis.

A schematic diagram of a typical CE system is shown in Figure 10. The basic instrumental set-up consists of a fused silica capillary, two buffer reservoirs, two electrodes, a high voltage power supply and an on-column detector.
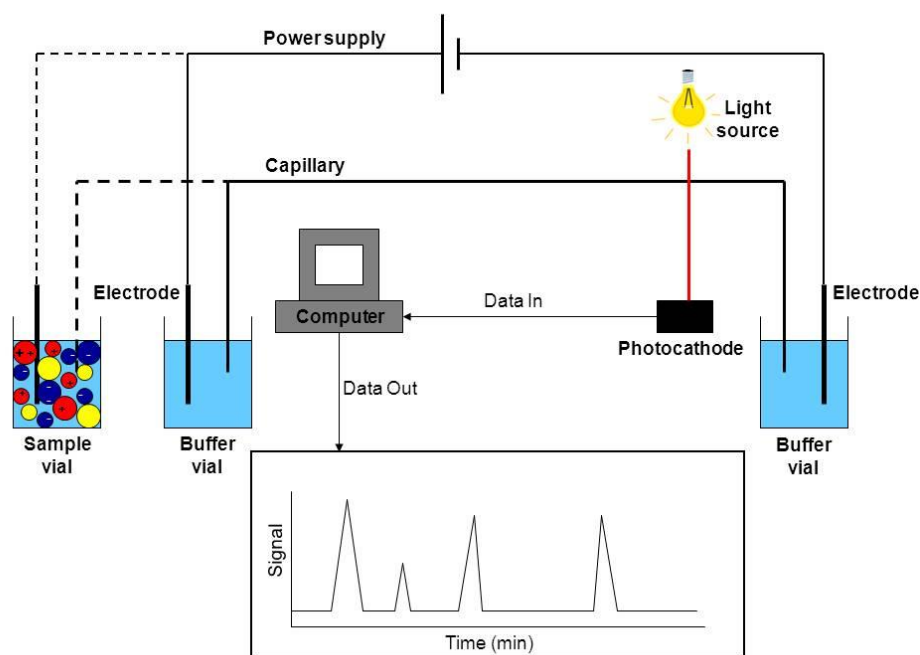

Figure 10. Schematic representation of a CE system, adapted from [97].

The separation of compounds by CE is dependent on the differential migration of analytes in an electric field. The electrophoretic migration velocity (v) of an analyte is defined by Equation 1:

v = μ_E · E   Equation 1

where   v = ion velocity

             μ_E = electrophoretic mobility

             E = applied electric field

During the separation, two contrary forces act on an ionic species: on the one side the electrical force (F_E) and on the other the frictional force (F_F).

$$F_F = -6\pi \cdot \eta \cdot r_{St} \cdot v \qquad\qquad F_E = q \cdot E$$

where η = solution viscosity

             r_{St} = Stokes radius

             q = ion charge

After a short transient period a steady state, defined by the balance of F_F and F_E, is attained:

-F_F = F_E

$6\pi \cdot \eta \cdot r_{St} \cdot v = q \cdot E$ Equation 2

Solving for velocity and substituting Equation 2 into Equation 1 yields μ_E which is then described in terms of physical parameters:

$$\mu_E = \frac{q}{6\pi \cdot \eta \cdot r}$$

                                                            Equation 3

Equation 3 shows that only charged ions are affected by the electric field, neutral analytes are poorly separated by CE and require additives. Small, highly charged species exhibit high mobilities whereas large, minimally charged species have low mobilities.

The velocity of migration of an analyte in CE is also dependent of the electroosmotic flow (EOF) of the buffer solution. The EOF is the bulk movement of the liquid in the capillary as a consequence of the surface charge of the interior capillary wall [98]. In fused silica capillaries the interior wall is negatively charged because the silanol (Si-OH) groups are deprotonated at pH > 3. The cations of the buffer solution are attracted to the silanol anions and form a diffuse double-layer (Figure 11). The inner or fixed layer is held tightly to the silanoate groups. The outer layer is further from the silanoate groups and called the mobile or diffuse layer. When a positive potential is applied at the injection end of the capillary the cations forming the mobile layer migrate toward the cathode and drag along anions and neutrals, which results in the separation of positively, neutral and negatively charged species. Because of the potential, the EOF has a flat flow velocity profile which does not contribute to the broadening of solute zones. This is in contrast to a laminar or parabolic flow velocity profile which is generated by pressure.

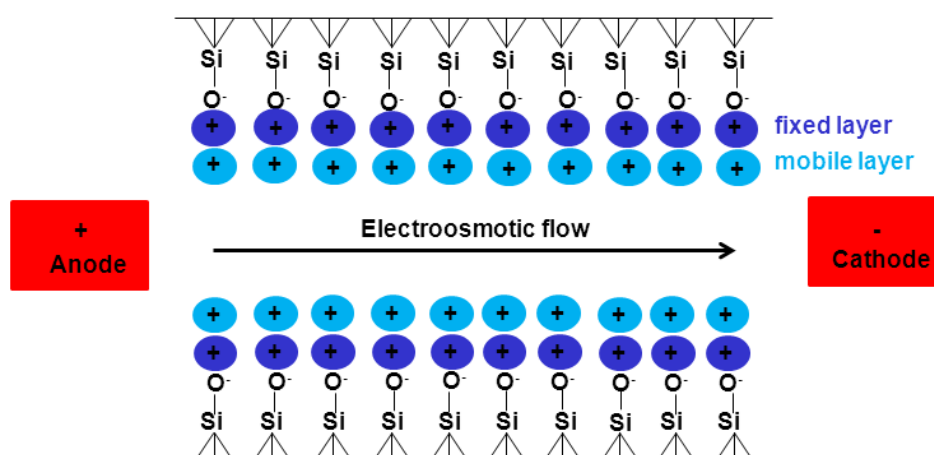**Figure 11.** Graphical depiction of the capillary walls in the presence of a buffer solution, adapted from [99].

The electroosmotic mobility can be determined by measuring the retention time of a neutral analyte and is defined as:

$$\mu_{EOF} = \frac{\varepsilon \cdot \xi}{\eta}$$

Equation 4

where μ_{EOF} = EOF mobility

ε = solution dielectric constant

ξ = zeta potential

The zeta potential in Equation 4 is strongly pH dependent, therefore the EOF can vary by more than an order of magnitude between pH 2 and pH 11 [94]. Under basic conditions (pH > 11) the surface is highly charged, the EOF is then too rapid to enable separation of the analytes before they reach the detector. On the contrary, at pH < 2 the silanol groups are protonated and the EOF is zero. Besides the pH of the background electrolyte (BGE), the EOF can be controlled by the following variables: electrical field (EOF changes proportionally with electrical field), ionic strength or BGE concentration (EOF increases at low ion strength), BGE composition (addition of organic modifiers to the electrolyte changes zeta potential and electrolyte viscosity), temperature (EOF changes due to viscosity change), and surfactants (anionic surfactants increase EOF, cationic surfactants decrease EOF) or coatings (can increase, decrease or even reverse the surface charge of the capillary) [94].

In a typical CE separation the EOF has an influence on the electrophoretic migration, therefore the resultant migration mobility of each species *i* is:

$$\mu_{eff,i} = \mu_{EOF} + \mu_{E,i} \hspace{4cm} \text{Equation 5}$$

If $\mu_{EOF} > \mu_{E,i}$ for all *i*, and this is generally the case for pH > 3, all species move in the same direction enabling single point detection of analytes:

$\mu_{eff,+} = \mu_{EOF} + \mu_{E,+}$	Positive ions
$\mu_{eff} = \mu_{EOF}$	Neutral molecules
$\mu_{eff,-} = \mu_{EOF} - \mu_{E,-}$	Negative ions

From these equations it is evident that small multiply charged cations migrate quickly whereas anions are retained longer in the capillary due to their conflicting electrophoretic mobilities (Figure 12).
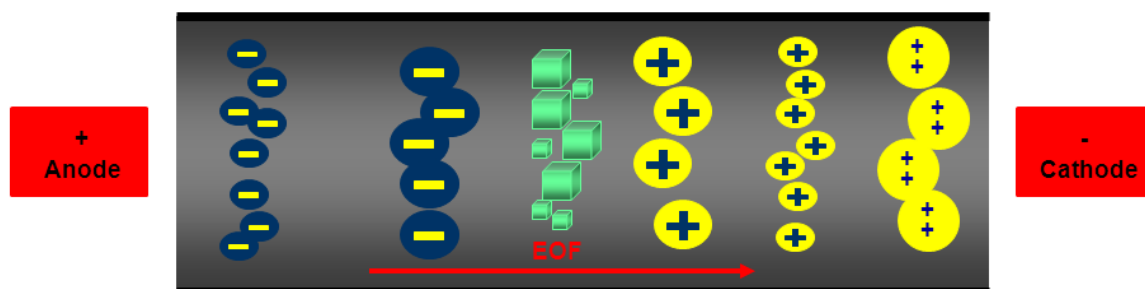

Figure 12. Schematic representation of separation in CE using fused silica capillaries [97].

The most widely used detection method is UV-visible absorption spectroscopy. Practically all commercial CE systems are equipped with this detector because it is suitable for many types of analytes. An optical window in the capillary allows online detection. The sensitivity with UV detection is proportional to the path length of the cell (Beer-Lambert law), which in this case is the internal diameter of the capillary (10-100 µm). Due to this short path length the detection limit with UV/vis absorbance is relatively high. In order to improve the detection limit, fluorescence and mass spectrometry are also used as detection techniques.

Several modes of CE operation have been developed in the last years. They differ in the composition of the BGE and can be divided according to their separation modes in the following main categories: capillary zone electrophoresis (CZE), micellar electrokinetic chromatography (MEKC), microemulsion electrokinetic chromatography (MEEKC), capillary gel electrophoresis (CGE), capillary isoelectric focusing (CIEF), capillary isotachophoresis (CITP) and capillary electrochromatography (CEC) [94].

To date, CZE has been the most popular CE mode because of its simplicity of operation and versatility. However, more and more sophisticated capillary based separation techniques have been developed in recent years and applied for a multitude of analytical problems.

2.2. Microemulsion Electrokinetic Chromatography

Microemulsion electrokinetic chromatography (MEEKC) is a separation mode applied in CE, which offers the possibility of highly efficient separations of both charged and neutral analytes. This electrodriven separation technique uses microemulsion buffers to resolve solutes based on both their hydrophobicities and electrophoretic mobilities. In general, an oil-in-water microemulsion is utilized in MEEKC which consists of an aqueous buffer, oil, surfactant and co-surfactant. Borate and phosphate are used as typical buffers in the pH range 7-9 in MEEKC, because of their relatively high EOF velocities. Octane or heptane are most frequently used to generate the oil droplets. These droplets are coated with a surfactant to reduce the surface tension between the two liquid layers and which allows the emulsion to form. Sodium dodecyl sulphate (SDS) is the most widely utilized emulsifier in MEEKC. The surfactant molecules position themselves at the oil-water interface, with the tail groups orientated towards the oil droplet and the negatively charged hydrophilic sulphate groups orientated towards the aqueous phase (Figure 13). Electrostatic repulsion of the negatively charged head groups of SDS prevents highly efficient packing and formation of an emulsion. Therefore a co-surfactant, usually a medium chain length alkyl alcohol such as butan-1-ol, is

essential for the formation of the microemulsion. Co-surfactant molecules position themselves between the sulphate group of the surfactant molecules and reduce the surface tension of the system.
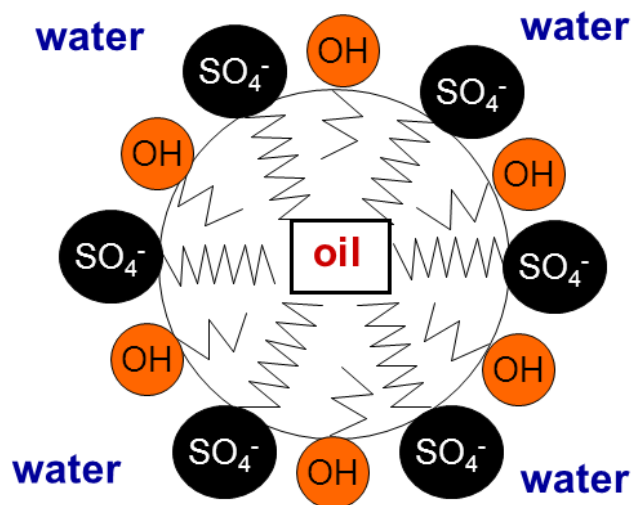
Figure 13. Schematic drawing of a surfactant coated oil droplet.

SDS induces negative charges to the droplets, which enables them to migrate towards the anode when voltage is applied. Under most conditions, however, anionic oil droplets still migrate along the separation axis toward the detector (near the cathode) because their electrophoretic velocity is usually not large enough to overcome the EOF. The chromatographic separation is based on the partition of the solutes between the aqueous phase and moving oil droplets. The more hydrophobic the solute is, the more it interacts with the oil droplet and the longer the migration time. Conversely uncharged, highly hydrophilic solutes reside in the aqueous phase of the microemulsion and migrate quickly with the EOF towards the detector. The retention factor (capacity factor *k*) of a solute in an MEEKC system is defined as the ratio n_{me}/n_{aq} (n_{me} = total number of moles of solute in the microemulsion phase, n_{aq} = total number of moles of solute in the aqueous phase) and this mass distribution coefficient can be calculated according to:

$$k = \frac{t_R - t_o}{t_o(1 - \frac{t_R}{t_{me}})}$$

Equation 6

where t_o = migration time of an unretained substance (EOF marker)

t_{me} = migration time of the microemulsion

t_R = solute migration time

Higher *k* values indicate slower migration and stronger partitioning of the solute into the oil droplet.

MEEKC is a relatively new technique but is widely applied to a range of application types [100, 101]. This method is very useful for the determination of log P values of neutral solutes [102, 103], but MEEKC can also be applied to the analysis of vitamins [104], bioanalysis [105], natural products [106] and antibiotics [107].

2.3. Inductively Coupled Plasma Mass Spectrometry

Inductively coupled plasma mass spectrometry (ICP-MS) is a useful and powerful technique for trace element analysis which was commercialized in 1983 [108]. Beside its sub-parts-per trillion detections limits, ICP-MS offers further advantages like multi-element and multi-isotope capability as well as a wide linear dynamic range [109]. Therefore this method has found applications in the semiconductor, biomedical, nuclear and pharmaceutical industry. ICP-MS is based on the atomization and ionization of the analytical sample in the plasma and the separation of the formed ions in the mass spectrometer. An ICP-MS system usually consists of six parts: a sample-introduction system, a plasma source, an interface region, an ion focusing system, a mass analyzer and a detector (Figure 14).
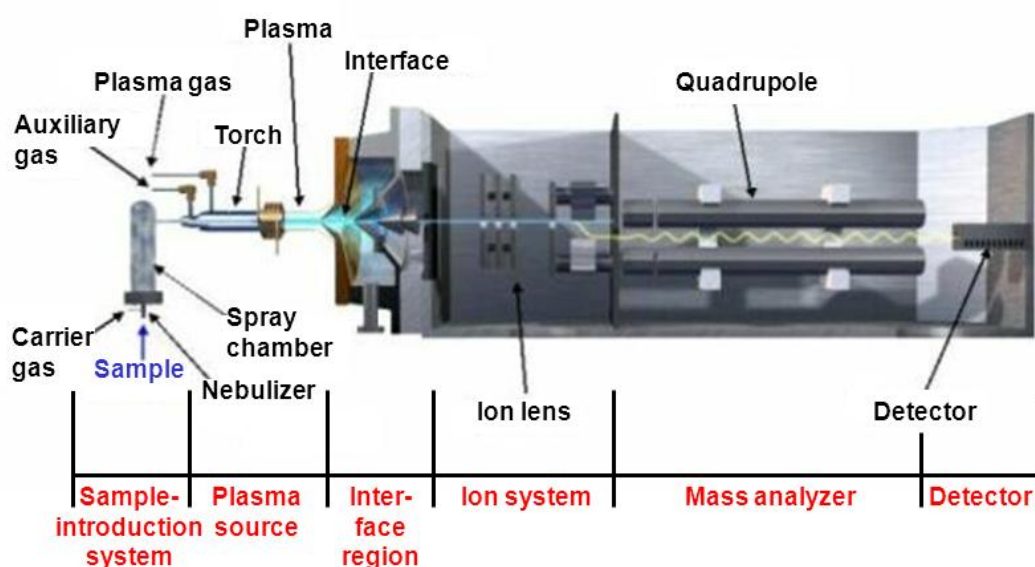

Figure 14. Schematic representation of an ICP-MS system, adapted from [110].

Depending on the sample, two different introduction systems exist for ICP-MS. For a liquid sample an introduction system consisting of a nebulizer and a spray chamber is normally used. In the nebulizer the liquid sample is dispersed into a fine aerosol by a pneumatic action of gas flow. Only small droplets are transferred into the plasma. Solid samples can be introduced into the ICP-MS by two different ways. They can be digested with heat and/or strong acids and introduced into the ICP-MS in liquid form. But this process is time consuming and the adding of chemicals like hydrofluoric acid to dissolve the sample can give rise to matrix-based interferences forming in the plasma. An alternative introduction system for solid samples is laser-ablation (LA). This technique requires minimal sample preparation. High-energy UV or IR photons are emitted by the laser and release ablation particles as a fine dense aerosol which is then transported from the laser cell using a carrier gas to the plasma source. The generation of the plasma with a temperature of approximately 6000 K, requires a plasma torch, a radio frequency (RF) coil and an RF power supply. A flow of argon gas is introduced into a series of concentric tubes of the torch that is wrapped at one end by an RF coil [111]. An electrical spark is applied to the gas, which causes some electrons to be stripped from their argon atoms. These electrons are accelerated in the magnetic field of the induction coil and collide with other argon atoms leading to the emission of electrons. This collision-induced ionization of the argon continues in a chain reaction, resulting in what is known as an inductively coupled plasma discharge. During their voyage into the plasma the sample aerosol goes through a number of physical changes [112]. In the preheating zone the liquid droplets are dried and become small solid particles. As the sample moves further into the plasma, the solid particles are transferred into the gas phase. These ground state atoms are converted to ideally simply charged ions through the collision with energetic argon electrons (Figure 15).
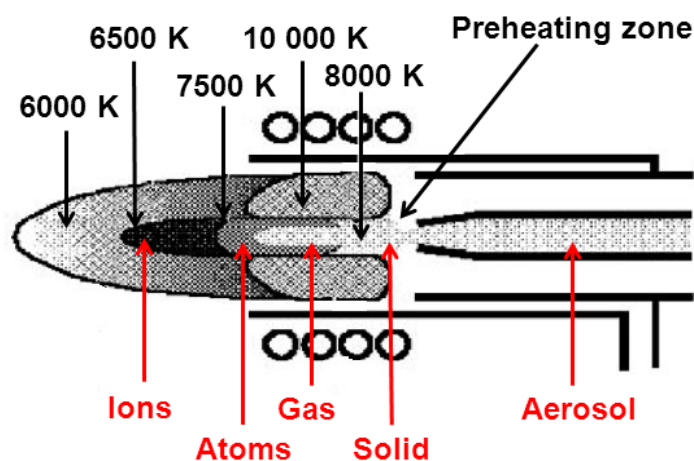

Figure 15. Conversion of a droplet to an ion in the ICP, adapted from [112].

The ions are transported from the plasma and directed into the interface of the mass spectrometer. The interface is responsible for the transport of the ions from the atmospheric pressure region of the torch to the mass spectrometer analyzer region, which is at 10^{-6} Torr [113]. Immediately behind the interface a lens focusing system is positioned. It focus the ion beam into the mass analyzer and blocks both photons and neutrals from passing any further into the spectrometer which results in low background levels, low detection limits and stable signals in real-world sample matrices [114]. The ions exiting the lens system are separated according to their mass-to-charge (*m/z*) ratio by the mass analyzer. Quadrupole mass filters, double focusing magnetic sector and time-of-flight are the mass analyzers which are used in commercial ICP-MS systems. 90% of all ICP mass spectrometers sold are equipped with a quadrupole mass analyzers which consists of four cylindrical or hyperbolic metallic rods [115]. By placing a direct current field on one pair of rods and a RF field on the other, only ions of a selected *m/z* ratio can reach the detector, whereas ions that do not have the selected *m/z* pass through the spaces between the rods and are ejected from the quadrupole (Figure 16). The settings of the quadrupole can be changed quickly, allowing to measure all the analytes in a multielement sample. In real-world samples 25 elements can be determined in duplicate with precision in 1-2 min [115].
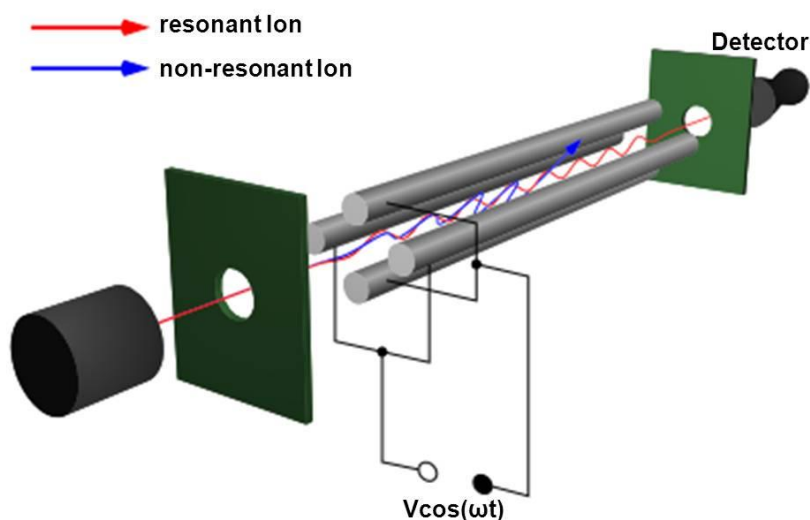

Figure 16. Schematic representation of a quadrupole mass filter [116].

Ions that make it through the mass analyzer are converted into electrical pulses and are detected by an electron multiplier. The magnitude of the electrical pulses corresponds to the concentration of analyte ions present in the sample.

2.4. Capillary Electrophoresis-Inductively Coupled Plasma Mass Spectrometry

Selectivity and sensitivity are important factors in (bio)analysis. Selectivity can be achieved by separation techniques like high-performance liquid chromatography (HPLC), gas chromatography (GC) and CE. To study proteins CE is one of the techniques of choice. With this separation technique protein analysis is carried out under mild conditions and, in contrast to HPLC, there is no need of organic solvents or very high salt concentrations. This enables the study of proteins under real-world conditions with minor influences on an existing equilibrium, i.e., conformational changes or protein degradation are unlikely to occur during analysis. Additionally, CE separations are characterized by high resolution, minimal sample consumption and short separation times, but CE has a serious drawback by its lack of sensitivity when ordinary UV-Vis detectors are used.

ICP-MS is a multielement, highly sensitive and specific detector. The drawback of ICP-MS for bioanalysis lies in the selectivity. During ICP ionization proteins are atomized and ionized, owing to this destructive detection principle, no information of the chemical form of a protein can be obtained with ICP-MS detection.

CE and ICP-MS have large potential in bioanalysis and in their combination, limitations of the one technique are offset by properties of the other. The hybrid technique CE-ICP-MS was for the first time described in 1995 [117] and finds nowadays application in metal-protein binding studies, tracing the metabolism of drugs in the human body, metal-speciation analysis, isoform analysis of metalloproteins and studies of metal-transmembrane transporation [118]. The challenges in the hyphenation of CE to ICP-MS are the adaptation of the low flow rate of the CE to the flow rate of the nebulizer of the ICP-MS, the maintenance of the electrical connection and the avoidance of laminar flow in the capillary, which could destroy the EOF based separation. Since 1995, several interfaces like concentric nebulizers, cross-flow nebulizers, oscillating capillary nebulizers and ultrasonic nebulizers were developed [119]. One of the most widely distributed interfaces is the microconcentric nebulizer developed by Schaumlöffel and Prange [120], which is commercially available as the CEI-100 interface from CETAC. The instrument set-up of the CE-ICP-MS system using the CEI-100 interface is shown in Figure 17. The CEI-100 interface involves the use of a sheath liquid in order to allow closing the electrical circuit for CE and to increase the linear velocity of the flow of CE effluent to match the sample flow rate of the ICP-MS. Because of easy clogging and breaking of the micronebulizers, on-line CE-ICP-MS analyses are still far from routine. Especially quantitative measurements are critical due to changes in sensitivity between runs which lead to poor repeatability [121]. Therefore, the addition of a trace element to the make-up-liquid is

necessary. The average intensity of the external standard is then used to normalize the signals of the analytes.

Depending on the research topic and the analytes different CE separation modes have to be used. So far mostly CZE was combined with ICP-MS and only a few other modes of CE have been used hyphenated to ICP-MS. With capillary electrochromatography (CEC) the absorption of bio-species on the capillary wall is reduced and the separation efficiency of some analytes is improved. Lin *et al.* used CEC-ICP-MS for the separation of selenoamino acids [122]. Capillary isoelectric focusing (CIEF) is known for its extremely high resolving power. This CE mode was interfaced to ICP-MS and used by Michalke *et al.* for the analysis of organic Se species [123]. We have developed MEEKC-ICP-MS and used this method for the separation of neutral complexes and the analysis of lipophilicity of anticancer platinum compounds [124].
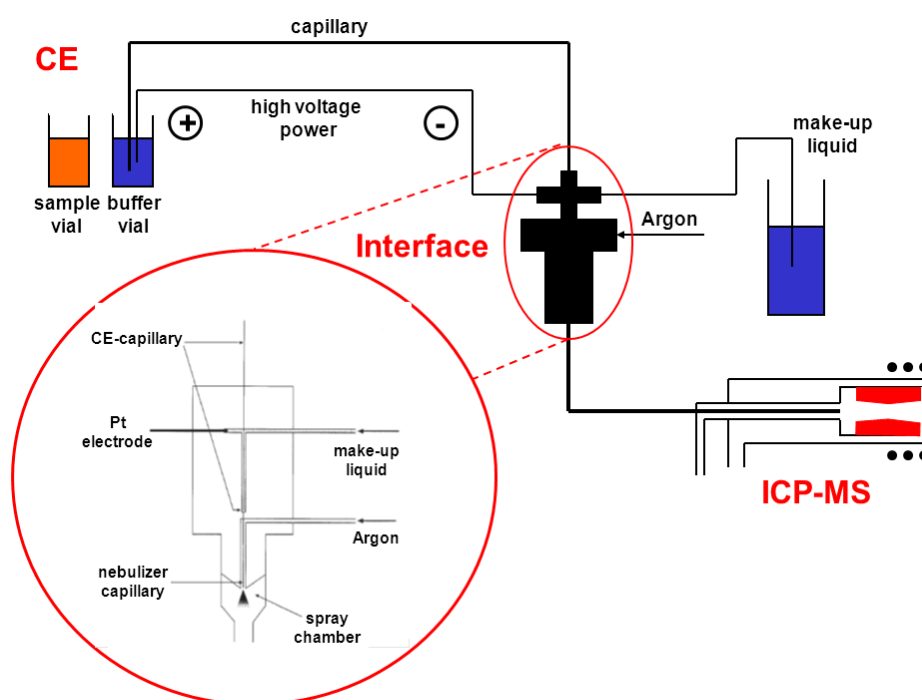

Figure 17. CE-ICP-MS system with a microconcentric nebulizer, adapted from [120].

2.5. Electrospray Ionization Mass Spectrometry

Electrospray ionization mass spectrometry (ESI-MS) is nowadays a basic tool in different research areas including analysis of pharmaceuticals with a relatively small molecular mass up to biological macromolecules. It is a soft ionization technique and is therefore especially useful in studying labile species such as peptides, proteins, organometallics, coordination compounds, oligosaccharides and polymers. Electrospray as an ionization technique for mass spectrometry was developed by Dole *et al.* in the late 1960s [125] and improved by Yamashita and Fenn who in 1984 coupled an electrospray source to a quadrupole mass analyzer [126-128]. The success of ESI started when Fenn *et al.* demonstrated that with this ionization technique multiply charged ions were obtained from proteins [129, 130]. Before this development the mass spectral analysis of proteins and other macromolecules was problematic because of limited transfer into the gas phase. Fenn was awarded for this contribution with the 2002 Nobel Prize in Chemistry.

The process of electrospray ionization can be divided in 4 steps: formation of ions, nebulization, desolvation and ion evaporation. Ion formation can occur already in solution before nebulization. In this case the analyte ion abundance is high as is the electrospray sensitivity. Analytes that do not ionize in solution can be charged during the process of nebulization, desolvation and ion evaporation. The nebulization starts when the sample solution enters the spray chamber through a needle to which a high potential difference is applied (Figure 18). The combination of the nebulizing gas, which often enters the spray chamber concentrically through a tube that surrounds the needle, and the strong electrostatic field forces the spraying of charged droplets from the needle with a surface charge of the same polarity as of the needle. As the charged droplets pass down the potential gradient toward the source sampling cone on the counter electrode, solvent evaporation occurs. With the aid of a counter flow of warm nitrogen gas the charged droplets are continuously reduced in size by evaporation of the solvent, leading to an increase of surface charge density and a decrease of the droplet radius. When the force of the Coulomb repulsion equals that of the surface tension of the droplet (the Rayleigh limit), the droplet is ripped apart. This produces smaller droplets with a high surface charge density which can undergo a cascade of ruptures, yielding smaller and smaller droplets until the analyte is free of solvent and single ions move to the mass analyzer.
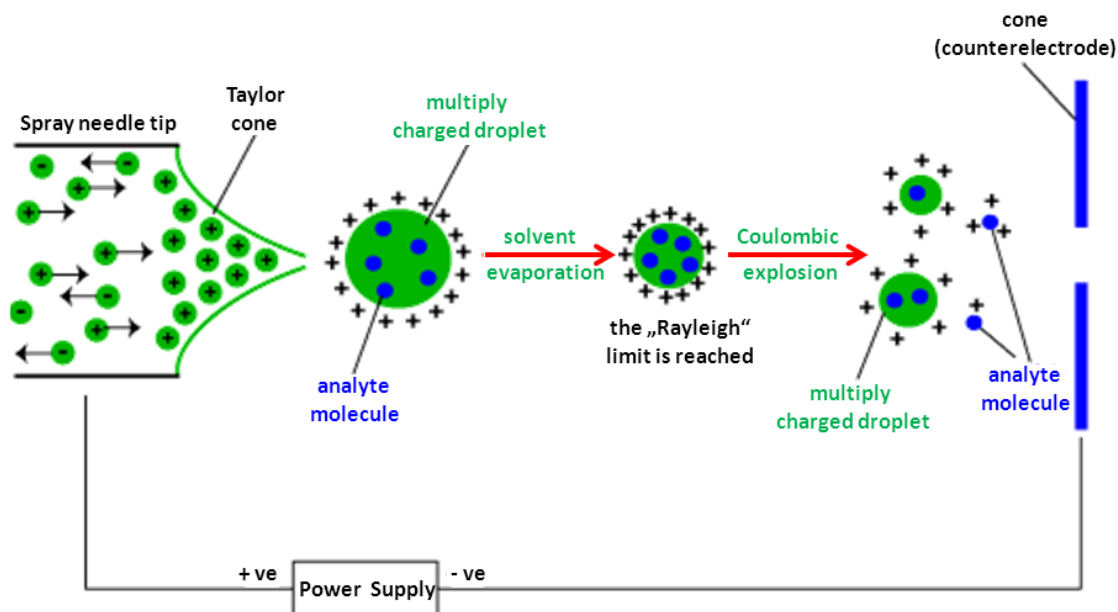
Figure 18. The spraying process at the nebulizer tip of an ESI-MS instrument [131].

The process of ion formation has been the subject of many scientific investigations but the exact mechanism of the process is still discussed controversially. Two different theories exist that explain the final production of gas-phase ions: the ion evaporation model that says that ions are emitted directly from the charged droplets into the gas phase and the charged residue model that suggests that electrospray droplets undergo evaporation leading to droplets that contain on average one analyte ion.

ESI is an example of atmospheric pressure ionization (API). Sample ionization under atmospheric pressure has the advantage of a 10^3-10^4 times greater ionization efficiency as in a reduced-pressure chemical ionization (CI) source [130]. The analyzer compartment is situated in the high vacuum region of the mass spectrometer (10^{-5} Torr) in order to prevent unwanted interactions between the molecular ions and atmospheric components which can affect the determined *m/z* ratio. Therefore, the ions have to pass a series of skimmer cones and are guided electrostatically into the vacuum of the mass analyzer. There are five types of mass analyzers that can be used in ESI-MS systems: quadrupolar analyzers, ion trap analyzer, magnetic and electromagnetic analyzers, time-of-flight analyzers and ion resonance analyzers. The combination of several analyzers in sequence is also possible (tandem mass spectrometry) and is becoming increasingly common.

As already mentioned above, the great benefit of ESI is the formation of multiply charged species which makes the measurement of biological macromolecules possible. Generally it can be said that a protein will tend to carry one charge per 1000 Da. This value is dependent of the number of basic amino acids in the protein, and the measurement conditions. If there

are only few basic amino acids the number of charges decreases [130]. Therefore, nearly all proteins can be detected in the mass range up to 3000 *m/z*, regardless of their actual molecular weight. The ESI-mass spectrum of apo-Tf is shown in Figure 19; it is protonated between 27 and 35 times and provides individual peaks in the range of 2200-3000 *m/z*. With the help of deconvolution algorithms the multiple peaks can be transformed into a single peak given the molecular weight.
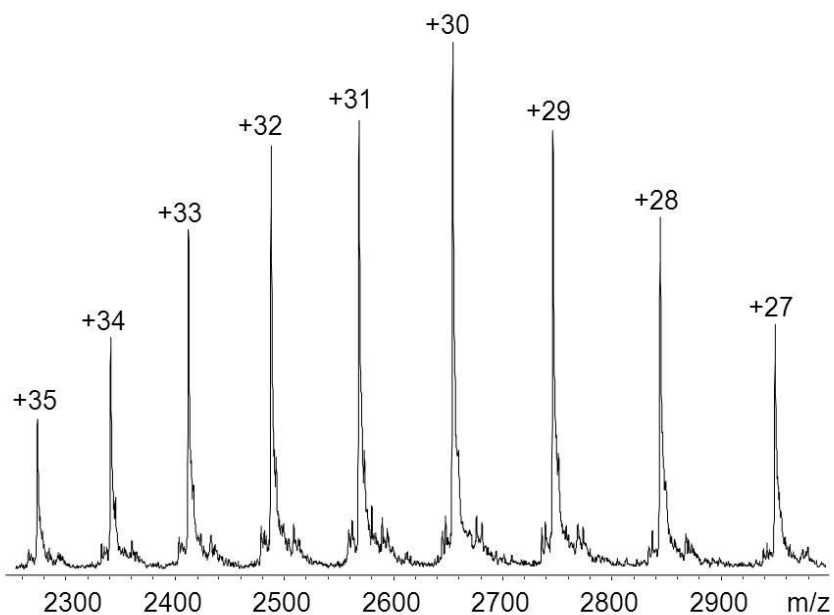

Figure 19. ESI-mass spectrum of apo-transferrin. The number of charges are indicated on each peak. The molecular weight of this glycoprotein is 79570 ± 7 Da.

3. Results

This Ph.D.-thesis can be divided in three research topics and is based on the following publications/manuscripts:

The influence of lipophilicity on the antiproliferate properties of anticancer platinum complexes

The first example of MEEKC-ICP-MS coupling and its application for the analysis of anticancer platinum complexes

Bytzek A.K., Reithofer M.R., Galanski M., Groessl M., Keppler B.K., Hartinger C.G.
Status: published in **Electrophoresis**, 2010, *31*, 1-7. (Cover article)

The first example of the coupling of MEEKC to ICP-MS was presented and used for the separation of Pt(II) and Pt(IV) anticancer drugs and drug candidates. The MEEKC-ICP-MS system was found to be more sensitive than MEEKC with conventional UV/vis detection and the analysis of UV/vis silent compounds is now achievable.

To achieve an effective separation of the Pt complexes, I have optimized at first the MEEKC method by using different compositions of microemulsions. Afterwards the coupling of MEEKC to ICP-MS was performed and the collected data was compared with standard ultraviolet/visible (UV/vis) spectroscopy detection. I have drafted the manuscript and contributed to the discussion of the data.

Tuning of lipophilicity and cytotoxic potency by structural variation of anticancer platinum(IV) complexes

Reithofer M.R., Bytzek A.K., Valiahdi S.M., Kowol C.R., Groessl M., Hartinger C.G., Jakupec M.A., Galanski M., Keppler B.K.
Status: published in **Journal of Inorganic Biochemistry**, 2010, *105*, 46-51.

The IC_{50} values of a series of bis(carboxylato)dichlorido(ethane-1,2-diamine)platinum(IV) compounds were correlated with the compounds lipophilicity, reduction potential and their cellular accumulation in cancer cells *in vitro*. It was found that the antiproliferative properties of the complexes correlated with their lipophilicity as well as their accumulation, whereas differences in antiproliferative potency could not be explained by reduction potentials.

I have contributed ocantol/water partition coefficient data on the lipophilicity by the shake flask method as well as by microemulsion electrokinetic chromatography. Furthermore, a significant contribution to the discussion of the results was made during the preparation of the manuscript.

Studies on the biodistribution of oxaliplatin and its methyl derivatives in tumor bearing mice

Bytzek A.K., Jungwirth U., Berger W., Galanski M., Hartinger C.G., Keppler B.K.
Status: in preparation

The influence of the lipophilicity of Pt- complexes on the anticancer activity *in vivo* was studied in tumor-bearing mice. Oxaliplatin and its methyl derivatives KP1537 and KP1691 were administered intravenously and their biodistribution and especially their accumulation in the tumor were determined 1 and 6 h post-injection.

I have mineralized the tissue samples by microwave digestion and analyzed them for their Pt content by ICP-MS. Data analysis and correlation with biophysical properties of the enantiomeric compounds was done.

Understanding the behavior and properties of the ruthenium drug candidate KP1339 *in vivo*

LC- and CZE-ICP-MS approaches for the *in vivo* analysis of the anticancer drug candidate sodium *trans*-[tetrachloridobis(1*H*-indazole)ruthenate(III)] (KP1339) in mouse plasma

Bytzek A.K., Boeck K., Hann S., Herman G., Keppler B.K., Hartinger C.G., Koellensperger G.
Status: submitted to **Metallomics**

To improve the understanding of the mode of action of the drug candidate KP1339, the Ru complex was given intravenously to mice. CZE and SEC-IC (size exclusion/anion exchange chromatography) were coupled to ICP-MS in order to characterize the interaction of KP1339 with mice plasma proteins *in vivo*. The samples of the mice terminated after 24 hours showed a 2-2.5 lowered albumin content as compared to the untreated control group and the mice

which were terminated after 7 days. It was found that KP1339 bind to a high degree to albumin. At a dose higher then 50 mg/kg the formation of albumin aggregates was observed and confirmed by matrix-assisted laser desorption ionization mass spectrometry (MALDI MS).

My contribution to this paper was the optimization of a CZE-ICP-MS method for the measurement of Ru in the plasma samples as well as the investigation of the interaction with serum proteins. Additionally, I performed MALDI measurements of the fractionated plasma samples and drafted significant parts of the manuscript, especially the discussion with regard to the mode of action of the drug candidate.

Biodistribution of the anticancer drug candidate sodium *trans*-[tetrachloridobis(1*H*-indazole)ruthenate(III)] (KP1339)

Bytzek A.K., Koellensperger G., Keppler B.K., Hartinger C.G.

Status: in preparation

The Ru complex KP1339 is a promising anticancer agent, currently undergoing clinical trials. In this work package, pharmacokinetic aspects of KP1339 in non-tumor bearing mice in a time frame of 24 h were investigated. KP1339 was administered intravenously and the accumulation in tissues was determined at several time points. The highest Ru levels were found in colon, lung, liver kidney and thymus. The peak Ru concentrations in these tissues were reached 1-6 h after administration and declined slowly over time. Apart from the Ru content in the blood also the interaction with serum proteins was investigated. It was found that a large majority of the total Ru content was attached to mouse serum albumin (MSA). Beside the MSA adduct, a higher molecular weight species was observed probably stemming from MSA conjugates.

I contributed the mineralization of the tissue samples by microwave digestion and the analysis of their Ru content by ICP-MS to this paper. The partition of the Ru between the major serum proteins was investigated by CZE-ICP-MS. Additionally, I performed an NCI anticancer drug discovery screen compare analysis for the parent compound KP1019 which indicated that the mode of action of this Ru compound is different from those of established drugs.

Serum protein binding of zinc complexes

Biodistribution of anti-diabetic Zn(II) complexes in human serum and *in vitro* protein-binding studies by means of CZE-ICP-MS

Bytzek A.K., Enyedy E.A., Kiss T., Keppler B.K., Hartinger C.G.

Status: published in **Electrophoresis***,* 2009, *30*, 4075-4082.

Zn(II) compounds are under development as insulin-enhancing drugs with potential use in the treatment of diabetes. Herein, CZE-ICP-MS studies on the interaction of Zn(II)-maltolato, -2-picolinato and -2,6-dipicolinato complexes with human serum proteins were performed and modeling calculations were confirmed by these experimental results. The investigated Zn(II)-complexes showed a high affinity to albumin.

For this study I adapted a CZE-ICP-MS method for the measurement of the Zn content attached to proteins. *In vitro* incubation of the Zn(II) complexes with transferrin, albumin and human serum were performed and the interaction with this proteins was determined.

3.1. The first example of MEEKC-ICP-MS coupling and its application for the analysis of anticancer platinum complexes

Bytzek A.K., Reithofer M.R., Galanski M., Groessl M., Keppler B.K., Hartinger C.G.
Status: published in **Electrophoresis**, 2010, *31*, 1-7. (Cover article)
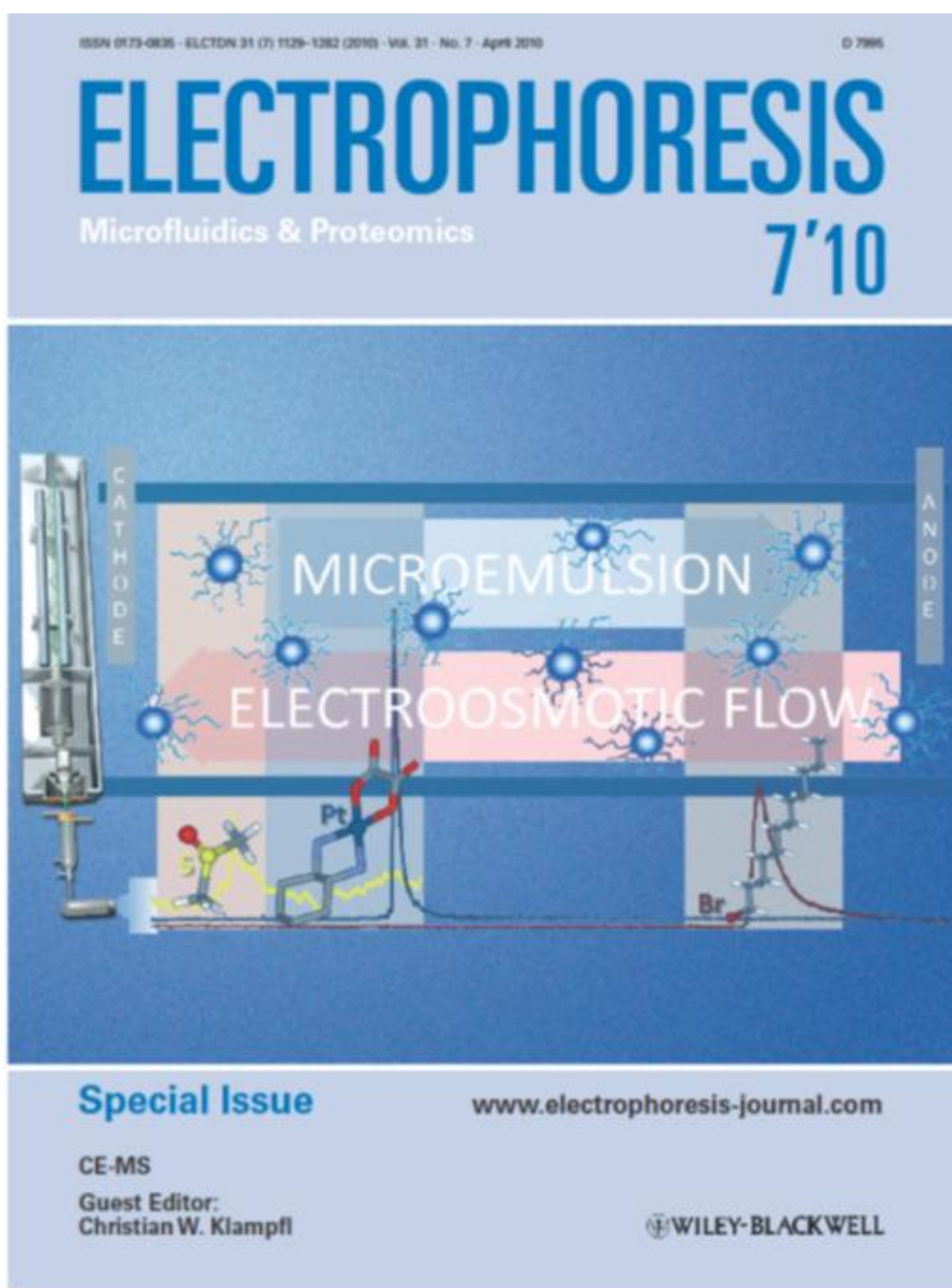
Anna K. Bytzek
Michael R. Reithofer
Markus Galanski
Michael Groessl
Bernhard K. Keppler
Christian G. Hartinger

Institute of Inorganic Chemistry,
University of Vienna, Vienna,
Austria

Research Article

The first example of MEEKC-ICP-MS coupling and its application for the analysis of anticancer platinum complexes*

MEEKC is a powerful electrodriven separation technique with many applications in different disciplines, including medicinal chemistry; however, up to now the coupling to highly sensitive and selective MS detectors was limited due to the ion suppressive effect of the commonly used surfactant SDS. Herein, the first example of the coupling of MEEKC to ICP-MS is presented and an MEEKC method for the separation of Pt(II) and Pt(IV) anticancer drugs and drug candidates was developed. Different compositions of microemulsions were evaluated and the data were compared with those collected with standard ultraviolet/visible (UV/vis) spectroscopy detection. The MEEKC-ICP-MS system was found to be more sensitive than MEEKC-UV/vis and the analysis of UV/vis silent compounds is now achievable. The migration behavior of the Pt(II) and Pt(IV) compounds under investigation is correlated to their different chemical structures.

1 Introduction

Commercially available CE instruments have been traditionally equipped with ultraviolet/visible (UV/vis) detectors, at best with a DAD device. These detectors provide sufficient sensitivity for many applications, however, with the disadvantage of low selectivity. In the last decade, CE hyphenated to mass spectrometers has gained considerable attention and the number of applications has increased steadily [1–3]. CE can be operated in different separation modes and more and more of these techniques are coupled to MS detectors, though some of these separation modes, especially when containing non-volatile components, have initially been considered as limited in their compatibility to MS coupling. Today, CE-MS is applied in many different fields of research, including, *e.g.* the analysis of pharmaceuticals and their metabolites, often in difficult biological matrices, environmental samples or technical products [4, 5].

One of such applications is the analysis of platinum(II) compounds, often used in the chemotherapeutic schemes of cancer patients [6]. Platinum complexes have been applied for

more than 30 years in the clinic but yet their mode of action has not unambiguously been identified [7]. The most important part in their activity appears to be related to the binding to DNA, whereas attachment to proteins, in particular to plasma proteins, being the first potential binding partners after intravenous administration, is believed to contribute to their side effects [8]. These adverse effects comprise nephrotoxicity, ototoxicity, vomiting, *etc.*, which are often observed during chemotherapy. However, the major limitation of healing tumor patients appears to be intrinsic and acquired resistance [7]. Oxaliplatin **1** (*SP*-4-2)-[(1*R*,2*R*)-]cyclohexane-1,2-diamine-$\kappa^2 N,N$](oxalato-$\kappa^2 O,O$)platinum(II) (Fig. 1) has been used in clinics for several years and more recently Pt(IV) compounds also moved into the focus of interest, due to potential oral administration which would improve the living quality of cancer patients significantly [9, 10]. Several examples of Pt(IV) complexes underwent clinical trials, most recently satraplatin [(*OC*-6-43)-bis(acetato-κO)amminedichlorido(cyclohexylamine-κN)platinum(IV); formerly JM216], but so far none of them made it to clinical application. One of the chemical features of the compound class exploitable for drug development is that they are relatively inert and are not significantly metabolized with respect to ligand substitution reactions after administration, but can be reduced in the hypoxic environment of the tumor, consequently enhancing the selectivity of the chemo-

Correspondence: Dr. Christian G. Hartinger, Institute of Inorganic Chemistry, University of Vienna, Waehringer Street 42, A-1090 Vienna, Austria
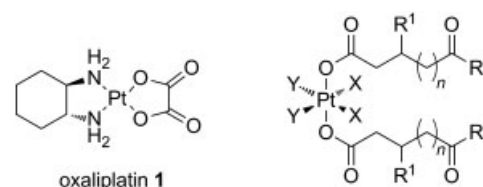**E-mail:** christian.hartinger@univie.ac.at
Fax: +43-1-4277-9526

*Dedicated to Professor Andreas Rizzi on the occasion of his 60th birthday.

therapeutics. The axial ligands were found to influence the redox potential of the Pt$^{IV/II}$ couples and eventually after reduction structurally related compounds to those used in clinics are formed. Recently, the synthesis of a series of such Pt(IV) compounds was reported (Fig. 1) and promising *in vitro* anticancer activity was demonstrated [11–13].

In recent years, CE has become an established technique in metallodrug research [14–16], especially for metallo-drug–protein-binding studies [17–22]. Initially, hydrolysis of the established anticancer agents such as cisplatin, carboplatin and oxaliplatin (neutral compounds which become positively charged after the exchange of the chlorido or biscarboxylato ligands by aqua groups) was studied in CZE mode [16]. Other major CE-based investigations include the binding of such compounds and related non-platinum anticancer metallodrug candidates to DNA building blocks [16], *i.e.* nucleotides and proteins under conditions, often chosen to resemble the physiological situation [16, 18, 23, 24]. Although the use of unspecific UV/vis detection appears limited, coupling to MS, in particular to element-specific ICP-MS (which also becomes of increasing importance in proteomics [25]), provides an additional degree of selectivity and also outstanding sensitivity [17, 26]. Hyphenation to the soft and ICP-complementary ionization technique ESI-MS yields structural information, not available from ICP-MS [17, 26, 27].

An important feature in the modes of action of (metallo)drugs is the cellular uptake [28]. This process is often influenced by active transport into the cell but also passive accumulation by diffusion is known to play an important role, especially in the case of the platinum compounds [29]. The diffusion of drugs through the cell membrane is related to the lipophilicity of a compound, which can be related to log k values in MEEKC. The separation in MEEKC mode relies on the different partition of the analytes in micro-emulsions (oil droplets suspended in an aqueous buffer, stabilized by a surfactant and co-surfactant) and a chroma-tography-type separation is achieved [30], thus enabling the efficient separation of neutral species as recently shown for

different isomers of new oxaliplatin derivatives [31]. The more lipophilic a compound is the higher will be its inclusion into the oil droplet [32]. Many different applications have been reported for this separation technique, including vitamins, proteins, peptides, drug compounds and agro-chemicals [30].

To the best of our knowledge, no coupling of MEEKC to ICP-MS was reported so far. Herein, this new methodology was applied in anticancer metallodrug research in a proof of principle study and the potential was evaluated in the analysis of oxaliplatin and several new neutral Pt(IV) anti-cancer drug candidates.

2 Materials and methods

2.1 Instrumentation

CE separations were carried out on an HP^{3D} CE system (Agilent, Waldbronn, Germany) equipped with an on-column DAD. Detection was carried out either by UV/vis at 200 nm or with an Agilent 7500ce ICP-MS interfaced utilizing a CETAC CEI-100 microconcentric nebulizer [33]. For all measurements with UV-detection, capillaries of 48.5 cm total length (40 cm effective length; 50 μm id) were used (Polymicro Technologies, Phoenix, AZ, USA), in the case of ICP-MS detection the capillary length was extended to 60 cm. Capillary and sample tray were thermostatted at 37°C. The sample injection was carried out by hydrodynamic injection at 10 mbar for 15 s or at 25 mbar for 4 s for UV/vis and ICP-MS detection, respectively, and the separation voltage was 20–25 kV. New capillaries were conditioned with 0.1 M HCl, water, 0.1 M NaOH, and again with water (10 min each). As a daily routine, the capillary was flushed with 0.1 M NaOH, water, and BGE for 5 min each before the first run. Before each injection, the capillary was purged with 0.1 M NaOH, water and the BGE for 2 min each. The operational values for the MEEKC-ICP-MS interface are listed in Table 1. The nebulizer was employed in self-aspiration mode with the sheath liquid closing the electrical circuit and spraying a fine aerosol. Analyses were started only if a sufficiently stable signal (RSD ^{115}In < 5%) was attained. Instrument control as well as data analysis was carried out using ChemStation software (B.03.07).

2.2 Reagents and solutions

SDS, dodecanophenone, 1-bromododecane, 1-butanol and sodium monohydrogenphosphate were purchased from Sigma-Aldrich (Vienna, Austria). Sodium hydroxide solution (0.1 M), hydrochloric acid, heptanes and sodium dihydrogenphosphate were obtained from Fluka (Buchs, Switzerland) and DMSO from Fisher Scientific, Austria. The ICP-MS tuning solution containing lithium, yttrium, cerium, thallium and cobalt in 2% HNO$_3$ (each 10 mg/L) was obtained from Agilent Technologies (Vienna, Austria) and the ^{115}In standard was from CPI international (Santa

Figure 1. Structures of the platinum anticancer drug oxaliplatin **1** and Pt(IV) drug candidates **2–11**. chxn = cyclohexanediamine

2	$n = 0$, X = Cl, Y$_2$ = en, R = OCH$_3$, R^1 = H
3	$n = 0$, X = Cl, Y$_2$ = en, R = OC$_2$H$_5$, R^1 = H
4	$n = 0$, X = Cl, Y$_2$ = en, R = OC$_3$H$_7$, R^1 = H
5	$n = 0$, X = Cl, Y$_2$ = en, R = OC$_4$H$_9$, R^1 = H
6	$n = 0$, X = Cl, Y$_2$ = en, R = NHC$_3$H$_7$, R^1 = H
7	$n = 1$, X = Cl, Y$_2$ = en, R = NHC$_3$H$_7$, R^1 = H
8	$n = 1$, X = Cl, Y$_2$ = en, R = OCH$_3$, R^1 = CH$_3$
9	$n = 1$, X = Cl, Y$_2$ = en, R = OC$_2$H$_5$, R^1 = CH$_3$
10	$n = 0$, X = Cl, Y$_2$ = en, R = NH(cyclopentyl), R^1 = H
11	$n = 0$, X$_2$ = oxalate, Y$_2$ = (1R,2R)-chxn, R = NHC$_3$H$_7$, R^1 = H

Table 1. ICP-MS operational parameters

Sampler	Ni (0.1 mm orifice)
Skimmer	Ni (0.4 mm orifice)
Plasma RF power, W	1500
Isotopes recorded	^{34}S, ^{79}Br, ^{115}In, ^{195}Pt
Nebulizer gas flow rate (L/min)	1.14
Sheath liquid	10 mM phosphate buffer with 20 μg/L In
BGE	Microemulsion: 1.43% SDS, 91.15% phosphate buffer (10 mM, pH 7.4), 0.85% heptane, 6.57% butanol

Rosa, USA). High-purity water used throughout this study was obtained from a Millipore Synergy 185 UV Ultrapure Water system (Molsheim, France). Oxaliplatin **1** and the Pt(IV) compounds **2–11** (Fig. 1) were synthesized as described elsewhere [11–13, 34].

2.3 Preparation of the microemulsion

For the preparation of the MEEKC solutions, different ratios of SDS, 1-butanol, heptane and a small portion of buffer (mass%) were mixed by sonication for 5 min. The residual buffer was then slowly added to the mixture. Phosphate buffer (20 and 10 mM for MEEKC-UV/vis and -ICP-MS, respectively; pH 7.4) was used for the preparation of the microemulsions. The solution was kept for 24 h at room temperature before use.

2.4 Sample preparation

The analytes were dissolved in the microemulsions to give concentrations between 0.4 and 0.6 mg/mL (UV/vis detection) and *ca.* 0.1 mg/mL (ICP-MS detection). For the MEEKC-UV/vis studies, DMSO and dodecanophenone were used as markers for the EOF and the microemulsion droplets, respectively; to 1 mL of the sample solution, 1 μL DMSO and 10 μL dodecanophenone (18 mg/mL in methanol) were added. In the case of ICP-MS detection, DMSO (^{34}S) and 1-bromododecane (^{79}Br) were used as markers (1 mL of the sample contained 3 μL DMSO and 1 μL 1-bromododecane (diluted 1:1 with 1st issue correction1-butanol)).

2.5 Calculations

The capacity factor, *k*, is defined as the ratio n_{me}/n_{aq} (n_{me} = total number of moles of solute in the microemulsion phase, n_{aq} = total number of moles of solute in the aqueous phase) and this mass distribution coefficient can be calculated according to Eq. (1) (t_o = migration time of an unretained substance (EOF marker), t_{me} = migration time

of the microemulsion, t_R = solute migration time).

$$k = \frac{t_R - t_0}{t_n(1 - t_R/t_{me})} \tag{1}$$

The LODs and LOQs for ICP-MS and UV/vis detection were calculated using Eqs. (2) and (3) (σ = residual standard deviation of the calibration curve, *S*, its slope).

$$LOD = \frac{3.3\sigma}{s} \tag{2}$$

$$LOQ = \frac{10\sigma}{s} \tag{3}$$

3   Results and discussion

Oral administration of drug compounds does not only require a certain degree of chemical inertness but also sufficient bioavailability, a factor, which depends at least partly on the lipophilicity of a drug. In a recent report, the lipophilicity of oxaliplatin derivatives was related to the *k* factors determined by an MEEKC-UV/vis method [31]. It is a few years since MEEKC-MS has been introduced, as the coupling with ESI-MS is limited due to the suppressive effect of the commonly used surfactant SDS on ESI [35]. However, the development of atmospheric pressure photo ionization with ionization by high-energy photons [36] enabled the hyphenation of the two methods [37], and different pharmaceuticals have been analyzed with this technique [38, 39]. ICP-MS is an element specific and highly sensitive method [25, 26], which is in contrast to ESI-MS not influenced by ion suppression.

3.1 Analysis of oxaliplatin by MEEKC-ICP-MS, method development and initial performance tests

Many parameters such as the choice of oil phase, surfactant and co-surfactant, pH of the BGE, and the hydrophobicity of the analytes influence the separation performance of an MEEKC system and the complexity of the microemulsion allows optimization in several directions. Since the developed method is aimed to be eventually used in the analysis of samples in biological environment, the pH of the buffer composition was set to 7.4 and a phosphate buffer was used for the preparation of the microemulsion with the surfactant SDS. In order to generate the oil droplets, heptane was added and 1-butanol was used as the co-surfactant. Before injection, the sample was diluted with the microemulsion in order not to disrupt the separation system [32].

A satisfying result for the analysis of **1** was obtained with an MEEKC system consisting of 1.43% SDS, 0.85% heptane, 6.57% 1-butanol and 91.15% phosphate buffer (10 mM, pH 7.4; Fig. 2). Microemulsions of such composition were demonstrated to possess high stability in other reports [40]. Due to the low flow through the capillary, the interface
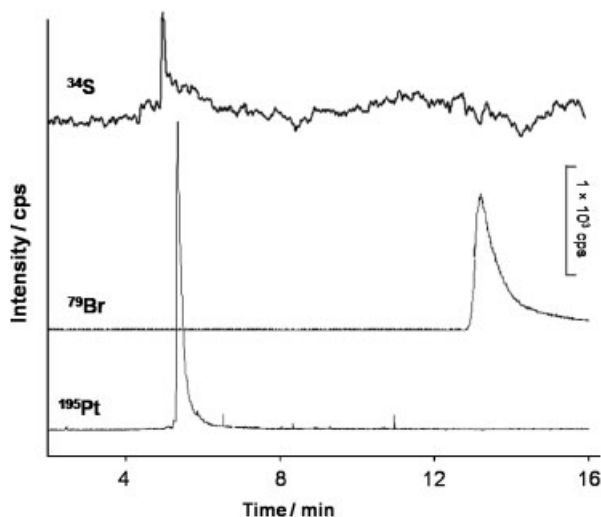
Figure 2. MEEKC-ICP-MS of oxaliplatin **1**. Shown are the traces of ^{195}Pt, the EOF marker (^{34}S) and the marker of the microemulsion droplets (^{79}Br).

Table 2. Comparison of the log k values obtained for **1**, **2**, **5**, **9** and **10** by MEEKC-UV/vis and -ICP-MS with 1.44% SDS, 6.48% 1-butanol, 0.82% heptane, 91.26% phosphate buffer as microemulsion ($n = 3$)

Compound	Detection method	
	UV/vis	ICP-MS
Oxaliplatin **1**	-0.863 ± 0.004	-0.890 ± 0.025
2	-1.130 ± 0.004	-1.100 ± 0.171
5	0.553 ± 0.003	0.616 ± 0.035
9	0.098 ± 0.002	0.170 ± 0.015
10	0.105 ± 0.002	0.061 ± 0.023

oxaliplatin samples were prepared. Linear calibration curves with high correlation coefficients were obtained for both detection methods: in the case of UV/vis detection, the standards covered the range of 0.35–5 mM (Fig. 3), in the case of ICP-MS detection 0.125–1.000 mM. The LODs and LOQs were slightly lower when ICP-MS detection was used (Table 3); however, addition of an internal standard was required in that case (the peak area of oxaliplatin was divided by the peak area of 1-bromododecane as a function of the analyte concentration), whereas the MEEKC-UV/vis system was easier to handle in terms of operation. Furthermore, high recovery rates of about 90% were obtained.

between the CE system and the ICP-MS requires addition of a sheath liquid (phosphate buffer containing 20 µg/L In), which is also used to close the electrical circuit of the CE system and to introduce an external standard in order to monitor the stability of the spraying conditions. The oxaliplatin sample was spiked with DMSO and 1-bromododecane to mark the EOF and the microemulsion droplets, respectively, and the ICP-MS was operated to record in parallel ^{195}Pt, ^{34}S and ^{79}Br, in order to detect all three sample components. Furthermore, the capacity factors for **1** and the Pt(IV) complexes **2**, **5**, **9** and **10** were determined for MEEKC-UV/vis and -ICP-MS. These compounds were chosen due to their different structures and therefore expected differing log k values. The data obtained for all compounds were found to be very similar with the two detection systems (Table 2; the small differences might be related to inaccuracies stemming from broad S and Br signals); however, **9** and **10** were not separable with the applied method. These results also prove that 1-bromododecane is a suitable but UV/vis-silent marker for the microemulsion droplets. It appears that the presence of the surfactant does not influence the ionization efficiency of the ICP-MS and the analysis is not altered by such processes.

In order to determine the LOD and LOQ for the MEEKC-UV/vis and the -ICP-MS systems, calibration curves with
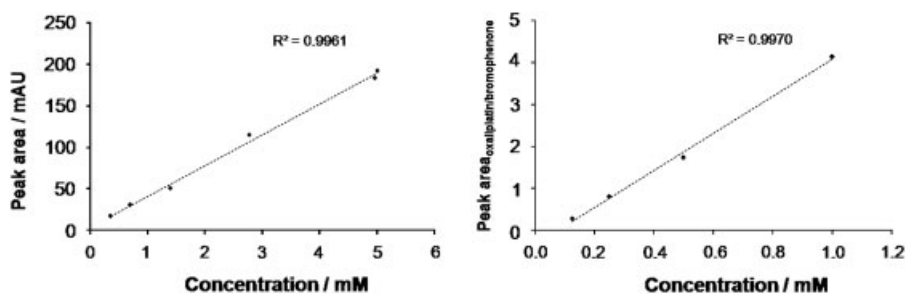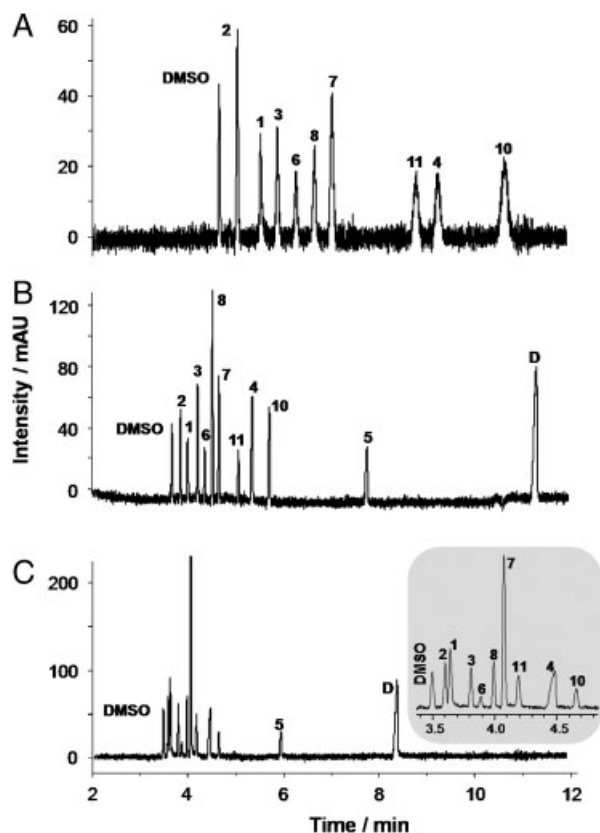
3.2 Separation of oxaliplatin and platinum(IV) complexes with MEEKC and UV/vis detection

In order to maintain the stability of the separation system, oil-in-water microemulsions require specific ratios of the respective components. These ratios can only be varied within a very narrow range and a standard microemulsion consists of approximately 90% aqueous buffer, 3% surfactant, 6% co-surfactant, and ∼1% oil [32]. The separation conditions of **1**, its Pt(IV) precursor **11** and a series of Pt(IV) anticancer drug candidates, were optimized by changing the composition of the microemulsion (Fig. 4; the differing intensities of the peaks are due to using freshly prepared sample mixtures). The microemulsion consisting of 1.44% SDS, 6.48% 1-butanol, 0.82% heptane and 91.26% phosphate buffer was identified as a good compromise (over 1.89 and 0.85% SDS in the microemulsion) between separation performance and analysis time for the separation of **1–8**, **10**

Figure 3. Calibration graph for the quantification of oxaliplatin **1** with the MEEKC-UV/vis and -ICP-MS systems.

Table 3. LOD and LOQ as determined by MEEKC-UV/vis and -ICP-MS for the anticancer drug oxaliplatin **1**

Method	CE-UV/vis	CE-ICP-MS
LOD (mM)	0.39	0.25
LOQ (mM)	1.18	0.76

Figure 5. log *k* values for **1–11** as obtained by MEEKC analysis with different microemulsion compositions ((A) 1.89% SDS, 5.94% 1-butanol, 0.59% heptane, 91.59% phosphate buffer; (B) 1.44% SDS, 6.48% 1-butanol, 0.82% heptane, 91.26% phosphate buffer; (C) 0.85% SDS, 6.68% 1-butanol, 1.06% heptane, 91.41% phosphate buffer). For all log *k* values SDs of about 5% or less were determined (*n* = 3).

In an attempt to correlate the structure of the analytes with the log *k* values, as determined from analyses with three different MEEKC systems, no clear-cut relationship was observed (Fig. 5). All MEEKC systems show the same order of migration, and the separation of the compounds in structurally related groups allows drawing the following conclusions: in the case of compounds **2–5**, the increase of lipophilicity by changing from the methyl ester to ethyl, propyl and butyl residues is clearly reflected by increasing log *k* values, as was also observed for the methyl and ethyl esters **8** and **9**. In the case of the propyl amides of the succinate **6** and glutarate **7** derivatives, the latter possesses, as expected, a more lipophilic character. Compounds **10** and **11** are difficult to compare with any of the other compounds due to their structural difference. However, the Pt(IV) precursor **11** for **1** is significantly more lipophilic than the clinically established compound.

3.3 Analysis of platinum(IV) complexes with MEEKC-ICP-MS

In order to assay the separation performance of MEEKC-ICP-MS (1.43% SDS, 91.15% phosphate buffer (10 mM, pH 7.4), 0.85% heptane, 6.57% butanol), mixtures of Pt compounds were analyzed consisting of the complexes **2–5**, **7** and **10**, varying only in the aliphatic ester functionality and with widely differing log *k* values in the MEEKC-UV/vis experiment (Fig. 6). Peak tailing leading to partial peak overlapping, possibly caused by the dilution of the sample in the CE-MS interface and a memory effect of the ICP-MS detection, was observed in these studies, which limits the number of compounds to be analyzed. However, the separation is sufficient to determine the log *k* values of the compounds studied on basis of these results.

Figure 4. Effect of the SDS surfactant concentration on the migration of the platinum complexes **1–8**, **10** and **11** in MEEKC-UV/vis mode (D, dodecanophenone). (A) 1.89% SDS, 5.94% 1-butanol, 0.59% heptane, 91.59% phosphate buffer; (B) 1.44% SDS, 6.48% 1-butanol, 0.82% heptane, 91.26% phosphate buffer; (C) 0.85% SDS, 6.68% 1-butanol, 1.06% heptane, 91.41% phosphate buffer.

and **11** (**9** was not added to the sample mixture due to expectable overlaps based on the log *k* determination; Fig. 5). Higher SDS concentrations resulted in a lower EOF and therefore significantly longer analysis times as well as peak broadening [41]. In contrast, lowering of the SDS concentration to 0.85% reduced the separation efficiency and lead to partially unresolved peaks. These studies have to be considered as preliminary studies with regard to the biological applications (therefore all experiments were carried out at 37°C, and the phosphate buffer was adjusted to pH 7.4), *e.g.* for the detection of oxaliplatin and its potentially orally administerable Pt(IV) precursor in biological tissue.
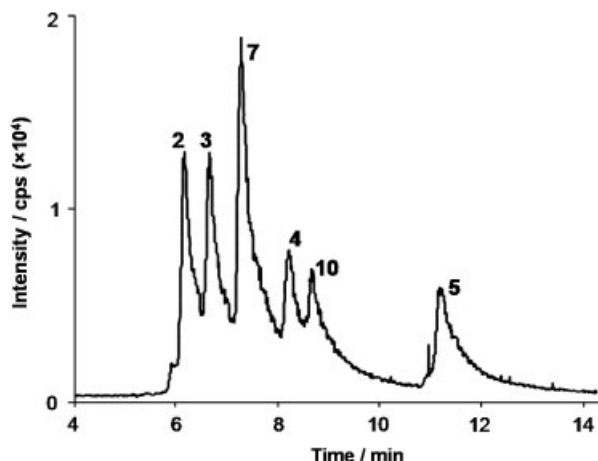
Figure 6. Electropherogram obtained by MEEKC-ICP-MS for the separation of **2–5, 7** and **10** by monitoring the ^{195}Pt trace.

4 Concluding remarks

MEEKC was found to be an efficient separation system for the analysis of Pt(II) and Pt(IV) anticancer agents, which were assigned according to the migration times (both with UV/vis and ICP-MS detection). The application of MEEKC was for a long time limited in the choice of detectors and only recently it was hyphenated to MS detectors with atmospheric pressure photo ionization. In this article, the coupling of MEEKC with the element-specific ICP-MS is presented for the first time. The high selectivity and sensitivity of the ICP-MS was used to detect in parallel the platinum compounds and the EOF and microemulsion droplet markers DMSO and 1-bromododecane, respectively. Initial performance tests revealed slightly higher sensitivity of the ICP-MS system as compared with UV/vis, which in addition suffers from unspecificity, especially when analyzing clinical samples with complex matrix. However, MEEKC-UV/vis was the more stable system in terms of operation; high linearity of the calibration curve was obtained without addition of internal standards. An advantage of the ICP-MS technology is that UV/vis-silent compounds (such as 1-bromododecane) can be detected without prior derivatization.

When comparing the lipophilicity of the Pt compounds, a clear-cut trend is only observable as long as minor structural changes are made, *e.g.* from methyl **2** to ethyl **3**, propyl **4** and butyl esters **5**. To establish a more general rule, a broader series of compounds is required. Additionally, further studies on the correlation of octanol–water coefficients, a widely used indicator for the distribution of a drug within an organism, with the log k values obtained by ICP-MS detection are desirable and would broaden the area of application of the method.

5 References

[1] Schmitt-Kopplin, P., Englmann, M., *Electrophoresis* 2005, *26*, 1209–1220.

[2] Gaspar, A., Englmann, M., Fekete, A., Harir, M., Schmitt-Kopplin, P., *Electrophoresis* 2008, *29*, 66–79.

[3] Klampfl, C. W., Buchberger, W., *Anal. Bioanal. Chem.* 2007, *388*, 533–536.

[4] Schmitt-Kopplin, P., *Electrophoresis* 2009, *30*, 1609.

[5] Klampfl, C. W., *Electrophoresis* 2006, *27*, 3–34.

[6] Jakupec, M. A., Galanski, M., Arion, V. B., Hartinger, C. G., Keppler, B. K., *Dalton Trans.* 2008, 183–194.

[7] Galanski, M., Arion, V. B., Jakupec, M. A., Keppler, B. K., *Curr. Pharm. Des.* 2003, *9*, 2078–2089.

[8] Reedijk, J., *Chem. Rev.* 1999, *99*, 2499–2510.

[9] Hall, M. D., Mellor, H. R., Callaghan, R., Hambley, T. W., *J. Med. Chem.* 2007, *50*, 3403–3411.

[10] Galanski, M., Jakupec, M. A., Keppler, B. K., *Curr. Med. Chem.* 2005, *12*, 2075–2094.

[11] Reithofer, M., Galanski, M., Roller, A., Keppler, B. K., *Eur. J. Inorg. Chem.* 2006, 2612–2617.

[12] Reithofer, M. R., Valiahdi, S. M., Jakupec, M. A., Arion, V. B., Egger, A., Galanski, M., Keppler, B. K., *J. Med. Chem.* 2007, *50*, 6692–6699.

[13] Reithofer, M. R., Schwarzinger, A., Valiahdi, S. M., Galanski, M., Jakupec, M. A., Keppler, B. K., *J. Inorg. Biochem.* 2008, *102*, 2072–2077.

[14] Hartinger, C. G., Timerbaev, A. R., Keppler, B. K., *Electrophoresis* 2003, *24*, 2023–2037.

[15] Timerbaev, A. R., Hartinger, C. G., Keppler, B. K., *Trends Anal. Chem.* 2006, *25*, 868–875.

[16] Hartinger, C. G., Keppler, B. K., *Electrophoresis* 2007, *28*, 3436–3446.

[17] Timerbaev, A. R., Hartinger, C. G., Aleksenko, S. S., Keppler, B. K., *Chem. Rev.* 2006, *106*, 2224–2248.

[18] Groessl, M., Reisner, E., Hartinger, C. G., Eichinger, R., Semenova, O., Timerbaev, A. R., Jakupec, M. A., Arion, V. B., Keppler, B. K., *J. Med. Chem.* 2007, *50*, 2185–2193.

[19] Groessl, M., Hartinger, C. G., Polec-Pawlak, K., Jarosz, M., Dyson, P. J., Keppler, B. K., *Chem. Biodiversity* 2008, *5*, 1609–1614.

[20] Groessl, M., Hartinger, C. G., Polec-Pawlak, K., Jarosz, M., Keppler, B. K., *Electrophoresis* 2008, *29*, 2224–2232.

[21] Groessl, M., Bytzek, A., Hartinger, C. G., *Electrophoresis* 2009, *30*, 2720–2727.

[22] Bytzek, A. K., Enyedy, É. A., Kiss, T., Keppler, B. K., Hartinger, C. G., *Electrophoresis* 2009, in press.

[23] Groessl, M., Hartinger, C. G., Dyson, P. J., Keppler, B. K., *J. Inorg. Biochem.* 2008, *102*, 1060–1065.

[24] Polec-Pawlak, K., Abramski, J. K., Semenova, O., Hartinger, C. G., Timerbaev, A. R., Keppler, B. K., Jarosz, M., *Electrophoresis* 2006, *27*, 1128–1135.

[25] Bettmer, J., Montes Bayon, M., Ruiz Encinar, J., Fernandez Sanchez, M. L., Fernandez de la Campa, M. d. R., Sanz Medel, A., *J. Proteomics* 2009, *72*, 989–1005.

[26] Sun, X., Tsang, C.-N., Sun, H., *Metallomics* 2009, *1*, 25–31.

[27] Schluga, P., Hartinger, C. G., Egger, A., Reisner, E., Galanski, M., Jakupec, M. A., Keppler, B. K., *Dalton Trans.* 2006, 1796–1802.

[28] Egger, A., Arion, V. B., Reisner, E., Cebrian-Losantos, B., Shova, S., Trettenhahn, G., Keppler, B. K., *Inorg. Chem.* 2005, *44*, 122–132.

[29] Jung, Y., Lippard, S. J., *Chem. Rev.* 2007, *107*, 1387–1407.

[30] Mahuzier, P.-E., Aurora Prado, M. S., Clark, B. J., Kedor-Hackmann, E. R. M., Altria, K. D., *LC-GC Eur.* 2003, *16*, 22–29.

[31] Rappel, C., Galanski, M., Yasemi, A., Habala, L., Keppler, B. K., *Electrophoresis* 2005, *26*, 878–884.

[32] Altria, K. D., Mahuzier, P.-E., Clark, B. J., *Electrophoresis* 2003, *24*, 315–324.

[33] Schaumlöffel, D., Prange, A., *Fresenius J. Anal. Chem.* 1999, *364*, 452–456.

[34] Habala, L., Galanski, M., Yasemi, A., Nazarov, A. A., von Keyserlingk, N. G., Keppler, B. K., *Eur. J. Med. Chem.* 2005, *40*, 1149–1155.

[35] Ryan, R., Donegan, S., Power, J., McEvoy, E., Altria, K., *Electrophoresis* 2009, *30*, 65–82.

[36] Robb, D. B., Covey, T. R., Bruins, A. P., *Anal. Chem.* 2000, *72*, 3653–3659.

[37] Schappler, J., Guillarme, D., Rudaz, S., Veuthey, J.-L., *Electrophoresis* 2008, *29*, 11–19.

[38] Himmelsbach, M., Haunschmidt, M., Buchberger, W., Klampfl, C. W., *J. Chromatogr. A* 2007, *1159*, 58–62.

[39] Himmelsbach, M., Haunschmidt, M., Buchberger, W., Klampfl, C. W., *Anal. Chem.* 2007, *79*, 1564–1568.

[40] Ishihama, Y., Oda, Y., Uchikawa, K., Asakawa, N., *Anal. Chem.* 1995, *67*, 1588–1595.

[41] Klotz, W. L., Schure, M. R., Foley, J. P., *J. Chromatogr. A* 2001, *930*, 145–154.

3.2. Tuning of lipophilicity and cytotoxic potency by structural variation of anticancer platinum(IV) complexes

Reithofer M.R., Bytzek A.K., Valiahdi S.M., Kowol C.R., Groessl M., Hartinger C.G., Jakupec M.A., Galanski M., Keppler B.K.

Tuning of lipophilicity and cytotoxic potency by structural variation of anticancer platinum(IV) complexes

Michael R. Reithofer, Anna K. Bytzek, Seied M. Valiahdi, Christian R. Kowol, Michael Groessl, Christian G. Hartinger, Michael A. Jakupec, Markus Galanski *, Bernhard K. Keppler *

University of Vienna, Institute of Inorganic Chemistry, Waehringer Str. 42, A-1090 Vienna, Austria

ABSTRACT

A series of bis(carboxylato)dichlorido(ethane-1,2-diamine)platinum(IV) compounds with IC_{50} values ranging between 142 μM and 18 nM was investigated with respect to their lipophilicity (by the shake flask method as well as microemulsion electrokinetic chromatography), reduction potential, as well as their cellular accumulation in cancer cells in vitro. In general, the antiproliferative properties of the complexes correlated with their lipophilicity as well as their accumulation, whereas differences in antiproliferative potency could not be explained by reduction potentials since they do not vary significantly within the investigated series of compounds. Only minor effects for complexes featuring polar end groups were detected.

© 2010 Elsevier Inc. All rights reserved.

1. Introduction

The successful story of metal containing anticancer drugs started more than 40 years ago with the discovery of the antiproliferative activity of cisplatin (*cis*-diamminedichloridoplatinum(II)) by Barnett Rosenberg [1]. Besides cisplatin, two further platinum-based anticancer drugs are used routinely in the clinics today, namely carboplatin, *cis*-diammine(cyclobutane-1,1-dicarboxylato)platinum(II), and oxaliplatin, (R,R)-cyclohexane-1,2-diamine(oxalato)platinum(II) [2]. Along with the discovery of cisplatin, platinum(IV) compounds were found to act as potential anticancer drugs. In this context it is worthwhile mentioning that platinum(IV) compounds show some advantages over their platinum(II) analogs. Firstly, platinum(IV) compounds exhibit a higher coordination number (six *vs.* four) than their platinum(II) counterparts, and therefore the fine-tuning of pharmacologically important properties such as kinetic stability, lipophilicity and reduction potential can be performed more easily [3]. Secondly, platinum(IV) compounds are kinetically inert compared to platinum(II) complexes, which puts forth the possibility of oral drug administration [4,5]. The first platinum(IV) anticancer drugs which were investigated in clinical trials, tetraplatin and iproplatin (Fig. 1), were both abandoned, because of unfavorable pharmacological properties.

In the case of tetraplatin, the toxicity was too high [6], whereas iproplatin was found to be not active enough [7]. In this context it has to be mentioned that platinum(IV) compounds act as prodrugs, whereby the biologically more active platinum(II) species is obtained *via* reduction of its platinum(IV) analog (activation by reduction) [5,8]. Thus the different biological activity of tetraplatin and iproplatin (systemic toxicity *vs.* low efficacy) can be explained based on their reduction potentials. The use of chloride as axial ligands results in a high reduction potential (tetraplatin: $E_p = -90 \pm 20$ mV *vs.* Ag/AgCl) [9], therefore tetraplatin is reduced easily in the blood within seconds. Complexes having axial hydroxido ligands display a much lower reduction potential (iproplatin: $E_p = -730 \pm 100$ mV *vs.* Ag/AgCl), therefore reduction to the active platinum(II) compound is slow in the body and as a result, the compounds are not properly activated.

A breakthrough was achieved with the carboxylation of *trans*-dihydroxidoplatinum(IV) compounds, resulting in bis(carboxylato)platinum(IV) analogs, which showed a reduction potential situated between compounds with either chlorido or hydroxido axial ligands. So far, two bis(carboxylato)platinum(IV) compounds, namely satraplatin, (OC-6-43)-bis(acetato)amminedichlorido(cyclohexylamine)platinum(IV) (formerly JM216) and LA-12, (OC-6-43)-bis(acetato)adamantylamine(ammine)dichloridoplatinum(IV) (Fig. 1), have been investigated in clinical trials. Satraplatin was investigated in advanced phase III clinical trials in hormone refractory prostate cancer in combination with prednisone [10], and is currently in a phase II trial against non-small cell lung carcinoma. The satraplatin derivative LA-12 has finished phase I clinical trials and has shown promising *in vivo* activity in ADJ/PC6 plasmacytoma and A2780 ovarian carcinoma tumor mice [11–13].

Recently, platinum(IV) chemistry has made considerable progress due to a new carboxylation method. The use of succinic, maleic, glutaric,
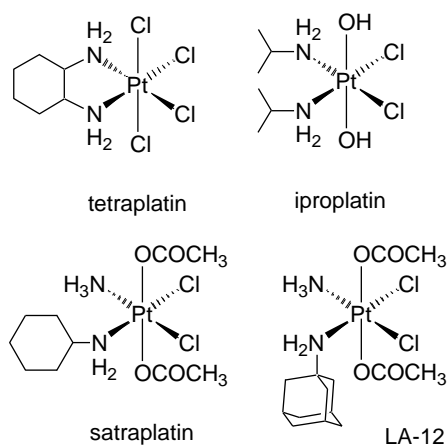

Fig. 1. Chemical structures of tetraplatin, iproplatin, satraplatin and LA-12.

or phthalic anhydride as carboxylation agents [14–19] resulted in bis(carboxylato)platinum(IV) complexes, displaying two free and unco-ordinated carboxylic acid groups, therefore opening up the possibility for further functionalization of the axial ligands. Derivatization of the axial ligands is of great importance, when taking into account, that these ligands are released during the activation of the platinum(IV) complex in the body. A specific targeting of established platinum(II) drugs (*e.g.* cisplatin) *via* their platinum(IV) analogs seems now promising, since a derivatization of the equatorial ligands is no longer necessary [20–22].

Recently, we reported on the synthesis, characterization and cytotoxicity of a series of bis(carboxylato)platinum(IV) complexes with exceptionally high antiproliferative properties using succinic and glutaric anhydride as carboxylation agents [17–19]. Further derivati-zation was performed using amines and alcohols, which resulted in formation of the corresponding amides or esters, respectively. With the aim of gaining a deeper insight into the mechanism of action and in order to understand the structure–activity relationships and to optimize the effects achievable with this class of compounds, we determined the lipophilicity, the reduction potential as well as the cellular accumulation of the respective platinum(IV) complexes and compared them with their cytotoxic properties.

2. Experimental section

2.1. Compounds and reagents

The platinum(IV) complexes were synthesized following a published procedure [17–19]. Sodium dodecyl sulfate (SDS), dodeca-nophenone, 1-butanol and sodium monohydrogenphosphate were purchased from Sigma-Aldrich (Vienna, Austria). Sodium hydroxide solution (0.1 M), hydrochloric acid, and heptane sodium dihydrogen-phosphate were obtained from Fluka (Buchs, Switzerland) and DMSO was from Fisher Scientific. High purity water used throughout this work was obtained from a Millipore Synergy 185 UV Ultrapure Water system (Molsheim, France).

2.2. Electrochemistry

Cyclic voltammograms were measured in a three-electrode cell using a 2.0 mm-diameter glassy carbon disc working electrode, a platinum auxiliary electrode, and a Ag|Ag$^+$ reference electrode containing 0.10 M AgNO$_3$, the potential of which was corrected using an internal standard of ferrocenium/ferrocene. Measurements were performed at room temperature using an EG & G PARC 273A potentiostat/galvanostat. Deaeration of solutions was accomplished by passing a stream of argon through the solution for 5 min prior to the measurement and then maintaining a blanket atmosphere of

argon over the solution during the measurement. The potentials were measured at a scan rate of 100 mV s^{-1} in 0.20 M [n-Bu$_4$N][BF$_4$]/DMF (dimethylformamide), using [Fe(η^5-C$_5$H$_5$)$_2$] (E$_{1/2}$ = +0.72 V *vs.* NHE) [23] as the internal standard, and were quoted relative to the normal hydrogen electrode (NHE).

2.3. log k determination

The log k values were determined by MEEKC (microemulsion electrokinetic chromatography) carried out with an HP^{3D} CE system (Agilent, Waldbronn, Germany) equipped with an on-column diode-array detector. Detection was carried out by UV at 200 nm. For all measurements, capillaries of 48.5 cm total length (40 cm effective length; 50 μm ID) were used (Polymicro Technologies, Phoenix, AZ, USA). Capillary and sample tray were thermostatted at 37 °C. The sample injection was carried out by hydrodynamic injection at 10 mbar for 15 s and the separation voltage was 25 kV. New capillaries were conditioned with 0.1 M HCl, water, 0.1 M NaOH, and again with water (10 min each). As a daily routine, the capillary was flushed with 0.1 M NaOH, water, and BGE (background electrolyte) for 5 min each before the first run. Before each injection, the capillary was purged with 0.1 M NaOH, water and the BGE for 2 min each.

The microemulsion was prepared using the following component ratios (wt.%) to establish a stable microemulsion: 91.26% sodium phosphate buffer (20 mM, pH 7.4), 0.82% heptane, 1.44% SDS, and 6.48% 1-butanol. For the preparation of the MEEKC solutions, surfactant, alcohol, oil, and a small portion of buffer were mixed by ultrasonication for 5 min. The residual buffer was then slowly added to the mixture. Afterwards, the solution was let to stand for 30 min at the room temperature before use.

The analytes were dissolved in the microemulsion to give concentrations between 0.45 and 0.6 mg/ml. DMSO and dodecano-phenone were used as markers for the EOF (electroosmotic flow) and the microemulsion droplets, respectively: to 1 ml of the sample solution 1 μl DMSO and 10 μl dodecanophenone (18 mg/ml in methanol) were added.

The retention factor, k, is defined as the ratio n$_{me}$/n$_{aq}$ (n$_{me}$ = total number of moles of the solute in the microemulsion phase, and n$_{aq}$ = total number of moles of the solute in the aqueous phase) and this mass distribution coefficient can be calculated according to Eq. (1) [t$_o$ = migration time of an unretained substance (EOF marker), t$_{me}$ = migration time of the microemulsion, and t$_R$ = solute migration time].

$$k = \frac{t_R - t_0}{t_0 \left(1 - \frac{t_R}{t_{me}}\right)} \tag{1}$$

2.4. log P determination

For the log P determination, the guidelines for the shake flask method described recently in Ref. [24] were slightly modified. Weighted amounts of platinum complexes were dissolved in HPLC-grade water, which was pre-saturated with octanol, and mixed by sonication for 5 min. Afterwards, the solutions were centrifuged for 5 min and the concentration of Pt was determined by ICP-MS (inductively coupled plasma-mass spectrometry). Weighted amounts of that solutions were mixed with the same volume of octanol and shaken for 15 min. After phase separation, the Pt concentration in the aqueous phase was again determined by ICP-MS and the partition coefficients were calculated.

The platinum content in the aqueous phase was determined by ICP-MS (Agilent 7500ce, Waldbronn, Germany), equipped with a CETAC ASX-520 autosampler (Neuss, Germany), a Scott double pass spray chamber, and a MicroMist nebulizer. For the analysis, the samples were diluted 1:1000 with 2.5% HCl. Every sample contained 0.5 ppb In as the internal standard (CPI International, Santa Rosa, CA, USA).

2.5. Cellular accumulation

SW480 cells (colon carcinoma, human) were kindly provided by Brigitte Marian (Institute of Cancer Research, Department of Medicine I, Medical University of Vienna, Austria). Cells were grown in 75 cm^2 culture flasks (Iwaki/Asahi Technoglass) as adherent monolayer cultures in complete culture medium, i.e., minimal essential medium (MEM) supplemented with 10% heat-inactivated fetal bovine serum, 1 mM sodium pyruvate, 4 mM L-glutamine, and 1% non-essential amino acids (100×) (all purchased from Sigma-Aldrich Austria) without antibiotics. Cultures were maintained at 37 °C in a humidified atmosphere containing 5% CO$_2$ and 95% air. For cellular accumulation experiments, exponentially growing cells were harvested from culture flasks by trypsinization and seeded in complete culture medium in densities of 3×10^5 cells/well in 6-well plates (3 plates per substance). Corresponding adsorption blanks were located on the same plate. Cells were allowed to settle and resume adherent characteristics for 24 h at 37 °C. Then, 0.278 ml/well of 10× solutions of the test compounds were added, followed by incubation for 2 h at 37 °C. In the meantime, the cell number was determined in 3 wells, and the average cell number per well was calculated. After exposure, the medium was removed completely and wells were washed twice with PBS, followed by solubilization of cells by addition of 0.5 ml/well of subboiled HNO$_3$ for >1 h. Subsequently, aliquots of 400 μl/well were transferred into 15 ml polypropylene tubes, filled to a total volume of 8 ml with Milli-Q water and internally standardized with In (0.5 ppb). The amount of Pt was determined by ICP-MS (Agilent 7500ce, Waldbronn, Germany), equipped with a CETAC ASX-520 autosampler (Neuss, Germany), a Scott double pass spray chamber, and a MicroMist nebulizer, at a sample delivery rate of approx. 0.25 ml per min. Platinum and indium standards were obtained from CPI International (Amsterdam, The Netherlands). The instrument was tuned with a solution containing 1 ppb each of lithium, yttrium, cerium, thallium, and cobalt in 2% HNO$_3$ (Agilent Technologies, Vienna, Austria).

3. Results and discussion

Bis(carboxylato)Pt(IV) compounds are among the most promising platinum-based drug candidates for the treatment of cancer. In order to rationalize the observed cytotoxic activity of a series of Pt(IV) complexes reported recently, the compounds were evaluated with regard to their lipophilicity, redox potentials, in vitro antiproliferative properties, and cellular accumulation. For these studies, a series of nine bis(carboxylato)platinum(IV) complexes (Fig. 2) was chosen that covers a broad range of cytotoxicity and lipophilicity [17–19].
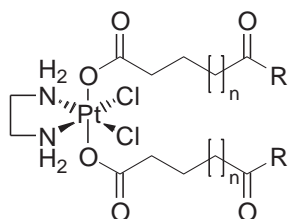
1	n = 0,	R = OH
2	n = 0,	R = OCH$_3$
3	n = 0,	R = OC$_2$H$_5$
4	n = 1,	R = OC$_2$H$_5$
5	n = 0,	R = OC$_3$H$_7$
6	n = 0,	R = OC$_4$H$_9$
7	n = 0,	R = NHC$_2$H$_4$OH
8	n = 0,	R = NHC$_3$H$_7$
9	n = 0,	R = NH(cyclopentyl)

Fig. 2. Chemical structures of dichlorido(ethane-1,2-diamine)platinum(IV) complexes.

The complexes feature ethane-1,2-diamine and chloride as equatorial ligands and either succinate (Fig. 2, n = 0) or glutarate (n = 1) esters and amides in axial positions.

3.1. log P and log k determination

A good estimate for a drug's ability to accumulate in (cancer) cells is its lipophilicity, which is generally expressed by the octanol–water partition coefficient, log P, and a number of direct and indirect methods can be applied for its determination. An electrokinetic chromatography method used in determining the lipophilicity is microemulsion electrokinetic chromatography (MEEKC) [25,26]. The separation in MEEKC occurs not only due to the electrophoretic mobility of the analytes but is also based on their hydrophobic interaction with microemulsion droplets. The migration times of the analytes in comparison to those of the electroosmotic flow (EOF) and microemulsion droplet markers can be used to calculate capacity factors as a measure of the lipophilicity. Additionally, log P values were determined using the traditional shake flask method [24]. log k and log P values of complexes **2–9** are listed in Table 1. Complex **1** equipped with a carboxylic acid functionality could not be included in the investigations, since its lipophilicity is dependent on the pH value.

Correlating the MEEKC data with the chemical structures of compounds **2–6** bearing ester moieties, it appears that with the length of the alkyl ester group, the lipophilicity as expressed by the capacity factors increases (compound **4** is a special case with an additional methylene group separating the dicarboxylic acid functionalities, being situated in terms of capacity factor between **3** and **5**; order of lipophilicity: **2**<**3**<**4**<**5**<**6**).

In the case of amides the situation is a bit more complicated since the structures of terminal groups vary significantly. Complex **7** with the hydroxyethyl moiety showed the smallest capacity factor and it was also the least lipophilic compound (of both ester and amide series). Increased lipophilicity was found for the propyl (**8**) and the cyclopentylamine (**9**) derivatives, respectively.

The shake flask method yielding the log P values for the compounds drew a similar picture as observed by the MEEKC method. Correlation of capacity factors with octanol–water partition coefficients of the ester derivatives (**2–6**), resulted in a linear dependency ($R^2 = 0.99089$, Fig. 3), showing that, within this class of complexes, the methods are complementary to each other.

3.2. Electrochemistry

Since platinum(IV) compounds act as prodrugs (activation by reduction), the reduction potential is an important pharmacological parameter to estimate the reactivity/activity of the drugs. When the reduction potential is high (*e.g.* tetraplatin: $E_p = -90 \pm 20$ mV *vs.* Ag/AgCl or $+110 \pm 20$ mV *vs.* NHE) [9] reduction occurs rather fast in the blood, resulting in a number of severe side effects as in the case of tetraplatin. On the other hand, if the reduction potential is too low (iproplatin: $E_p = -730 \pm 100$ mV *vs.* Ag/AgCl or -530 ± 100 mV *vs.* NHE), the drug is not reduced fast enough in the body and is excreted

Table 1
log P values determined *via* the shake flask method and log k values obtained by MEEKC measurements.

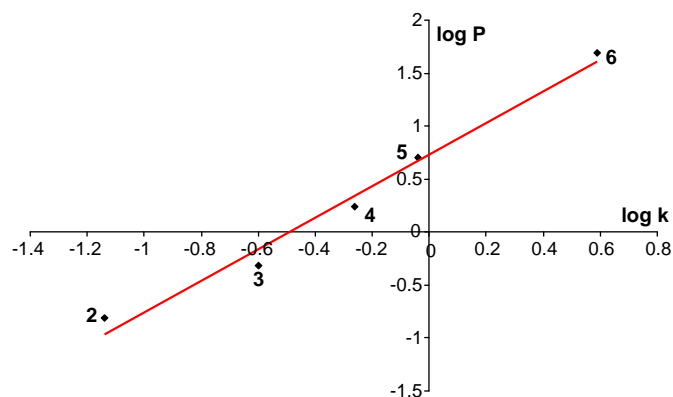|	Complex	log k	log P
Ester derivatives	**2**	−1.14	−0.81 ± 0.02
	3	−0.60	−0.32 ± 0.01
	4	−0.26	0.24 ± 0.01
	5	−0.04	0.70 ± 0.01
	6	0.59	1.69 ± 0.02
Amide derivatives	**7**	−1.94	−1.45
	8	−0.47	−0.43 ± 0.04
	9	0.09	0.61 ± 0.03

Fig. 3. Plot of log P values, obtained *via* the shake flask method, *vs.* log k derived from MEEKC experiments for ester derivates **2**, **3**, **4**, **5**, and **6**.

intact to a significant amount. As delineated earlier, the differences in the reduction potential are the consequence of different axial ligands (chlorido *vs.* hydroxido). Thus, to reach a balance of an appropriate (medium-scale) degree of reactivity, a change of the axial ligands to *e.g.* carboxylate, resulting in complexes with an intermediate reduction potential, is required.

All compounds were investigated by cyclic voltammetry in DMF solution at a scan rate of 100 mV s^{-1} using 0.20 M [n-Bu$_4$N][BF$_4$] as supporting electrolyte. Since the solubility of these compounds was too low in water, DMF was the solvent of choice (stability for several days was demonstrated by ^{1}H-NMR spectroscopy). The cyclic voltammogram displayed only one irreversible reduction peak corresponding to Pt$^{IV/II}$ reduction (Fig. 4), which is common for Pt(IV) compounds. This fact can be explained by loss of the axial ligands, which results in a change of the coordination geometry (octahedral *vs.* square planar). Reduction potentials of all compounds are given in Table 2. With the exception of compounds **1** and **7**, the reduction potentials of all other compounds are very similar (Table 2). Thus, the chain length of the carboxylato ligand does not influence the reduction potential. However, a polar end group (COOH in **1** and CH$_2$OH in **7**) leads to an increase in the reduction potential by about 0.07 V.

3.3. Cytotoxicity

The cytotoxicity of all compounds was determined in four different cell lines, representing both, cisplatin sensitive (CH1, HeLa) and cisplatin resistant (SW480, SK-OV-3) cancer cells, yielding the IC$_{50}$ values listed in Table 3 [18,19]. Generally, there is a fairly good inverse correlation between IC$_{50}$ and log P values (the more lipophilic a complex, the lower its IC$_{50}$ values). This correlation is particularly strong within the series of ester derivatives featuring the succinate residue (**2**, **3**, **5**, and **6**) and within the series of amide complexes (**7**, **8**, and **9**).
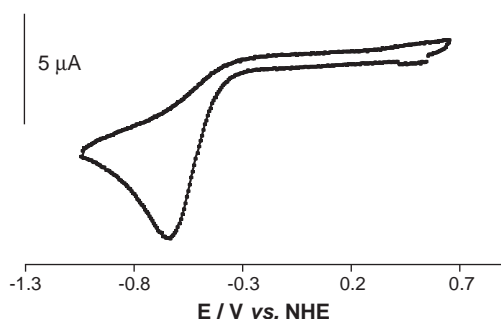

Fig. 4. Cyclic voltammogram of **6** in DMF containing 0.20 M [n-Bu$_4$N][BF$_4$] at a scan rate of 0.10 V s^{-1} using a glassy carbon working electrode.

Table 2
Summary of the electrochemical data.

	Functional group	Compound	E$_p$/Pt^{IV}→Pt^{II}
Amide derivatives	COOH	**1**	−0.56
	CH$_2$OH	**7**	−0.56
	–	**8**	−0.63
Ester derivatives	–	**9**	−0.63
	–	**2**	−0.65
	–	**3**	−0.65
	–	**4**	−0.65
	–	**5**	−0.63
	–	**6**	−0.64

Potentials in V ± 0.02 *vs.* NHE measured at a scan rate of 100 mV s^{-1} in 0.20 M [n-Bu$_4$N][BF$_4$]/DMF.

As expected, the methylester derivative **2** is the least cytotoxic of the ester derivatives, whereas the butylester derivative **6** shows the highest cytotoxicity in all four cell lines. In the case of complex **4** (containing a glutarate instead of a succinate moiety), the lipophilicity is intermediate between those of complexes **3** and **5**, but its cytotoxic properties, in particular in the more sensitive CH1 and HeLa cells, are lower than might be expected on the basis of lipophilicity (Fig. 5). Therefore, it may be argued that an ethyl spacer is more favorable for cytotoxicity than a propyl spacer.

Taking into account the small changes in the reduction potentials of **1**–**9**, cytotoxicity obviously depends mainly on the lipophilic properties of the complexes, which should reflect in different extents of cellular accumulation. Consequently, cellular platinum accumulation in one of the cell lines was investigated.

3.4. Cellular accumulation

Cellular platinum content upon 2 h of exposure of SW480 cells to the complexes could be quantified by ICP-MS in all cases. Values vary within two orders of magnitude from 4.9 fg Pt/cell (**7**) to 541 fg Pt/cell (**6**) (Table 3). Assuming an average cell volume of ca. 4200 μm^3 (corresponding to the mean diameter of ca. 20 μm measured for suspended SW480 cells), these values suggest that **6** and **5**, the compounds that are taken up to the highest extent, may even have been accumulated (about 660 μM and 240 μM, respectively, according to this calculation) beyond the extracellular concentration (50 μM) within the short exposure time of 2 h.

Plotting IC$_{50}$ values of all complexes against cellular accumulation in the same cell line yields an approximately hyperbolic correlation, which can roughly be linearized by logarithmic transformation of both axes (Fig. 6).

Table 3
Cellular accumulation of platinum(IV) complexes upon 2 h of exposure of SW480 cells and antiproliferative activity in four human cancer cell lines. Values are means ± standard deviations obtained from at least three independent experiments.

Compound	Pt accumulation (fg/cell)	IC$_{50}$ (μM)[a]			
	SW480	SW480	CH1	HeLa	SK-OV-3
1	6.6 ± 0.2	95 ± 5	5.5 ± 2.2	14 ± 4	76 ± 17
2	19.7 ± 1.0	16 ± 1	0.68 ± 0.20	3.6 ± 1.3	17 ± 3
3	59.8 ± 3.8	4.1 ± 0.5	0.34 ± 0.11	0.68 ± 0.04	3.7 ± 1.2
4	61.7 ± 3.3	3.5 ± 0.1	1.1 ± 0.2	2.1 ± 1.0	3.7 ± 1.1
5	197.3 ± 14.0	0.63 ± 0.20	0.068 ± 0.024	0.11 ± 0.01	1.0 ± 0.3
6	541.4 ± 93.5	0.22 ± 0.08	0.018 ± 0.007	0.032 ± 0.007	0.35 ± 0.08
7	4.9 ± 0.7	142 ± 23	24 ± 3	82 ± 2	131 ± 16
8	41.3 ± 13.2	31 ± 15	2.3 ± 1.1	9.2 ± 2.0	66 ± 23
9	9.9 ± 2.2	19 ± 9	1.9 ± 0.2	2.9 ± 1.4	29 ± 5

[a] 50% inhibitory concentrations in CH1, HeLa, SW480 and SK-OV-3 cells (MTT assay, 96 h of exposure) [18,19].
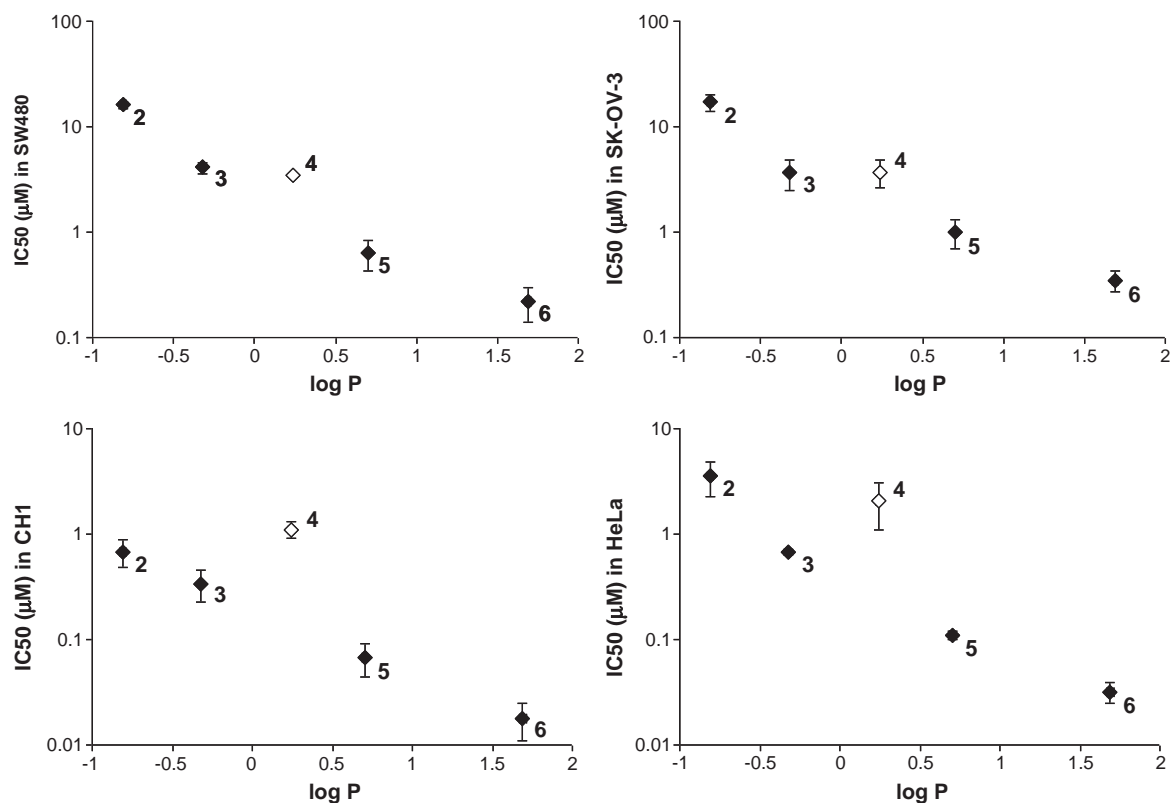
Fig. 5. Correlation of cytotoxicity (IC$_{50}$ in four human cancer cell lines) with lipophilicity (log P) of ester derivatives **2–6**. Note that compound **4** (with axial ligands derived from glutaric acid) deviates from the correlation observed for the other compounds (with axial ligands derived from succinic acid), indicating that cytotoxicity is also dependent on the position where the carbon chain of the axial ligands is elongated and not on lipophilicity alone.

The complexes **5** and **6**, which were previously identified as highly cytotoxic [19], are accumulated by the cells in the highest amounts. Thus, the strong biological effects of these compounds are most likely the consequence of their high capacity of penetrating the cell, which results from the higher chain length and lipophilicity of the ester moiety of the axial carboxylato ligands. Whereas elongation of the ester carbon chain results in an increase of both cellular accumulation and antiproliferative potency with each addition of a single methylene moiety (**2**<**3**<**5**<**6**), chain elongation by one methylene moiety between the carboxylato carbon atoms has no effect whatsoever (**3**≈**4**).

In the case of amides (**7**, **8**, and **9**), an expectedly low accumulation was found for complex **7** exhibiting a hydroxyethyl moiety. Surprisingly, the highest accumulation was observed for the propyl derivative and not for the cyclopentyl congener. In addition, the difference in accumulation is not reflected in the cytotoxicity of those

compounds. One would expect that a higher accumulation results in a higher cytotoxicity, but compound **9** displays lower IC$_{50}$ values in all tested cell lines, consistent with its high lipophilicity, even though cellular accumulation of this compound is lower than that of **8** (Table 3). However, it should be born in mind that cellular accumulation was measured after 2 h, whereas the IC$_{50}$ values were determined after 96 h of exposure time. Therefore, we cannot exclude that complex **9** is simply accumulated slower than compound **8**.

In the case of the esters (**2–6**), cellular accumulation is in good agreement with the IC$_{50}$ values and with the log P values (cellular accumulation increases with increasing lipophilicity). Each additional methylene group in the ester moiety (methyl-, ethyl-, propyl- and butylester) leads to an approximately threefold increase of cellular accumulation, which results in a significant enhancement of cytotoxicity. Since the reduction potentials of compounds **2–6** are very similar, the differences in cytotoxicity are clearly based on cellular concentrations of the complexes. Consistent with the structure–activity relationships mentioned earlier, an exception is compound **4**, which contains a propyl instead of an ethyl spacer between the carboxylic carbon atoms. Compound **3** shows almost the same cellular accumulation as compound **4**, but the IC$_{50}$ values of **3** are about three times lower in CH1 and HeLa cells than the IC$_{50}$ values of **4**, indicating that cellular accumulation cannot (just as little as reduction potential) explain why an ethyl spacer is more advantageous than a propyl spacer in terms of cytotoxic potency.

4. Conclusions

Novel Pt(IV) complexes have shown to exhibit extraordinary cytotoxic properties. In order to better understand their chemical behavior and their effect on the biological activity, a series of experiments was conducted including determination of lipophilicity, redox potentials, in vitro antiproliferative activity and cellular
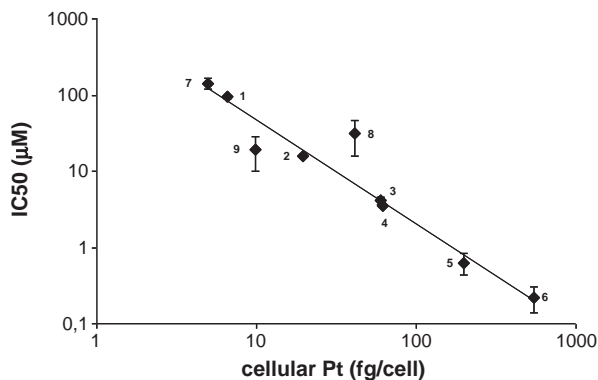

Fig. 6. Correlation of cellular accumulation of platinum(IV) complexes and their antiproliferative activity in SW480 cells.

accumulation. With the selected series of bis(carboxylato)platinum (IV) compounds, a wide range of cytotoxicity against human tumor cells (IC$_{50}$ values from nM to high μM) and lipophilicity (from relatively hydrophobic to lipophilic) was covered. The cytotoxic properties of the studied ester derivatives correlated well with the lipophilicity as well as the accumulation of the complexes in tumor cells. It appeared that the differences in cytotoxicity of the compounds are not caused by differences in reduction potentials. Future *in vivo* studies will guide us to the development of compounds with properties fitting in the ideal window of lipophilicity, toxicity and activity.

Acknowledgements

References

[1] M. Rosenberg, L. VanCamp, T. Krigas, Nature 205 (1965) 698–699.
[2] M.A. Jakupec, M. Galanski, B.K. Keppler, Rev. Physiol. Biochem. Pharmacol. 146 (2003) 1–54.
[3] M. Galanski, M.A. Jakupec, B.K. Keppler, Curr. Med. Chem. 18 (2005) 2075–2094.
[4] M.D. Hall, T.W. Hambley, Coord. Chem. Rev. 232 (2002) 49–67.
[5] M.D. Hall, R.C. Dolman, T.W. Hambley, Met. Ions Biol. Sys. 42 (2004) 297–322.
[6] R.J. Schilder, F.P. LaCreta, R.P. Perez, S.W. Johnson, J.M. Brennan, A. Rogatko, S. Nash, C. McAleer, T.C. Hamilton, D. Roby, R.C. Young, R.F. Ozols, P.J. O'Dwyer, Cancer Res. 54 (1994) 709–717.
[7] C. Trask, A. Silverstone, C.M. Ash, H. Earl, C. Irwin, A. Bakker, J.S. Tobias, R.L. Souhami, J. Clin. Oncol. 9 (1991) 1131–1137.
[8] M.D. Hall, H.R. Mellor, R. Callaghan, T.W. Hambley, J. Med. Chem. 50 (2007) 3403–3411.
[9] S. Choi, C. Filotto, M. Bisanzo, S. Delaney, D. Lagasee, J.L. Whitworth, A. Jusko, C. Li, N.A. Wood, J. Willingham, A. Schwenker, K. Spaulding, Inorg. Chem. 37 (1998) 2500–2504.
[10] C.N. Sternberg, P. Whelan, J. Hetherington, B. Paluchowska, P.H.Th.J. Slee, K. Vekemans, P. Van Erps, C. Theodore, O. Koriakine, T. Oliver, D. Lebwohl, M. Debois, A. Zurlo, L. Collette, Oncology 68 (2005) 2–9.
[11] A. Kozubik, V. Horvath, L. Svihalkova–Sindlerova, K. Soucek, J. Hofmanova, P. Sova, A. Kroutil, F. Zak, A. Mistr, J. Turanek, Biochem. Pharmacol. 69 (2005) 373–383.
[12] J. Turanek, A. Kasna, D. Zaluska, J. Neca, V. Kvardova, P. Knotigova, V. Horvath, L. Sindlerova, A. Kozubik, P. Sova, A. Kroutil, F. Zak, A. Mistr, Anti-Cancer Drugs 15 (2004) 537–543.
[13] F. Zak, J. Turanek, A. Kroutil, P. Sova, A. Mistr, A. Poulova, P. Mikolin, Z. Zak, A. Kasna, D. Zaluska, J. Neca, L. Sindlerova, A. Kozubik, J. Med. Chem. 47 (2004) 761–763.
[14] A. Alvarez-Valdes, J.M. Perez, I. Lopez-Solera, R. Lannegrand, J.M. Continente, P. Amo-Ochoa, M.J. Camazon, X. Solans, M. Font-Bardia, C. Navarro-Ranninger, J. Med. Chem. 45 (2002) 1835–1844.
[15] K.R. Barnes, A. Kutikov, S.J. Lippard, Chem. Biol. 11 (2004) 557–564.
[16] W.H. Ang, I. Khalaila, C.S. Allardyce, L. Juillerat–Jeanneret, P.J. Dyson, J. Am. Chem. Soc. 127 (2005) 1382–1383.
[17] M. Reithofer, M. Galanski, A. Roller, B.K. Keppler, Eur. J. Inorg. Chem. 13 (2006) 2612–2617.
[18] M.R. Reithofer, S.M. Valiahdi, M.A. Jakupec, V.B. Arion, A. Egger, M. Galanski, B.K. Keppler, J. Med. Chem. 50 (2007) 6692–6699.
[19] M.R. Reithofer, A. Schwarzinger, S.M. Valiahdi, M. Galanski, M.A. Jakupec, B.K. Keppler, J. Inorg. Biochem. 102 (2008) 2072–2077.
[20] R.P. Feazell, N. Nakayama-Ratchford, H. Dai, S.J. Lippard, J. Am. Chem. Soc. 129 (2007) 8438–8439.
[21] S. Mukhopadhyay, C.M. Barnes, A. Haskel, S.M. Short, K.R. Barnes, S.J. Lippard, Bioconjugate Chem. 19 (2008) 39–49.
[22] S. Dhar, F.X. Gu, R. Langer, O.C. Farokhzad, S.J. Lippard, Proc. Nat. Acad. Sci. U.S.A. 105 (2008) 17356–17361.
[23] W.C. Barette Jr., H.W. Johnson Jr., D.T. Sawyer, Anal. Chem. 56 (1984) 1890–1898.
[24] OECD Guidelines for Testing of Chemicals, 107, OECD, Paris, 1995.
[25] C. Rappel, M. Galanski, A. Yasemi, V. Habala, B.K. Keppler, Electrophoresis 26 (2005) 878–884.
[26] A.K. Bytzek, M.R. Reithofer, M. Galanski, M. Groessl, B.K. Keppler, C.G. Hartinger, Electrophoresis 31 (2010) 1144–1150.

3.3. Studies on the biodistribution of oxaliplatin and its methyl derivatives in tumor bearing mice

Bytzek A.K.,[a] Jungwirth U.,[b] Berger W.,[b] Galanski M.,[a] Hartinger C.G.,[a,c] Keppler B.K.[a,c]
Status: in preparation.

[a] University of Vienna, Institute of Inorganic Chemistry, Waehringer Str. 42, A-1090 Vienna, Austria.

[b] Medical University of Vienna, Institute of Cancer Research, Borschkegasse 8a, A-1090 Vienna, Austria.

[c] University of Vienna, Research Platform 'Translational Cancer Therapy Research', Waehringer Str. 42, A-1090 Vienna, Austria.

Introduction

A new era of chemotherapy started with the introduction of cisplatin (*cis*-[diamminedichloridoplatinum(II)]) as an anticancer drug. This Pt complex is very effective against epithelioid malignancies of ovarian, testes, head and neck, esophageal and lung [1]. Due to the serious side effects of cisplatin, carboplatin {(*SP*-4-2)-diammine[1,1-cyclobutanediicarboxylato-κ*O*(2-)]platinum(II)} was introduced in the clinic in 1981 as a second generation compound with reduced side-effects [2]. The mode of action of carboplatin is analogous to that of cisplatin and therefore they share the same spectrum of treatable cancers [3]. The last world-wide approved anticancer Pt drug is the third generation complex oxaliplatin {(*SP*-4-2)-[(*1R,2R*)-cyclohexanediamine-κ^2*N,N'*][ethanedioato(2-)-κ^2*O1,O2*]-platinum(II)}. In contrast to cisplatin and carboplatin, it has a different spectrum of activity [4] which can be explained by the formation of different DNA adducts due to the bulky cyclohexane ligand [5], and by different cellular uptake mechanisms. The accumulation of cisplatin and carboplatin in cells occurs mainly by passive diffusion but also facilitated transport plays an important role [6]. It was found that for these compounds the copper influx transporter CTR1 (copper transporter 1) can act as a transport system [7, 8]. Experiments indicated that deletion of the *Saccaromyces cerevisiae* CTR1 gene lowers accumulation, and increases resistance to cisplatin, and co-administration with copper inhibits cisplatin uptake in wild-type strains [9, 10]. The cellular uptake of oxaliplatin seems to be less dependent on CTR1 [11], but driven by passive diffusion and the human organic cation transporters (OCT) [12]. Passive diffusion is based on the concentration gradient for a drug across the cell membrane and is mainly dependent on the lipophilicity, size and charge of the compound [13]. Several studies investigated the impact of the lipophilicity of Pt-complexes on the *in vitro* anticancer activity. Thereby, higher lipophilicity of Pt complexes was frequently related to higher intracellular accumulation and lower IC$_{50}$ values [14-17]. Stewart *et al.* demonstrated that Pt accumulation is crucial for clinical efficacy. They investigated the Pt content in human autopsy samples and found that patients whose tumors responded to Pt-containing therapies had higher tumor Pt concentrations than those that failed to respond [18]. In recent years, a series of oxaliplatin derivatives were synthesized and tested on their anticancer activity. Especially oxaliplatin analogues with an additional methyl-group at the cyclohexan ring, namely KP1537 {(*SP*-4-2)-[(*1R,2R,4R*)-4-methyl-1,2-diaminecyclohexane-κ^2*N,N'*][ethanedioato(2-)-κ^2*O1,O2*]-platinum(II)} and KP1691 {(*SP*-4-2)-[(*1R,2R,4S*)-4-methyl-1,2-diaminecyclohexane-κ^2*N,N'*][ethanedioato(2-)-κ^2*O1,O2*]platinum(II)}, exhibited promising anticancer activity (Figure 1). The two oxaliplatin derivatives differ only in the orientation of the substituted alkyl group. Even though there is only this marginal difference, *in vitro* tests

indicated that the cytotoxic profile of KP1537 is similar to that of oxaliplatin, whereas KP1691 was more cytotoxic than oxaliplatin in the majority of the tested cell lines [19].
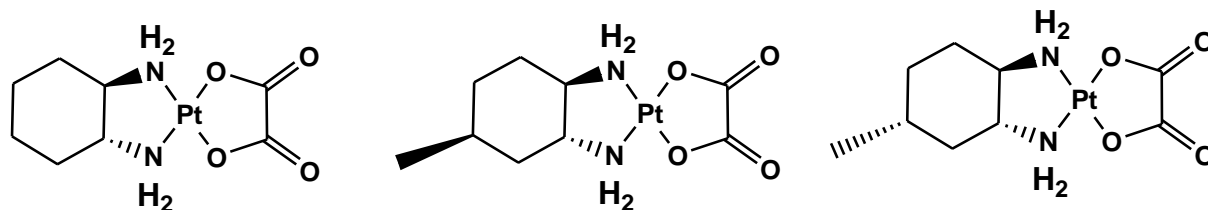

Figure 1. Chemical structures of oxaliplatin (left), KP1691 (middle) and KP1537 (right).

Interestingly, KP1537 -the in vitro less cytotoxic compound- was more active against an in vivo murine L1210 leukemia model than oxaliplatin and KP1691. First, it could be shown that KP1537 has a greater therapeutic window and can be administered at higher doses than oxaliplatin [19]. When equal doses of oxaliplatin and KP1537 were used no differences in the efficacy were seen (in accordance to the *in vitro* results). However, higher KP1537 doses, which were toxic in the case of oxaliplatin, had a superior therapeutic effect than oxaliplatin. KP1537 treatment resulted in five long-term survivors and an increase in life span of more than 200%, whereas the optimal oxaliplatin dose led to two long-term survivors and an increase in life span of 152% (Figure 2). KP1691, which was the most potent compound in the *in vitro* tests, showed an increased life span of only 122% and was less active than KP1537 and oxaliplatin. The mismatch between the *in vitro* and *in vivo* experiments on the one side and the differences in the activity between the two methyl derivatives on the other might be explained by altered transport, drug uptake and/or efflux pumps which might impact on the pharmacological characteristics of these stereoisomeric complexes *in vivo* but not *in vitro* [19].

In order to study the biodistribution of the Pt complexes *in vivo*, tumor and organ samples (brain, kidney, lung, liver and spleen) from tumor-bearing BalbC mice were analyzed for their Pt content 1 and 6 h post-treatment. As chronic neurotoxicitiy is the dose-limiting factor in oxaliplatin therapy [20, 21] the cellular uptake into the sciatic nerve was also investigated.
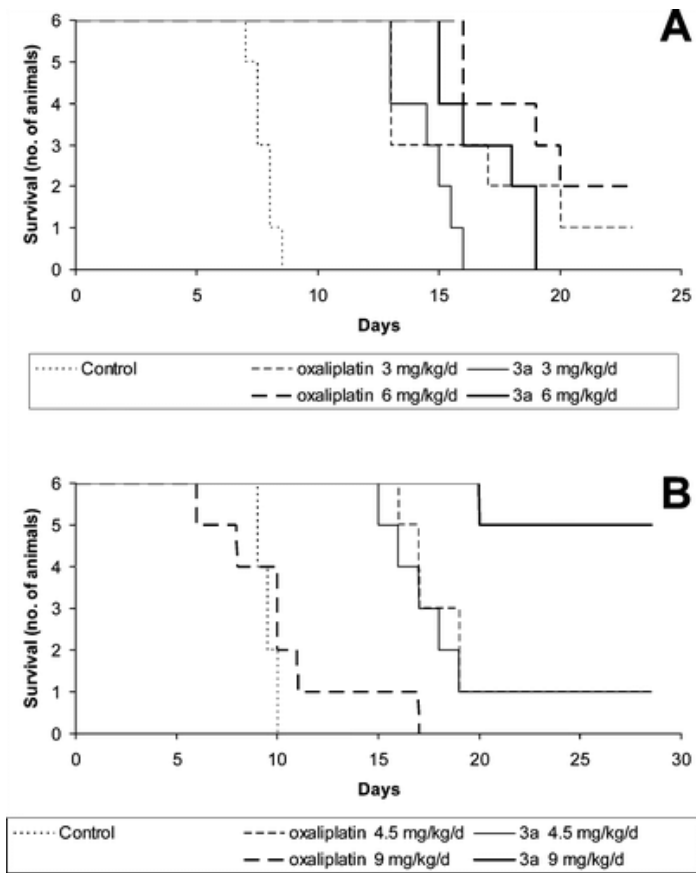
Figure 2: Kaplan-Meier plots demonstrating the survival of tumor-bearing mice treated with different doses of oxaliplatin and KP1537 in comparison to untreated controls [19].

Experimental

Animal treatment and sample preparation

The animals were kept in a pathogen-free environment and every procedure was done in a laminar airflow cabinet. The experiments were done according to the regulations of the Ethics Committee for the Care and Use of Laboratory Animals at the Medical University Vienna. 5×10^5 CT-26 cells in 50 µL serum-free RMPI medium were injected subcutaneously into the right flank of 6- to 8 weeks old female BalbC mice. Animals were randomly assigned to treatment groups and treated after one month with one intravenous bolus injection of oxaliplatin, KP1537 or KP1691 (9 mg/kg dissolved in 5% glucose). 1 or 6 h after drug application the

animals were sacrificed and blood, brain, kidney, liver, lung, sciatic nerve, spleen and tumor were collected and stored at –20 °C until microwave digestion and analysis for the Pt content.

Tumor platinum content

Instrumentation. The Pt content in the tissue was determined by ICP-MS (Agilent 7500ce, Waldbronn, Germany), equipped with a CETAC ASX-520 autosampler (Neuss, Germany), a Scott double pass spray chamber, and a MicroMist nebulizer. The ^{195}Pt and ^{115}In isotopes were recorded, the latter as internal standard. Instrument control and data analysis were carried out using Agilent ChemStation software (G1834B). The working conditions were optimized daily using a 1 µg L^{-1} tuning solution (Agilent) containing ^{7}Li, ^{89}Y and ^{205}Tl in 2% HNO$_3$. Doubly charged ions and oxide levels were minimized by using ^{140}Ce/^{70}Ce and Ce/CeO ratios and were typically < 2.5%. The instrument was calibrated daily using Pt standards of 0.5, 1, 5, 12, 23 and 30 ng Pt/mL in 3.5% HNO$_3$ spiked with 0.5 ppb In as internal standard (CPI International, Santa Rosa, CA, USA).

Sample preparation. Tissue sample aliquots of 10–35 mg were digested with 1 mL nitric acid (65% HNO$_3$ p.a. from Sigma Aldrich, further purified with a quartz sub-boiling system from Milestone-MLS GmbH, Leutkirch, Germany) and 1 mL water in a microwave system (MLS-Ethos1600, Milestone-MLS GmbH, Leutkirch, Germany). The samples were diluted with water to reach an end mass of approximately 10 g (0.5 ppb In as internal standard).

Results and Discussion

The pharmacokinetics and tissue distribution of drug compounds have a major influence on the therapeutic efficacy and adverse effects. Three groups of tumor bearing female BALB/c mice were treated either with oxaliplatin or its methyl derivatives KP1691 and KP1537 and the accumulation and biodistribution of the compounds were compared.

Tissue distribution after 1 h

One hour after administration of all three compounds, the highest Pt concentrations were found in blood. In order to study the distribution in the blood, the plasma was separated from the blood

cells by centrifugation. In the blood cells the Pt concentration was approximately 4.5 times higher than in the plasma after treatment with all three Pt complexes (Table 1). Similar observations were made for oxaliplatin by others. A high content of oxaliplatin in the blood is bound in erythrocytes which is supposed to inactivate the Pt complex [22, 23]. Mandal *et al.* investigated the oxaliplatin blood distribution of 19 colorectal cancer patients 1 and 48 h after the first infusion [24]. They found that the concentration of protein bound Pt complexes in erythrocytes did not change significantly in this time frame but the Pt levels in the plasma were reduced by about 50%, which can be attributed to drug transport, metabolism and clearance. Generally, the high affinity of Pt complexes to erythrocytes might explain the high Pt levels in lung, kidney and spleen which have a high blood supply and therefore are rich in erythrocytes. For example, the spleen is responsible for the filtration of the blood from worn-out erythrocytes. In contrast, low Pt levels were found in the brain after treatment with all three Pt complexes indicating that these compounds have a low potential to cross the blood brain barrier.

Table 1. Organ distribution of KP1691, KP1537 and oxaliplatin after 1 h in tumor bearing mice

	ng Pt / mg tissue		
compound	KP1691	KP1537	oxaliplatin
blood cells	3.43 ± 0.30	2.71 ± 0.48	2.38 ± 0.13
brain	0.05 ± 0.01	0.03 ± 0.01	0.03 ± 0.01
kidney	2.90 ± 0.02	2.49 ± 0.26	2.87 ± 0.39
liver	2.76 ± 0.36	2.28 ± 0.34	2.44 ± 0.14
lung	1.87 ± 0.15	1.78 ± 0.33	1.99 ± 0.15
plasma	0.74 ± 0.07	0.51 ± 0.10	0.62 ± 0.12
sciatic nerve	0.76 ± 0.03	0.37 ± 0.11	0.48 ± 0.05
spleen	2.64 ± 0.08	2.00 ± 0.43	2.12 ± 0.12
tumor	1.03 ± 0.02	0.78 ± 0.12	0.72 ± 0.12

When comparing the three different drugs to each other, in all analyzed tissues the highest Pt levels were found in mice treated with KP1691. The Pt tumor content in the KP1691 group was 1.03 ng Pt/mg tumor whereas the accumulation for KP1537 and oxaliplatin was similar and only 0.75 ng Pt/mg tumor. A similar picture was found in all other tissue samples.

Tissue distribution after 6 h

Tissues collected from mice sacrificed 6 h after drug administration showed for all three treatment groups the highest Pt concentrations again in kidney, liver, lung and spleen (Table 2). However, the absolute values after 6 h in comparison with the Pt content in the samples taken after 1h changed differently within the three Pt drugs. The Pt concentration in kidney, liver, lung and spleen slightly decreased in mice treated with KP1691, whereas only minor changes were found for KP1537 and a slight increase for oxaliplatin.

Table 2. Organ distribution of KP1691, KP1537 and oxaliplatin 6 h after treatment with the Pt complexes

	ng Pt / mg tissue		
compound	KP1691	KP1537	oxaliplatin
brain	0.03 ± 0.01	0.05 ± 0.02	0.06 ± 0.02
kidney	2.02 ± 0.61	2.62 ± 0.32	3.36 ± 0.51
liver	1.76 ± 0.53	2.29 ± 0.07	2.58 ± 0.52
lung	1.47 ± 0.50	1.61 ± 0.19	2.66 ± 0.94
sciatic nerve	0.39 ± 0.13	0.47 ± 0.11	0.70 ± 0.14
spleen	1.72 ± 0.56	1.78 ± 0.10	2.40 ± 0.28
tumor	0.63 ± 0.19	0.83 ± 0.02	0.99 ± 0.04

A similar trend was observed for all other tissue samples. After 6 h the highest Pt levels were found in the oxaliplatin group. Notably, the KP1691 concentration in the tumor decreased an

average by 40% whereas the Pt level after treatment with KP1537 remained constant (Figure 3). It appears as if the drug uptake and efflux are responsible for the different *in vitro* and *in vivo* anticancer activities of the investigated compounds. Furthermore, the enhanced efflux of KP1691 is most probably the reason for the lower anticancer activity *in vivo*. However, further investigations have to be performed to identify possible efflux mechanisms. Even though oxaliplatin accumulated over time to higher concentrations it was not more active in vivo and there is only a small difference to the in vivo more active KP1537. Taking into account that the uptake of oxaliplatin in the sciatic nerve is higher than for KP1537, the methyl derivative seems to be beneficial with regard to lower neurotoxicity.
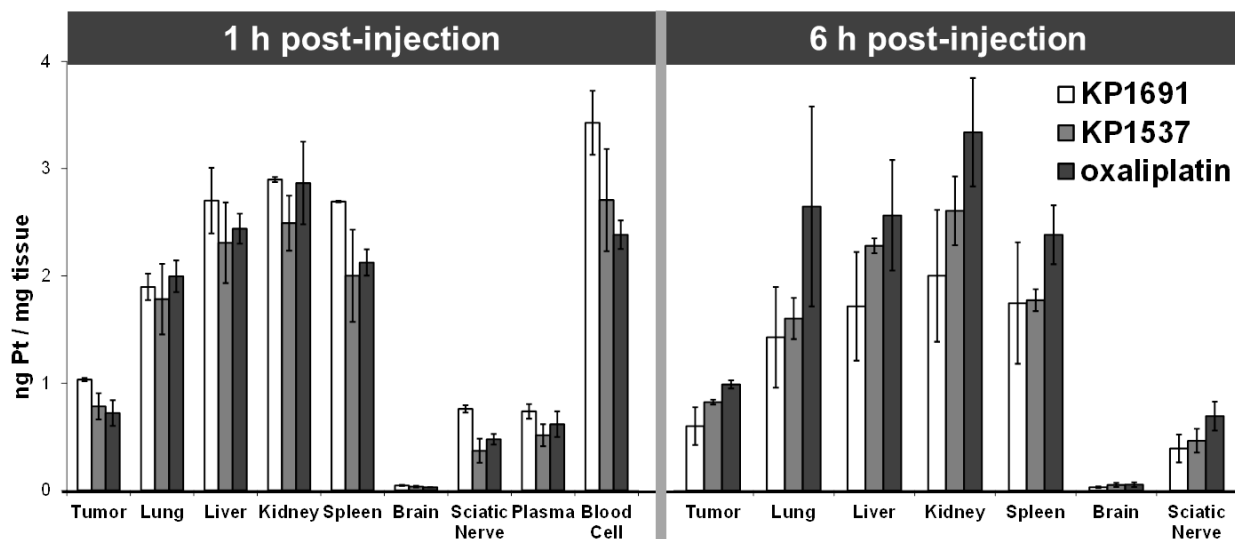
Figure 3. Pt content in tissue samples taken 1 and 6 h after intravenous administration of KP1691, KP1537 and oxaliplatin. The values are average of data from three independent experiments and the bars indicate the standard deviations.

Conclusion

In this study the biodistribution and accumulation of oxaliplatin and its methyl derivatives KP1691 and KP1537 were investigated in tumor-bearing mice. KP1691 is quickly accumulated in all analyzed tissue samples including the tumor. However, also a rather rapid efflux was detected which might explain the low anticancer activity of KP1691 observed in the L1210 murine leukemia model as compared to KP1537 and oxaliplatin [19]. In the same L1210 murine

leukemia model no differences in the anticancer activity between oxaliplatin and KP1537 were found when used at equal doses. A similar trend was observed in this study on the biodistribution of these two complexes; 6 h after administration the Pt tumor content in the KP1537 group was similar to that of oxaliplatin. Interestingly, KP1537 levels did not change between 1 and 6 h post-injection taken samples, whereas in the oxaliplatin group a slight increase was seen. Future studies should include long-term and repeated drug treatment groups to see if the Pt tumor levels for KP1537 and oxaliplatin remain similar or whether differences are found. Considering that neurotoxicity is a central problem of clinical application of oxaliplatin, the lower accumulation of KP1537 in the sciatic nerve makes it a promising drug for further (pre)clinical development.

Acknowledgment

References

1. T. Boulikas and M. Vougiouka, *Recent clinical trials using cisplatin, carboplatin and their combination chemotherapy drugs (Review).* Oncology Reports, 2004. **11**(3): p. 559-595.
2. F. M. Muggia, *Overview of Carboplatin - Replacing, Complementing, and Extending the Therapeutic Horizons of Cisplatin.* Seminars in Oncology, 1989. **16**(2): p. 7-13.
3. E. R. Jamieson and S. J. Lippard, *Structure, recognition, and processing of cisplatin-DNA adducts.* Chemical Reviews, 1999. **99**(9): p. 2467-2498.
4. O. Rixe, *Oxaliplatin, tetraplatin, cisplatin and carboplatin: the spectrum of activity in drug-resistant cell lines and in the cell lines of the National Cancer Institute's Anticancer Drug Screen panel.* Biochem. Pharmacol., 1996. **52**: p. 1855-1865.
5. B. Spingler, D. A. Whittington, and S. J. Lippard, *2.4 A crystal structure of an oxaliplatin 1,2-d(GpG) intrastrand cross-link in a DNA dodecamer duplex.* Inorg. Chem., 2001. **40**: p. 5596-5602.
6. M. D. Hall, et al., *The Role of Cellular Accumulation in Determining Sensitivity to Platinum-Based Chemotherapy.* Annu. Rev. Pharmacol.Toxicol., 2008. **48**: p. 495-535.
7. R. Safaei, *Role of copper transporters in the uptake and efflux of platinum containing drugs.* Cancer Letters, 2006. **234**(1): p. 34-39.
8. R. Safaei and S. B. Howell, *Copper transporters regulate the cellular pharmacology and sensitivity to Pt drugs.* Critical Reviews in Oncology Hematology, 2005. **53**(1): p. 13-23.

9.   S. Ishida, et al., *Uptake of the anticancer drug cisplatin mediated by the copper transporter Ctr1 in yeast and mammals.* Proceedings of the National Academy of Sciences of the United States of America, 2002. **99**(22): p. 14298-14302.

10.   X. J. Lin, et al., *The copper transporter CTR1 regulates cisplatin uptake in Saccharomyces cerevisiae.* Molecular Pharmacology, 2002. **62**(5): p. 1154-1159.

11.   G. Samimi and S. B. Howell, *Modulation of the cellular pharmacology of JM118, the major metabolite of satraplatin, by copper influx and efflux transporters.* Cancer Chemotherapy and Pharmacology, 2006. **57**(6): p. 781-788.

12.   S. Zhang, et al., *Organic cation transporters are determinants of oxaliplatin cytotoxicity.* Cancer Research, 2006. **66**(17): p. 8847-8857.

13.   S. Chillistone and J. Hardman, *Factors affecting drug absorption and distribution.* Anaesthesia and Intensive Care Medicine, 2008. **9**(4): p. 167-171.

14.   M. R. Reithofer, et al., *Tuning of lipophilicity and cytotoxic potency by structural variation of anticacer platinum(IV)complexes.* Journal of Inorganic Bichemistry, 2011. **105**(1): p. 46-51.

15.   S. P. Oldfield, M. D. Hall, and J. A. Platts, *Calculation of Lipophilicity of a Large, Diverse Dataset of Anticancer Platinum Complexes and relation to Cellular Uptake.* J. Med. Chem., 2007. **50**: p. 5227-5237.

16.   R. Song, et al., *Synthesis and cytotoxicity of new platinum (IV) complexes of mixed carboxylates.* J. Inorg. Biochem., 2003. **96**: p. 339-345.

17.   J. A. Platts, et al., *Meolecular and statistical modeling of reduction peak potentail and lipophilicity of platinum(IV) complexes.* J. Biol. Inorg. Chem., 2011. **16**: p. 361-372.

18.   D. J. Stewart, et al., *Platinum Concentrations in Human Autopsy Tumor Samples.* American Journal of Clinical Oncology-Cancer Clinical Trials, 1988. **11**(2): p. 152-158.

19.   S. A. Abramkin, et al., *{(1R,2R,4R)-4-methyl-1,2-cyclohexanediamine}oxalatoplatinum(II): a novel enantiomerically pure oxaliplatin derivative showing improved anticancer activity in vivo.* J Med Chem, 2010. **53**(20): p. 7356-64.

20.   L. Gamelin, et al., *Prevention of oxaliplatin-related neurotoxicity by calcium and magnesium infusions: A retrospective study of 161 patients receiving oxaliplatin combined with 5-fluorouracil and leucovorin for advanced colorectal cancer.* Clinical Cancer Research, 2004. **10**(12): p. 4055-4061.

21.   M. W. Saif and J. Reardon, *Management of oxaliplatin-induced peripheral neuropathy.* Therapeutics and Clinical Risk Management, 2005. **1**(4): p. 249-258.

22.   Ϥ. Π. Delord, et al., *Population pharmacokinetics of oxaliplatin.* Cancer Chemotherapy and Pharmacology, 2003. **51**(2): p. 127-131.

23.   T. Falta, et al., *Quantification of cisplatin, carboplatin and oxaliplatin in spiked human plasma samples by ICP-SFMS and hydrophilic interaction liquid chromatography (HILIC) combined with ICP-MS detection.* J. Anal. At. Spectrom., 2009. **24**: p. 1336-1342.

24.   R. Mandal, M. B. Sawyer, and X. F. Li, *Mass spectrometry study of hemoglobin-oxaliplatin complexes in colorectal cancer patients and potential association with chemotherapeutic responses.* Rapid Commun.Mass Spectrom., 2006. **20**(17): p. 2533-2538.

3.4. LC- and CZE-ICP-MS approaches for the *in vivo* analysis of the anticancer drug candidate sodium *trans*-[tetrachloridobis(1*H*-indazole)ruthenate(III)] (KP1339) in mouse plasma

Bytzek A.K.,[a] Boeck K.,[b] Hann S.,[b] Herman G.,[b] Keppler B.K.,[a,c] Hartinger C.G.,[a,c] Koellensperger G.[b]

Status: submitted to **Metallomics**

[a] University of Vienna, Institute of Inorganic Chemistry, Waehringer Str. 42, A-1090 Vienna, Austria.

[b] University of Natural Resources and Applied Life Sciences, Muthgasse 18, A-1180 Vienna, Austria.

[c] University of Vienna, Research Platform 'Translational Cancer Therapy Research', Waehringer Str. 42, A-1090 Vienna, Austria.
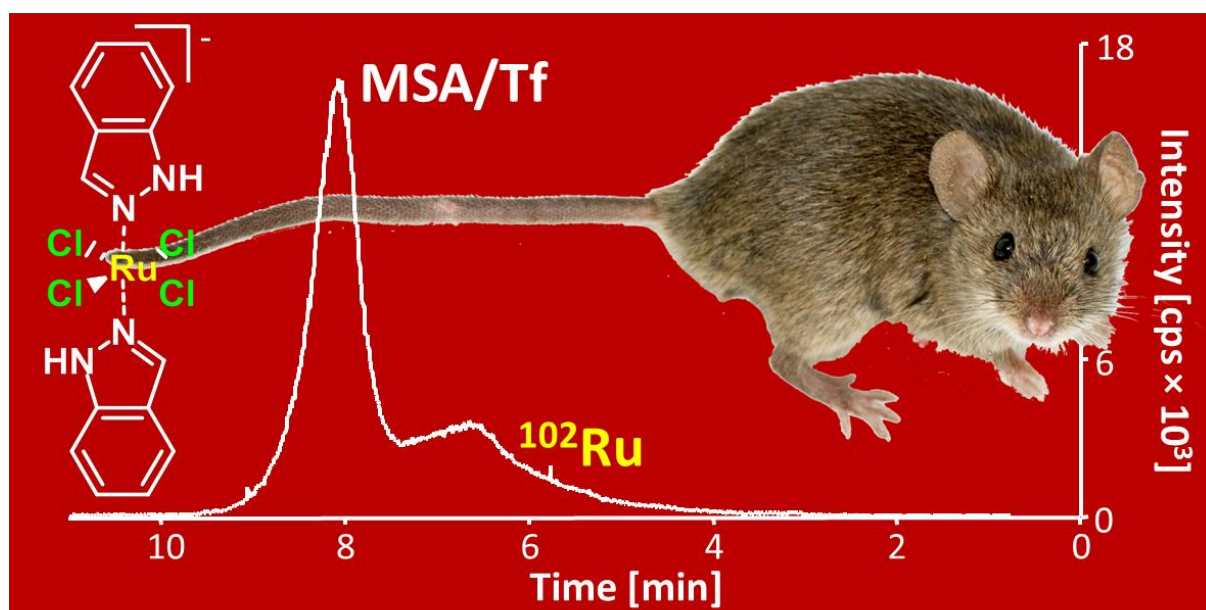
Abstract

The ruthenium-indazole complexes are promising anticancer agents undergoing clinical trials. KP1339 is administered intravenously (*i.v.*), where serum proteins are the first available biological binding partners. In order to gain a better insight into the mode of action, mice were treated with different doses of KP1339 *i.v.* and sacrificed at different time points. The blood serum was isolated from blood samples and analyzed by capillary zone electrophoresis (CZE) and size exclusion/anion exchange chromatography (SEC-IC) both combined online to inductively coupled plasma-mass spectrometry (ICP-MS). The performance of the analytical methodology was compared and the interaction of KP1339 with mouse plasma proteins characterized *in vivo*. Interestingly, the samples of the mice treated with 50 mg/kg and terminated after 24 h showed a by 2- to 2.5-fold lowered albumin content and increased formation of albumin aggregates as compared to the untreated control group and the 40 mg/kg group. The majority of Ru was bound to albumin and the stoichiometry of the KP1339 protein binding was determined through the molar Ru/S ratio. In general, good agreement of the data obtained with both techniques was achieved and the SEC-IC method was found to be more sensitive as compared to the CZE–ICP-MS approach. However, the latter benefits from shorter analysis time and lower sample consumption.

Introduction

Ruthenium compounds have become the best developed representatives of the non-platinum complexes with anticancer activity.[1-9] So far the two octahedral ruthenium(III) complexes indazolium *trans*-[tetrachloridobis(1*H*-indazole)ruthenate(III)] (KP1019; Figure 1) and imidazolium *trans*-[tetrachlorido(*S*-dimethylsulfoxide)(1*H*-imidazole)ruthenate(III)] (NAMI-A; Figure 1) have been tested in clinical phase I trials.[3,6,10,11] Only very moderate toxicities were observed in the case of KP1019,[3,6,11] and for NAMI-A blister formation was dose-limiting.[10]

In preclinical studies, KP1019 was found to be active against primary tumors and metastases in animal models, *e.g.*, in an autochthonous colorectal carcinoma of the rat which resembles colon cancer of humans,[11,12] whereas NAMI-A was shown to inhibit the metastasizing process.[13,14] In addition, the activity of KP1019 was investigated against more than 50 primary explanted human tumors, a model that has high predictability for the clinical situation,[15,16] showing activity

in more than 80% of the tumor models. These ruthenium(III) complexes are thought to have a distinct mode of action from platinum complexes[17,18] with DNA being not the primary target but interaction with proteins was demonstrated.[19] This behavior might also contribute to the low toxicity and side effects of such species, as does the "activation by reduction", *i.e.*, Ru(III) coordination compounds are thought to be activated in the tumor tissue by reduction under hypoxic conditions.[17,18,20,21]
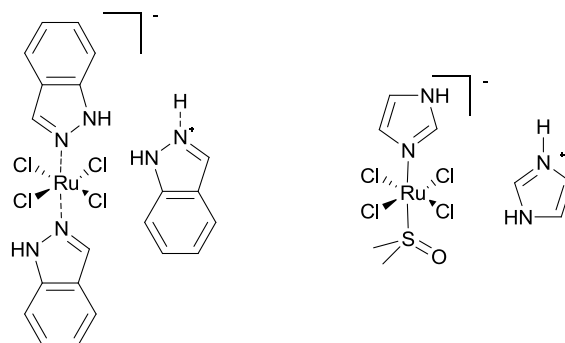

Figure 1. The structures of the two Ru[III] complexes in clinical trials: KP1019 (left) and NAMI-A (right).

The high affinity of the Ru[III] compounds to proteins, in particular to transferrin, was thought to play a major role in the uptake into cells *in vitro*,[22,23] and the distribution and transport to the tumor *in vivo*.[19,24-28] However, the main fraction of the Ru compound was found attached to human serum albumin in *in vitro* and *in vivo* samples and was estimated to be > 99% of the total Ru content.[26,27,29] The binding of the ruthenium compound to albumin was considered as a form of storage, as also hypothesized for cisplatin.[30]

The limitation in the application of KP1019 in the clinic was the low solubility and therefore the maximum tolerated dose was not reachable in clinical trials.[31] In an approach to obtain a compound with high water solubility, the indazolium counterion in KP1019 was replaced by sodium (KP1339).[3,6] With regard to the mode of action, a comparative study on the protein binding behavior of KP1019 and KP1339 revealed similar properties in terms of binding kinetics.[32]

The adduct formation of metal complexes with proteins was studied by several methods, including spectroscopic and separation methods (for recent reviews see refs. 19,33). Hyphenated liquid chromatography- (LC) and capillary zone electrophoresis-inductively-coupled plasma mass spectrometry (CZE–ICP-MS) methods were applied for the quantification of the

protein loading,[26,34-41] based on the metal-to-sulfur ratio as determined by ICP-MS as sensitive and element-specific detector.

Herein, we report the method development for characterization of the *in vivo* protein binding of the Ru anticancer compound KP1339 by LC– and CZE–ICP-MS and a comparison of these techniques with regard to detection and quantification limits. Data gained by means of the developed methods for the analysis of blood samples obtained from mice treated with KP1339 are presented.

Experimental

Mouse samples

KP1339 was administered *i.v.* to nude BALB/c mice (3 per group) in single doses of 40 (M40), 50 (M50) and 60 (M60) mg/kg and compared to the control (M0). When signs of terminal toxicity appeared, the experimental animals were terminated (control and M40-7: 7 days; M40-1: 1 day; M50-1: 1 day, M60-1: 1 day) and blood samples were taken. The collected blood was added to heparin-containing Eppendorf tubes and centrifuged (2500 rpm for 5 min). The obtained plasma was stored at -20 °C until analysis.

Sample preparation

Microwave-assisted digestion (MLS-1200-Microwave, MLS GmbH, Leutkirchen, Germany) was performed to mineralize the plasma samples for determination of total Ru concentration *via* ICP-MS. Therefore 20 mg plasma aliquots were digested according to the microwave user instructions. The digested samples were filled up with water to reach an end mass of 10 g. For the analysis, the samples were diluted 1 : 2.

For the elemental quantification by flow injection (FI)–ICP-MS and elemental speciation by SEC–ICP-MS the samples were diluted 1 : 20. For the 2D-SEC-IC–ICP-MS determination a dilution factor of 10 was applied. Calibration of metal-to-sulfur ratios was performed using FI of inorganic ruthenium and sulfur standards (Merck, Germany).

For CZE–ICP-MS, four sets of standards (incubated for 3 h at 37 °C in 10 mM phosphate buffer containing 100 mM NaCl at pH 7.4, in order to simulate physiological conditions) at molar KP1339/HSA ratios of 0.5, 1, 2 and 3 were utilized for calibration. The concentration of HSA

was kept constant at 100 µM. The *in vivo* samples were diluted 1 : 3 with the incubation buffer before analysis.

For protein fractionation, the plasma samples M0 and M60-1 were defrosted and diluted 1 : 10 with 20 mM Tris buffer containing 150 mM NaCl at pH 7.3. Prior to MS analysis, the fractions were lyophilized and redissolved in 10 µL water.

The samples for MALDI-MS were prepared using the dried droplet method with freshly prepared sinapinic acid (10 mg/mL in acetontrile/H_2O/trifluoroacetic acid = 50/50/0.1) as matrix. The protein samples and matrix were mixed 1 : 5 v/v and a 1 µL aliquot of the mixture was loaded onto the stainless steel MALDI target. The procedure was repeated three times.

LC–ICP-DRC-MS

The metal-free chromatographic system consisted of an AS 50 autosampler (including a custom made temperature control device), the ICS-3000 DP Dual pump system and the Chromeleon Chromatography Management System (Version 6.40), all from Dionex (Sunnyvale, California, USA). Injected samples were filtered in-line using a 0.45 µm PEEK filter located in front of the columns. The ICP-MS sample introduction system consisted of a PFA-nebulizer (CPI International, Amsterdam, Netherlands) and a cyclonic spray chamber. The ICP-MS used was a quadrupole-based system equipped with a dynamic reaction cell (ELAN DRC-II, PE SCIEX, Ontario, Canada) and oxygen (purity 4.5, Linde Gas GmbH, Vienna, Austria) was used as reaction gas.

Size exclusion chromatographic separation was achieved using a BioSuite[TM] 125 column (300 × 4.6 mm UHR SEC, 4 µm particle diameter) from Waters (Milford, Massachusetts, USA). The SEC eluent, containing 150 mM NaCl and 20 mM Tris-HCl, pH 7.4, was delivered at a flow rate of 350 µL·min^{-1}. A TSK-DEAE-NPR column (particle diameter 2.5 µm, TOSOH Bioscience GmbH, Stuttgart, Germany) made of PEEK (30 × 2 mm, Grom Chromatography GmbH, Rottenburg-Hailfingen, Germany) was used for anion exchange chromatography. The mobile phase was delivered by a gradient pump at a flow rate of 0.35 mL min^{-1} and consisted of water (A), 150 mM NaCl + 20 mM Tris, pH 7.4 (B) and 500 mM NaCl + 20 mM Tris, pH 7.4 (C). The initial composition was A/B 80/20, linear gradient elution was started simultaneously to switching of the transfer valve and ran to 100% C within 10 min. A more detailed description of the SEC-IC–ICP-MS experimental set-up is given elsewhere.[26] ICP-MS operation parameter are summarized in Table 1.

Table 1. ICP-MS operational parameters

Parameter	LC–ICP-DRC-MS	CZE–ICP- MS
Nebulizer	PFA nebulizer	CETAC CEI-100 microconcentric nebulizer
Spray chamber	Cyclon	-
Nebulizer gas flow, L min^{-1}	1.0	1.14
Auxiliary gas flow, L min^{-1}	1.275	0.4
Plasma gas flow, L min^{-1}	15	15
ICP RF power, W	1300	1500
O$_2$ flow rate, mL min^{-1}	0.8	-
RPQ	0.3 (SO), 0.6 (Ru)	-
Measured isotopes	^{48}SO, ^{101}Ru, ^{102}Ru	^{34}S, ^{72}Ge, ^{101}Ru, ^{102}Ru
Scan mode	Peak hopping	-
Sampler	Ni (0.1 mm orifice)	
Skimmer	Ni (0.4 mm orifice)	

CZE–ICP-MS

CZE experiments were performed with an HP^{3D} CE system (Agilent, Waldbronn, Germany) interfaced to an Agilent 7500ce ICP-MS with a CETAC CEI-100 microconcentric nebulizer. Capillaries of 60 cm total length (75 μm ID) were used (Polymicro Technologies, Phoenix, AZ, USA) for all experiments. Capillary and sample tray were thermostatted at 37 °C. Injections were performed by applying a pressure of 25 mbar for 4 s, and a constant voltage of -20 kV. Prior to the first use, the capillary was flushed at 1 bar with 0.1 M HCl, water, 0.1 M NaOH and again with water (10 min each). After this treatment the capillary was coated modifying the procedure described by Kelly *et al.* by subsequently rinsing with 1% PB solution containing 3v/v% ethylene glycol for 30 min at 50 mbar and water for 15 min at 1 bar.[42] Before each injection, the capillary was purged for 3 min both with water and the background electrolyte (BGE; 50 mM formic acid). The operational values for the CZE–ICP-MS analyses are shown in Table 1. The nebulizer was employed in self-aspiration mode with the sheath liquid (50 mM

formic acid with 20 ppb Ge) closing the electrical circuit and spraying a fine aerosol. Analyses were only started if a sufficiently stable signal (RSD ^{72}Ge < 5%) was attained.

SEC fractionation and subsequent LC-ESI-TOFMS and MALDI-MS analysis

The samples were fractionated with a Dionex Ultimate 3000 system. The size exclusion column for the separation was a Waters Biosuite 125 4 µm UHR SEC, 4.6 × 300 mm. The conditions were set to a flow rate of 350 µl min^{-1} of 20 mM Tris buffer containing 150 mM NaCl at pH 7.3. After a pre-run the collection, windows were set to collect fractions A (6.2–7.0 min), B (7.0–7.8 min), C (7.8–8.6 min) and D (8.6–9.4 min). The compounds were detected by UV spectroscopy at 215, 254 and 280 nm.

The analysis *via* LC-ESI-TOF-MS was carried out on an Agilent 6210 TOF-MS in combination with an Agilent 1200 SERIES HPLC system (Agilent, Waldbronn, Germany). The reversed phase column for the separation was an Ascentis Express C18 HPLC (Sigma Aldrich, Bellefonte, USA; column dimensions: 2.1 × 50mm). The injection volume was 2 µL of the collected fractions and the flow rate was set to 600 µL min^{-1}. Gradient elution was implemented starting with an aqueous phase containing 0.1% formic acid and 5% acetonitrile. The acetonitrile concentration was increased to 60% within 5 min followed by a further increase to 80% within 2 min. Afterwards the column was re-equilibrated within 2 min.

MALDI MS analyses were performed on an AXIMA-LNR instrument (Shimadzu Biotech-Kratos Analytical, Manchester, UK). The AXIMA-LNR was equipped with a pulsed nitrogen laser with a wavelength of 337 nm and a pulse width (FWHM) of about 4 ns and an integrated 1 GHz recorder. Analysis of the proteins was performed in linear mode with positive ionization at an acceleration voltage of 20 kV. Mass spectra were acquired by averaging 100 single laser shots and the spectra were recorded in the range from 30000 to 150000 *m/z*. For data processing and acquisition Kratos software version 2.3.5 was used.

Results and Discussion

In order to study the plasma protein distribution of the Ru compound KP1339 in an *in vivo* setup, three groups of mice were treated with the pharmaceutical formulation of 40 (M40), and 50 mg/kg (M50) and the data was compared to an untreated control group. The mice were sacrificed after 1 d (M40-1, M50-1) or after 7 days (M40-7). Plasma was obtained from the collected blood samples and the total Ru content in the M40-1 and M50-1 mouse blood plasma was determined by flow injection ICP-MS to be much higher than in M40-7 (Table 2). This was expectable based on results collected during a pharmacokinetic study accompanying a clinical phase I trial for the structurally related bis(indazole)-ruthenium compound KP1019.[31,43] The data were cross-validated with data obtained after microwave assisted digestion and the results are in good agreement.

Table 2. Total Ru concentrations in plasma.

Mouse	Dose	Time	µg Ru / g plasma
M40-1a	40 mg/kg	1d	22
M40-1b			28
M40-1c			20
M40-7a	40 mg/kg	7d	1.1
M40-7b			1.4
M40-7c			1.8
M50-1a	50 mg/kg	1d	23
M50-1b			22
M50-1c			22

LC–ICP-MS

In a semiquantitative determination of albumin using size exclusion chromatography (SEC)–ICP-MS monitoring of the ^{48}SO trace (Figure 2), the amount of protein in the 60–80 kDa fraction of the M50-1 plasma (22 ± 6 g/L), which contains mainly albumin (and *ca.* 5% transferrin), was

estimated to be lowered by 2–2.5 times, as compared to the untreated control (54 ± 1 g/L) and the M40-1 (47 ± 7 g/L) and M40-7 mouse plasma samples (44 ± 4 g/L). The concentration of protein was determined using inorganic sulfur standards for external calibration by flow injection or by employing HSA standards. Both approaches proved to be valid, revealing comparable results, but the use of albumin or drug-albumin adducts in SEC–ICP-MS and SEC-IC–ICP-MS allowed omitting the extra flow injection step in the analytical work flow.
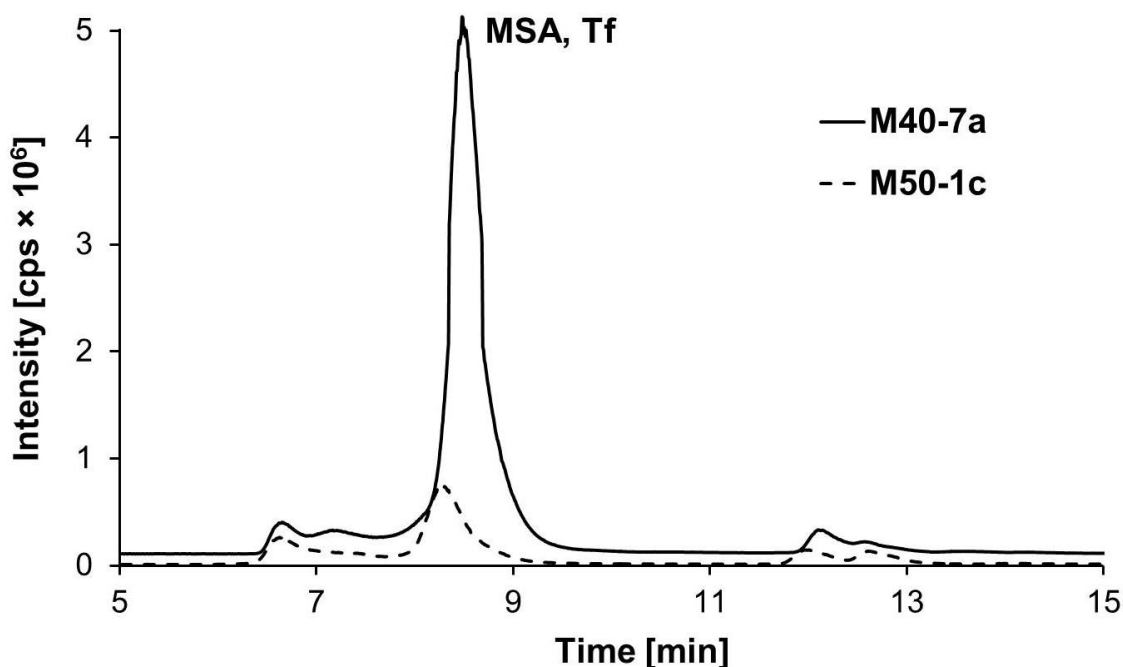

Figure 2. SEC-ICP-MS analysis (^{48}SO traces) of mouse plasma samples M40-7a and M50-1c ; The peak at 8 min represented the 60-80 kDa fraction containing the transporter proteins Tf, transferrin; and MSA, mouse serum albumin.

All mouse plasma samples contained as major component the protein fraction constituted primarily by albumin. However, at a dosage of 50 mg/kg KP1339, SEC-ICP-MS measurement revealed significantly changed relative distribution of the proteins (given by the sulfur peaks). At this dosage, not only a decrease in albumin content (peak at 8 min) along with a decrease of total protein content was observed in the mouse plasma, but also a shift towards higher molecular weight species. Two protein fractions increased to about 15% each, namely a fraction of proteins eluting at the size exclusion limit of the used SEC column corresponding to protein sizes > 150 kDa, and a fraction corresponding to 100–130 kDa proteins. Size ladder

experiments had shown that immunoglobulin and ferritin would elute at the time of the first SEC fraction. The latter fraction could represent an albumin dimer, since the peak was also found in albumin standards. Figure 3 shows the relative distribution of the three serum protein SEC fractions. At a dose of 40 mg/kg KP1339, the protein distribution was similar within the standard uncertainty, independent of the time of termination of the experiment.
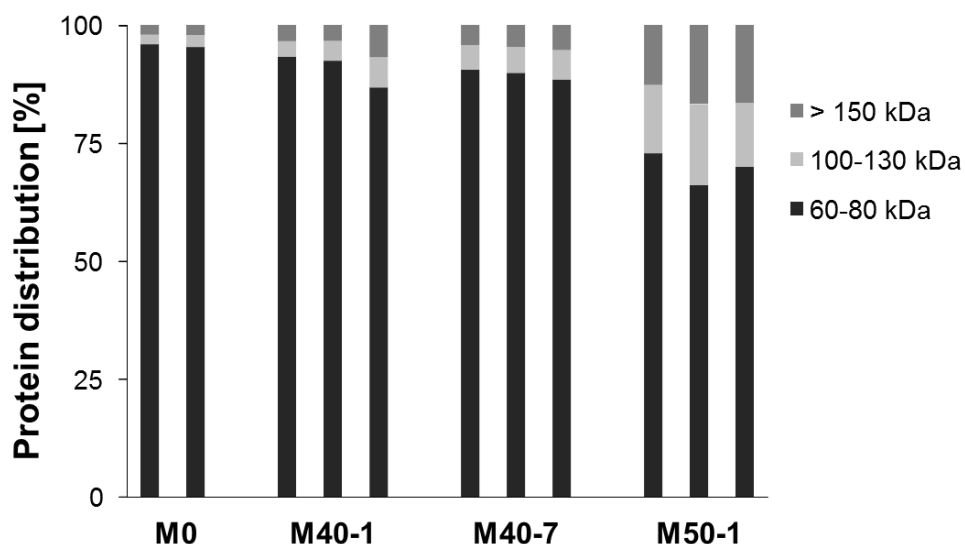

Figure 3. Changes in the relative protein distribution found in the plasma samples M40-1, M40-7 and M50-1 as compared to the control group M0.

Ru analysis by SEC–ICP-MS revealed that the decreased protein concentration and the changed serum protein distribution were related to an altered KP1339 protein binding pattern upon dosage increase from 40 to 50 mg/kg (Figure 4). Whereas in the case of the M40 mouse plasma samples the vast majority of the Ru was attached to 60-80 kDa fraction (90–95%), a broader distribution was found in the M50-1 group: the majority was still found at the albumin/transferrin fraction (*ca.* 60%), followed by a pronounced adduct formation with proteins > 100 kDa. The recovery rates for Ru with the used SEC column were satisfying ranging at 70%, whereas albumin is recovered quantitatively (tested with albumin standards).[44] For the mouse plasma samples M40-7, the concentration of Ru found attached to plasma proteins was significantly lower than in the M50-1 and M40-1 samples. This fact was in agreement to the data obtained by total Ru quantification of the plasma samples (Table 2) and expectable considering the longer time for *in vivo* processing of the protein adducts.
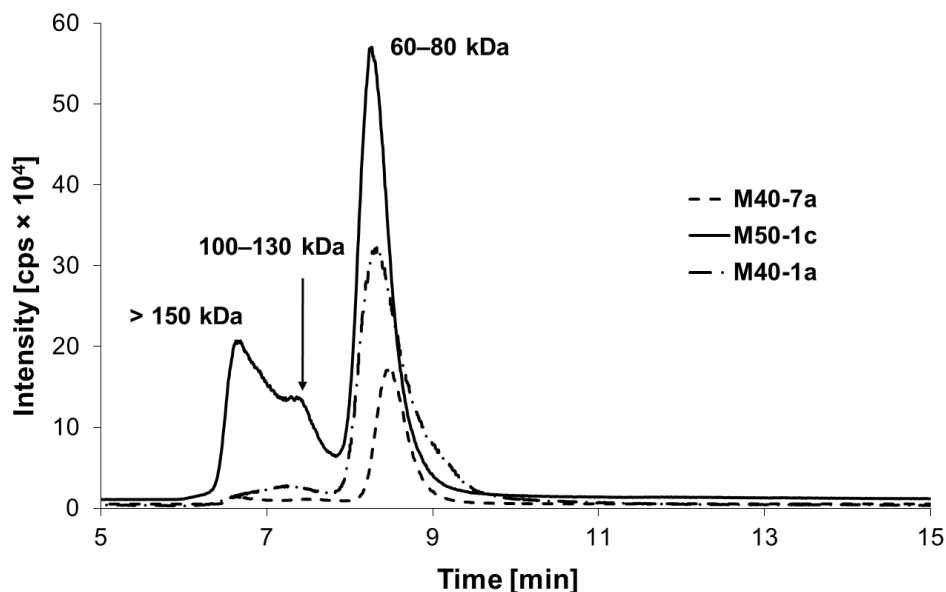
Figure 4. [101]Ru traces recorded by SEC–ICP-MS for mouse plasma samples M40-1a, M40-7a and M50-1c.

One possible explanation for these observations could be the agglomeration of serum albumin at KP1339 concentrations exceeding a certain dosage. Therefore experiments were carried out aiming at the characterization of the formed higher molecular weight species assumed to be agglomerated albumin-drug adducts. For this purpose an automated off-line SEC fraction collection was implemented. Samples of mice treated with a single dose of 50 and 60 mg/kg were investigated and sacrificed after 1 day. Figure 5 shows the SEC fractions, which were collected and subsequently analyzed by SEC-ICP-MS to confirm the quality of the fractionation, and by LC-TOF-MS and MALDI-MS to determine the molar masses of the proteins present in the collected fraction. As can be seen in Figure 5, the M60-1 sample contains a higher content of MSA agglomerates as compared to the M50-1 case (compare Figure 4), but no differences in the albumin fraction were observed.
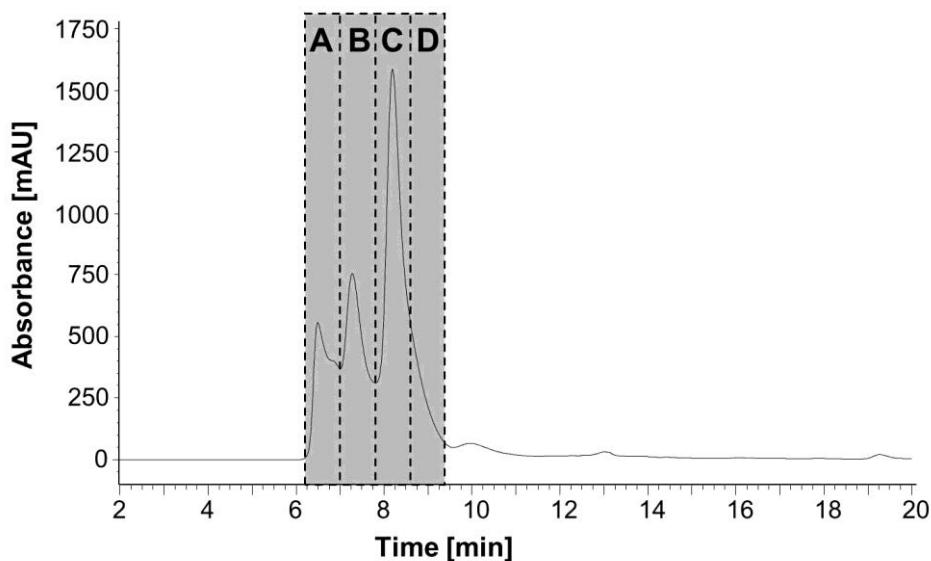
Figure 5. SEC fractionation of the M60-1 sample (M60-1_A, B, C and D); shown is the UV trace at 215 nm.

SEC-ICP-MS analysis of fractions M60_1_B, C and D revealed single peaks confirming the quality of fractionation. The analysis by LC-TOF-MS resulted for fractions C and D in mass spectra containing multiply charged protein ion patterns which were mathematically deconvoluted to give the molar masses of albumin. However, no proteins were identified in fraction B using the same approach. Most interestingly, mass spectra of fraction A contained again peaks assignable to albumin, similar to the data obtained for fractions C and D. However, in an off-line SEC-SEC-ICP-MS experiment not a single protein peak at 6–7 min was observed, but a similar distribution of proteins as without fractionation (Figure 6). These results point towards the fact that fraction A could contain agglomerated albumin-drug adducts, which were denatured during reversed phase LC-TOF-MS and already partly degraded *via* simple dilution as occurring in an SEC-SEC-ICP-MS experiment. Moreover, these assumptions were further strengthened by MALDI-MS studies. All collected fractions of a M60-1 mouse plasma sample were analyzed under identical conditions and compared to an HSA standard. In all four fractions, albumin was detectable, however, proteins with a mass of approximately 130 kDa were identified in fraction M60-1_B (Figure 7), which are neither present in the control mouse nor the other fractions. The molecular weight of these species indicates the formation of dimeric MSA aggregates. These data also fit nicely the molecular mass expectable from the retention times in the SEC experiment.
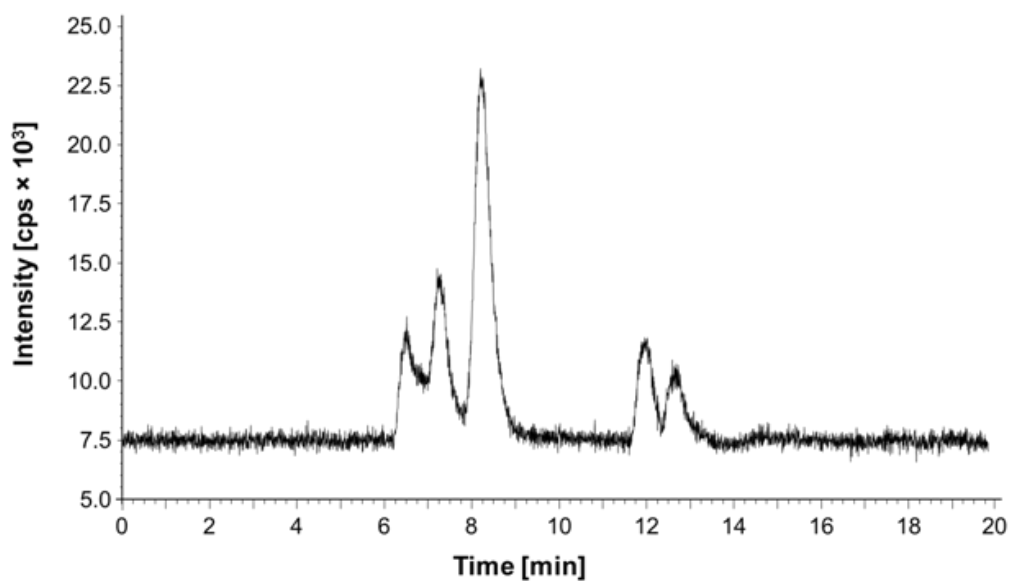
Figure 6. [48]SO trace recorded in an SEC-SEC-ICPMS run of fraction M60-1_A.
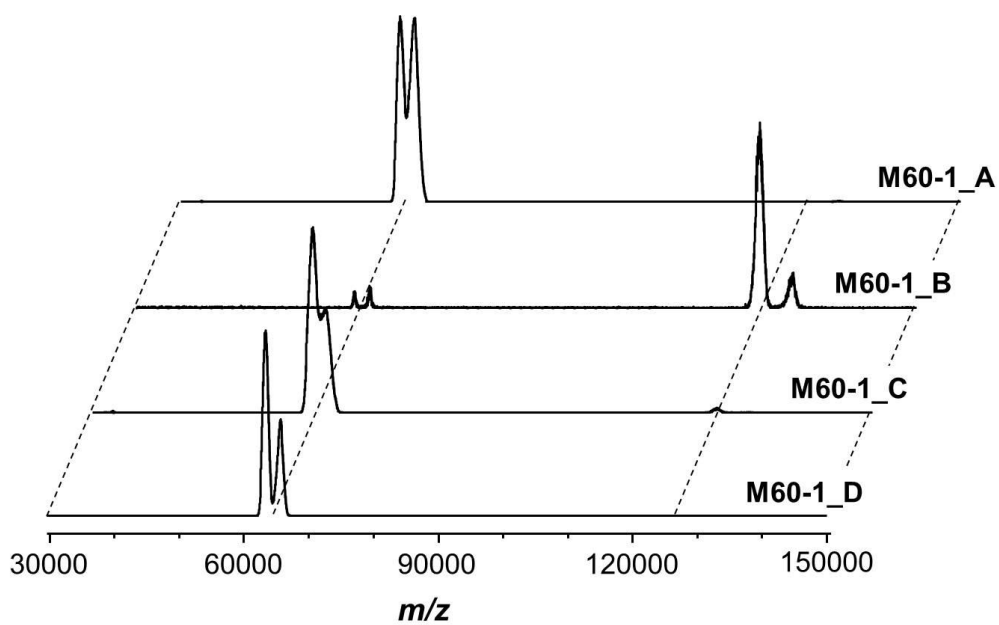
Figure 7. MALDI-mass spectra of fractions A–D collected from a M60-1 plasma sample.

SEC-IC-ICP-MS determination

Finally, the drug adduct formation in the 60-80 kDa fraction was analyzed on a quantitative basis following a two dimensional native separation scheme in combination with ICP-MS detection. The validity of the approach has been shown in the past.[26] As a key advantage, this method allows the separation of albumin and transferrin. In this work, the two-dimensional separation was achieved off-line. The LOD for transferrin was determined as 0.11 mg/mL and the LOQ as 0.36 mg/mL with regard to the sulfur signal (^{48}SO), whereas Ru limits of detection are lower by at least 1 order of magnitude. For all investigated samples the transferrin-KP1339 adduct was < LOD. Table 3 summarizes the obtained quantitative results for the albumin-KP1339 adducts.

CZE–ICP-MS

Capillary electrophoresis has been used for a long time in metallodrug research and in this study a method involving the use of PB-coated capillaries was directly compared to the SEC-IC–ICP-MS method described afore. External calibration was used with samples ranging from 0.5–3 eq. of KP1339 per HSA and as assessed by CZE–ICP-MS the binding was quantitative and yielded a linear calibration curve (Figure 8).

Figure 8. Calibration graph obtained for the analysis of HSA/KP1339 standards by CZE–ICP-MS.

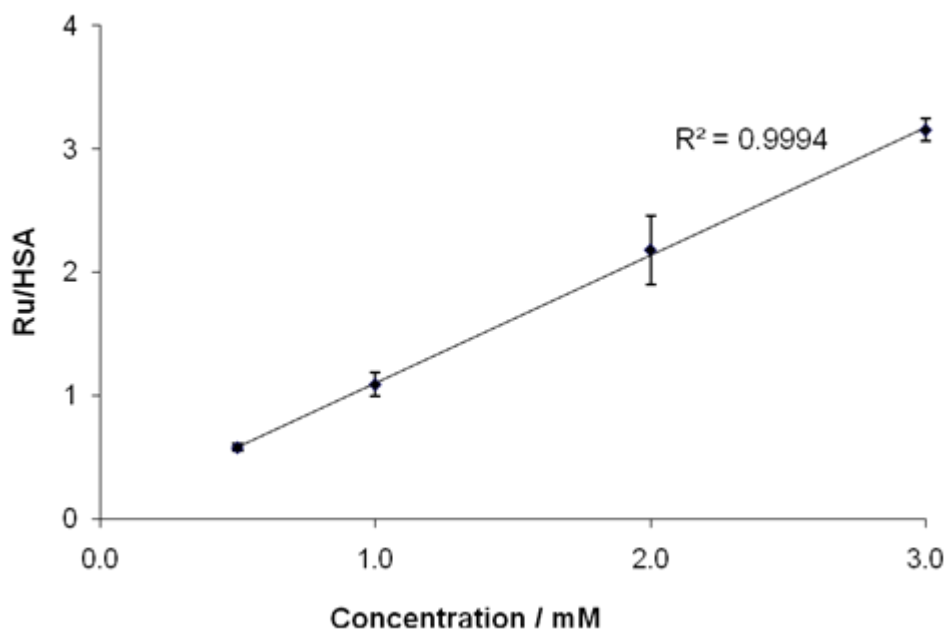The LOD and LOQ were determined for the Ru-to-HSA ratio as 0.22 and 0.66, respectively. In contrast to the SEC-IC–ICP-MS method, the concentration of albumin was measured by recording the ^{34}S trace. Due to the background of the ^{34}S trace caused by the interferences of $^{16}O^{18}O$, $^{16}O^{17}O^{1}H$ and $^{15}N^{16}O^{1}H$, only the trace of the most abundant protein in plasma, albumin (MSA contains 44 sulfur atoms[45]) was followed.

The electropherograms of the M40 and M50 mouse plasma samples contain two peaks in the Ru trace after treatment with KP1339 (Figure 9). The peak with the higher migration time corresponds to the KP1339–albumin adduct, whereas the second peak is assumed to stem in accordance to the LC data from albumin aggregates. Integration of the peaks demonstrates that the majority of the ruthenium drug is bound *in vivo* to albumin. The molar ratios of Ru/S for the KP1339-MSA adducts found with CZE-ICP-MS are summarized in Table 3 and compared to the results collected by SEC-IC-ICP-MS. The Ru/S ratios found with CZE technique are slightly higher than those obtained with SEC-IC–ICP-MS, but are still in good accordance taking into account the low sensitivity for ^{34}S (natural abundance 4.21%). In the plasma samples M40-1 and M40-7 almost 80 and 70%, respectively, of the total observed Ru content was found as albumin adduct, whereas the M50-1 samples contain significantly lower amounts of Ru attached to albumin (about 50%).
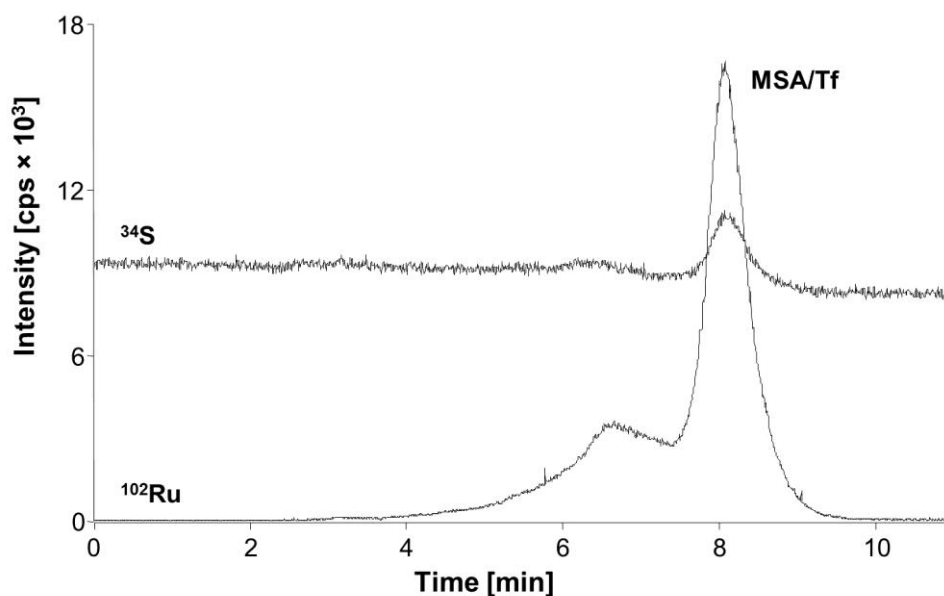
Figure 9. Electropherogram of the mouse plasma sample M40-1b. Shown are the traces of ^{102}Ru and ^{34}S (for MSA detection).

Table 3. Experimentally determined KP1339/MSA molar ratios.

Mouse	Dose	Ru/MSA [a]	
		CE–ICP-MS	SEC(-IC)–ICP-MS
M40-1a	40 mg/kg	0.83	0.72
M40-1b		0.88	0.71
M40-1c		0.84	0.94
M40-7a	40 mg/kg	0.15	0.04
M40-7b		0.12	0.04
M40-7c		0.15	0.05
M50-1a	50 mg/kg	0.93	0.70
M50-1b		- [b]	0.80
M50-1c		0.77	0.81

[a] The total combined uncertainties were estimated as 15%; [b] The volume of the plasma sample was too small to analyze it with all available methods.

Conclusions

Hyphenated methods, such as LC– and CE–ICP-MS approaches, are essential in metallomics research, especially when performing analyses in *in vivo* samples. The speciation analysis of metallodrugs in plasma samples obtained from mice is of major interest to identify essential parts of the mode of action, *i.e.*, the transport of the drugs through the bloodstream.

CZE– and 1D and 2D LC–ICP-MS methods were implemented in order to analyze plasma samples collected from mice treated with different amounts of the ruthenium-indazole anticancer complex KP1339 for 1 or 7 days. In general, the LC-based method was more sensitive, whereas the CZE approach is considerably quicker. The studies revealed a significant effect of the dosage on the total protein content and the species formed. In addition to the expected proteins, MSA agglomerates were identified, as shown by LC-TOF-MS and MALDI-MS after fractionation

of plasma samples. Furthermore, the protein and the drug-protein adduct distributions varied in dependence of the dose; for example, after treatment with 50 mg/kg the albumin contents along with the total protein content decreased significantly. Both, LC- and CZE-based ICP-MS experiments demonstrated that the majority of Ru was attached to albumin and good agreement was achieved for the molar ratio of Ru/MSA. In future, the developed methodology will be applied for the pharmacokinetic analysis of both *in vivo* samples collected from mice and eventually for accompanying experiments to clinical trials.

Acknowledgments

References

1.   J. M. Rademaker-Lakhai, D. Van Den Bongard, D. Pluim, J. H. Beijnen and J. H. M. Schellens, *Clin. Cancer Res.*, 2004, **10**, 3717-3727.
2.   W. H. Ang and P. J. Dyson, *Eur. J. Inorg. Chem.*, 2006, 4003-4018.
3.   C. G. Hartinger, S. Zorbas-Seifried, M. A. Jakupec, B. Kynast, H. Zorbas and B. K. Keppler, *J. Inorg. Biochem.*, 2006, **100**, 891-904.
4.   P. J. Dyson, *Chimia*, 2007, **61**, 698-703.
5.   P. J. Dyson and G. Sava, *Dalton Trans.*, 2006, 1929-1933.
6.   C. G. Hartinger, M. A. Jakupec, S. Zorbas-Seifried, M. Groessl, A. Egger, W. Berger, H. Zorbas, P. J. Dyson and B. K. Keppler, *Chem. Biodiversity*, 2008, **5**, 2140-2155.
7.   A. F. A. Peacock and P. J. Sadler, *Chem. Asian J.*, 2008, **3**, 1890-1899.
8.   C. G. Hartinger and P. J. Dyson, *Chem. Soc. Rev.*, 2009, **38**, 391-401.
9.   A. Levina, A. Mitra and P. A. Lay, *Metallomics*, 2009, **1**, 458-470.

10. J. M. Rademaker-Lakhai, D. van den Bongard, D. Pluim, J. H. Beijnen and J. H. Schellens, *Clin. Cancer Res.*, 2004, **10**, 3717-3727.

11. C. Dittrich, M. E. Scheulen, U. Jaehde, B. Kynast, M. Gneist, H. Richly, S. Schaad, V. B. Arion and B. K. Keppler, *Proc. Am. Assoc. Cancer Res.*, 2005, **46**, P472.

12. M. R. Berger, F. T. Garzon, B. K. Keppler and D. Schmaehl, *Anticancer Res.*, 1989, **9**, 761-765.

13. G. Sava, S. Pacor, G. Mestroni and E. Alessio, *Clin. Exp. Metastasis*, 1992, **10**, 273.

14. G. Sava, E. Alessio, A. Bergamo and G. Mestroni, *Top. Biol. Inorg. Chem.*, 1999, **1**, 143-169.

15. B. K. Keppler, K. G. Lipponer, B. Stenzel and F. Kratz, in *Metal Complexes in Cancer Chemotherapy*, ed. B. K. Keppler, VCH, Weinheim, 1993, pp. 187-220.

16. T. Pieper, K. Borsky and B. K. Keppler, *Top. Biol. Inorg. Chem.*, 1999, **1**, 171-199.

17. M. J. Clarke, F. Zhu and D. R. Frasca, *Chem. Rev.*, 1999, **99**, 2511-2533.

18. M. J. Clarke, *Coord. Chem. Rev.*, 2003, **236**, 209-233.

19. A. R. Timerbaev, C. G. Hartinger, S. S. Aleksenko and B. K. Keppler, *Chem. Rev.*, 2006, **106**, 2224-2248.

20. A. D. Kelman, M. J. Clarke, S. D. Edmonds and H. J. Peresie, *J. Clin. Hematol. Oncol.*, 1977, **7**, 274-288.

21. M. A. Jakupec, E. Reisner, A. Eichinger, M. Pongratz, V. B. Arion, M. Galanski, C. G. Hartinger and B. K. Keppler, *J. Med. Chem.*, 2005, **48**, 2831-2837.

22. M. Pongratz, P. Schluga, M. A. Jakupec, V. B. Arion, C. G. Hartinger, G. Allmaier and B. K. Keppler, *J. Anal. At. Spectrom.*, 2004, **19**, 46-51.

23. M. Groessl, E. Reisner, C. G. Hartinger, R. Eichinger, O. Semenova, A. R. Timerbaev, M. A. Jakupec, V. B. Arion and B. K. Keppler, *J. Med. Chem.*, 2007, **50**, 2185-2193.

24. F. Kratz, M. Hartmann, B. Keppler and L. Messori, *J. Biol. Chem.*, 1994, **269**, 2581-2588.

25. C. A. Smith, A. J. Sutherland-Smith, B. K. Keppler, F. Kratz and E. N. Baker, *J. Biol. Inorg. Chem.*, 1996, **1**, 424-431.

26. M. Sulyok, S. Hann, C. G. Hartinger, B. K. Keppler, G. Stingeder and G. Koellensperger, *J. Anal. At. Spectrom.*, 2005, **20**, 856-863.

27. K. Polec-Pawlak, J. K. Abramski, O. Semenova, C. G. Hartinger, A. R. Timerbaev, B. K. Keppler and M. Jarosz, *Electrophoresis*, 2006, **27**, 1128-1135.

28. C. G. Hartinger and B. K. Keppler, *Electrophoresis*, 2007, **28**, 3436-3446.

29. M. Groessl, C. G. Hartinger, K. Polec-Pawlak, M. Jarosz and B. K. Keppler, *Electrophoresis*, 2008, **29**, 2224-2232.

30. J. Reedijk, *Chem. Rev.*, 1999, **99**, 2499-2510.

31. F. Lentz, A. Drescher, A. Lindauer, M. Henke, R. A. Hilger, C. G. Hartinger, M. E. Scheulen, C. Dittrich, B. K. Keppler and U. Jaehde, *Anti-Cancer Drugs*, 2009, **20**, 97-103.

32. K. Polec-Pawlak, J. K. Abramski, J. Ferenc, L. S. Foteeva, A. R. Timerbaev, B. K. Keppler and M. Jarosz, *J. Chromatogr., A*, 2008, **1192**, 323-326.

33. X. Sun, C.-N. Tsang and H. Sun, *Metallomics*, 2009, **1**, 25-31.

34. J. Szpunar, *Analyst (Cambridge, U. K.)*, 2005, **130**, 442-465.

35. R. Lobinski, D. Schaumlöffel and J. Szpunar, *Mass Spectrom. Rev.*, 2006, **25**, 255-289.

36. S. Mounicou, J. Szpunar and R. Lobinski, *Chem. Soc. Rev.*, 2009, **38**, 1119-1138.

37. S. Hann, G. Koellensperger, K. Kanitsar, G. Stingeder, M. Brunner, B. Erovic, M. Mueller and C. Reiter, *Anal. Bioanal. Chem.*, 2003, **376**, 198-204.

38. S. Hann, G. Koellensperger, Z. Stefanka, G. Stingeder, M. Fuerhacker, W. Buchberger and R. M. Mader, *J. Anal. At. Spectrom.*, 2003, **18**, 1391-1395.

39. A. Prange and D. Profrock, *Anal. Bioanal. Chem.*, 2005, **383**, 372-389.

40. D. Pröfrock, P. Leonhard and A. Prange, *Anal. Bioanal. Chem.*, 2003, **377**, 132-139.

41. M. Groessl, C. G. Hartinger, P. J. Dyson and B. K. Keppler, *J. Inorg. Biochem.*, 2008, **102**, 1060-1065.

42. J. F. Kelly, S. J. Locke, L. Ramaley and P. Thibault, *J. Chromatogr., A*, 1996, **720**, 409-427.

43. M. Groessl, C. G. Hartinger, K. Polec-Pawlak, M. Jarosz and B. K. Keppler, *Electrophoresis*, 2008, **29**, 2224-2232.

44. S. Hann, T. Falta, K. Boeck, M. Sulyok and G. Koellensperger, *J. Anal. At. Spectrom.*, 2010, **25**, 861-866.

45. O. J. Bandele and N. Osheroff, *Biochemistry*, 2007, **46**, 6097-6108.

3.5. Biodistribution of the anticancer drug candidate sodium *trans*-[tetrachloridobis(1*H*-indazole)-ruthenate(III)] (KP1339)

Bytzek A.K.,[a] Koellensperger G.,[b] Keppler B.K.,[a,c] Hartinger C.G.[a,c]
Status: in preparation

[a] University of Vienna, Institute of Inorganic Chemistry, Waehringer Str. 42, A-1090 Vienna, Austria.
[b] University of Natural Resources and Applied Life Sciences, Muthgasse 18, A-1180 Vienna, Austria.
[c] University of Vienna, Research Platform 'Translational Cancer Therapy Research', Waehringer Str. 42, A-1090 Vienna, Austria.

Abstract

The ruthenium complex KP1339 is a promising anticancer agent, currently undergoing clinical trials. In order to get insight into the distribution and accumulation throughout a living organism, KP1339 was administered intravenously in non-tumor bearing nude BALB/c mice and the Ru content in blood cells and plasma, bone, brain, colon, kidneys, liver, lung, muscle, spleen, stomach and thymus was determined at several time points. The Ru concentration in blood cells and plasma was found to increase slightly within the first hours of analysis, with the Ru concentration being 3-times higher in plasma compared to blood cells. The plasma samples were subjected to analysis by capillary zone electrophoresis (CZE) and size exclusion/anion exchange chromatography (SEC-IC) both coupled to inductively coupled plasma-mass spectrometry (ICP-MS) and a large majority of the total Ru content was found attached to mouse serum albumin (MSA). Within 1 h, the peak ratio of approximately 1.2–1.5 Ru per albumin molecule is reached which declines to about 1 Ru per albumin molecule within 24 h. Beside the MSA adduct a higher molecular weight species is observed probably stemming from MSA conjugates. In addition, the tissue samples were mineralized by microwave digestion and analyzed for their Ru content. The highest Ru levels were found in colon, lung, liver, kidney and thymus. The peak Ru concentrations in these tissues were reached 1–6 h after administration and decline slowly over time. Additionally, the NCI's anticancer drug discovery screen for the parent compound KP1019 indicated high activity against leukemia. The high accumulation of KP1339 in the thymus and the high activity of KP1019 against leukemia make the two Ru drugs interesting candidates against lymphoblastic leukemia.

Introduction

Ruthenium compounds are considered the most likely candidates for the next generation of metal-based anticancer drugs and the Ru(III) complexes KP1019 {indazolium *trans*-[tetrachloridobis(1*H*-indazole)ruthenate(III)]} and NAMI-A {imidazolium *trans*-[tetrachloride(DMSO)(imidazole)ruthenate(III)]} (Figure 1) have finished clinical phase I trials [1-3].
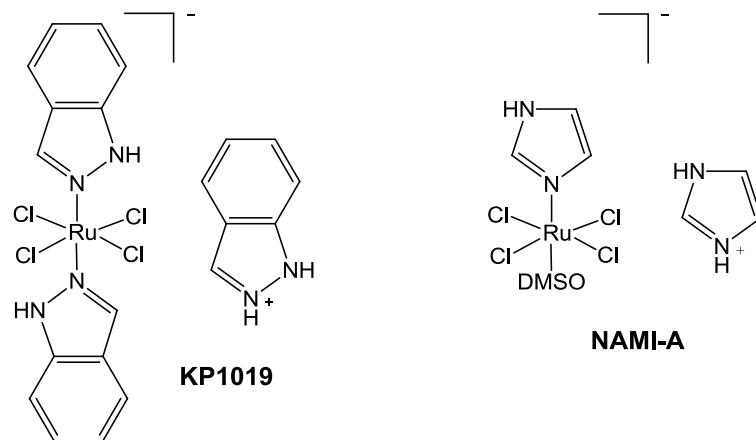
Figure 1. The structures of KP1019 {*trans*-[tetrachloridobis(1*H*-indazole)ruthenate(III)]} and NAMI-A {imidazolium *trans*-[tetrachloride(DMSO)(imidazole)ruthenate(III)]}.

The clinical and preclinical data indicate significant pharmacological differences between the different ruthenium compounds. Certain ruthenium compounds such as NAMI-A do not exhibit direct cytotoxicity in tumor cells and are considered only as anti-metastatic agents [4]. In contrast to these compounds, the bisindazole complex KP1019 and its analogues showed preclinical activity in several *in vivo* models against primary tumors and metastases. Most notable is the tumor-inhibiting potency in an autochthonous colorectal carcinoma of the rat, which resembles colon cancer of humans [5,6], and in more than 50 primary explanted human tumors, with a response rate of more than 80% of the tumor models [2]. In the KP1019 phase I clinical study, five of six patients experienced disease stabilization for 8–10 weeks, accompanied by only mild and non-drug-related toxic side effects [2,3]. The limitation in the application of KP1019 in the clinical trials was the low solubility and therefore the study endpoint was not reachable. Therefore, the sodium analogue of KP1019, called KP1339 {sodium *trans*-[tetrachloridobis(1*H*-indazole)ruthenate(III)]}, was selected for further development. KP1019 and KP1339 were found to share similar reactivity to proteins [7], modes of action and activity pattern [8,9]. These recent mechanism of action studies confirm that KP1019 and KP1339 differ from other ruthenium and platinum compounds. The primary target and mechanism of apoptosis induction for KP1019 and KP1339 appear to be cytosolic proteins and not DNA adduct formation. These studies indicate that KP1019 and KP1339 are novel apoptosis inducing agents.

The interaction of KP1019 and KP1339 with serum proteins is supposed to contribute to the selective transport to the tumor, being probably also related to the low adverse effects as compared to metal anticancer agents. KP1019 is almost exclusively bound to proteins in the

blood stream as shown both *in vitro* and *in vivo* [10-20]. Both major serum proteins, albumin and transferrin (Tf), represent potential binding partners. EPR studies revealed rapid non-covalent binding to the hydrophobic binding domains of HSA, followed by slow conversion to covalent interactions [20]. In contrast, the same experimental setup revealed covalent binding to apo-Tf. Competitive experiments with these two proteins indicated that less than 20% of the overall Ru content was bound to Tf in an equimolar mixture of Tf and HSA. When raising the HSA : Tf ratio to a physiologically relevant 10 : 1 ratio, this fraction declined to 2%. In the plasma samples of patients of the KP1019 clinical phase I trial, 80–90% of the Ru species were attached to HSA and the concentration of the KP1019-Tf adduct was below the quantification limit, but was estimated to be less than 1% of the total KP1019 content. The pharmacokinetic profile for humans comprises a small volume of distribution, low clearance and long half-life in blood plasma [8]. Renal excretion of Ru was very low, as secondary peaks were observed in the concentration-time curves, and biliary excretion might play a role in the overall elimination of ruthenium from plasma.

In order to understand the biodistribution of the drug candidate KP1339, non-tumor bearing mice were treated with the ruthenium compound and the Ru content was determined by ICP-MS in different tissues. Furthermore, CZE and LC both coupled to ICP-MS were employed to investigate the *in vivo* binding partner of KP1339 in the blood stream after *i.v.* administration. The collected data are compared to those of a pharmacokinetic study accompanying the clinical trial of KP1019, the parent compound of KP1339, and discussed with regard to data obtained within the NCI (National Cancer Institute, USA) anticancer drug discovery screening program.

Experimental

Animal treatment and sample preparation

The drug biodistribution study was carried out with nude BALB/c mice in groups of 3 mice each sacrificed after approximately 0.1, 1, 3, 6, 12 and 24 h. KP1339 was injected into the tail vein in a single dose of 40 mg/kg in citrate-saline buffer (5 mM citrate, 0.9% NaCl, pH 3.45) and blood, internal organs and tissues were harvested immediately after the animals were sacrificed at the given time points. Blood was taken from the heart and added to heparin-containing Eppendorf tubes and centrifuged (2500 rpm for 5 min), and liver, spleen, kidneys, stomach, colon, muscle, bone, lung, thymus and brain were collected. Animal handling was in accordance with standard animal keeping practice and regulation, animals were treated humanely and with regard for alleviation of suffering throughout the study.

Tissue metal content

Instrumentation. The Ru content in the tissue was determined by ICP-MS (Agilent 7500ce, Waldbronn, Germany), equipped with a CETAC ASX-520 autosampler (Neuss, Germany), a Scott double pass spray chamber, and a MicroMist nebulizer. The ^{101}Ru and ^{102}Ru isotopes as well as ^{115}In as internal standard were recorded. Instrument control and data analysis were carried out using Agilent ChemStation software (G1834B). The instrument parameters were optimized daily using a 1 µg L^{-1} tuning solution (Agilent) containing ^{7}Li, ^{89}Y and ^{205}Tl in 2% HNO_3. Doubly charged ions and oxide levels were minimized by using ^{70}Ce/^{140}Ce and ^{156}CeO/^{140}Ce and were typically < 2.5%. The instrument was calibrated daily using Ru standards of 0.5 - 22 ng Ru/mL in 3.5% HNO_3 spiked with 0.5 ppb In as internal standard (CPI International, Santa Rosa, CA, USA). The LOD and LOQ were determined as 0.98 and 2.98 ng/L.

Sample preparation. Tissue and blood cell sample aliquots of 10–50 mg were digested with 1 mL nitric acid (65% HNO_3 p.a. from Sigma Aldrich, further purified with a quartz sub-boiling system from Milestone-MLS GmbH, Leutkirch, Germany) and 1 mL water in a microwave system (Milestone-MLS GmbH, Leutkirch, Germany). The samples were diluted with water to reach an end mass of approximately 10 g. Every sample contained 0.5 ppb In as internal standard.

Plasma analysis/ Plasma metal content and metal distribution in plasma

Instrumentation. The ICP-MS used was a quadrupole-based system equipped with a dynamic reaction cell (ELAN DRC-II, PE SCIEX, Ontario, Canada). Oxygen (purity 4.5,

Linde Gas GmbH, Vienna, Austria) was used as reaction gas and the ^{102}Ru and ^{32}S^{16}O traces were recorded. The ICP-MS sample introduction system consisted of a PFA-nebulizer and a cyclonic spray chamber. For 2D SEC-IC-ICP-MS determinations a Meinhard nebulizer, ICP-MS operation parameters are given elsewhere [21].

The metal-free chromatographic system used consisted of an AS 50 autosampler (including a custom made temperature control device), an ICS-3000DP dual pump system and the Chromeleon Chromatography Management System (Version 6.40), all from Dionex (Sunnyvale, California, USA). The metal content in the plasma samples was assessed by flow injection analysis. In case of LC-ICP-MS determination, chromatographic separation was achieved using a BioSuite^{TM} 125 column (300 × 4.6 mm UHR SEC, 4 μm particle diameter) from Waters (Milford, Massachusetts, USA). The SEC eluent containing 150 mM NaCl and 20 mM Tris-HCl, pH 7.4 was delivered at a flow rate of 350 μL·min^{-1} and directly transferred to the ICP-MS introduction system.

Sample preparation. For both type of analysis, the samples were diluted by a factor of 20 in 150 mM NaCl. For the 2D-SEC–IC–ICP-MS determination a dilution factor of 10 was applied.

CZE–ICP-MS

Instrumentation. CZE experiments were performed with an HP^{3D} CZE system (Agilent, Waldbronn, Germany) interfaced to an Agilent 7500ce ICP-MS with a CETAC CEI-100 microconcentric nebulizer. For all experiments capillaries of 60 cm total length (75 μm ID) were used (Polymicro Technologies, Phoenix, AZ, USA). Capillary and sample trays were thermostatted at 25 °C. Injections were performed by applying a pressure of 25 mbar for 4 s, and a constant voltage of –30 kV. Prior to the first use, the capillary was flushed at 1 bar with 0.1 M HCl, water, 0.1 M NaOH and again with water (5 min each). After this treatment the capillary was coated by rinsing with 1% PB solution containing 3v/v% ethylene glycol for 30 min at 50 mbar and water for 15 min at 1 bar [22,23]. Before each injection, the capillary was purged for 2 min with NaOH, water and the background electrolyte (BGE). The operational values for the CZE–ICP-MS interface are shown in Table 1. The nebulizer was employed in self-aspiration mode with the sheath liquid closing the electrical circuit and spraying a fine aerosol. Analyses were only started if a sufficiently stable signal (RSD ^{72}Ge < 5%) was attained.

Sample preparation. For calibration, four sets of standards (incubated for 3 h at 37 °C in 10 mM phosphate buffer containing 100 mM NaCl at pH 7.4 in order to simulate physiological conditions) at four different stoichiometries, namely at molar KP1339/HSA ratios of 0.5, 1, 2 and

3 were utilized. The concentration of HSA was kept constant at 100 μM. Human serum as well as the plasma samples were diluted 1 : 3 with the incubation buffer before analysis.

Table 1. ICP-MS operational parameters

Parameter	LC–ICP-DRC-MS	CZE–ICP-MS
Nebulizer	PFA nebulizer	CETAC CEI-100 microconcentric nebulizer
Spray chamber	Cyclon	-
Nebulizer gas flow, L min^{-1}	1.0	1.14
Auxiliary gas flow, L min^{-1}	1.275	0.4
Plasma gas flow, L min^{-1}	15	15
ICP RF power, W	1300	1500
O$_2$ flow rate, mL min^{-1}	0.8	-
RPQ	0.3 (SO), 0.6 (Ru)	-
Measured isotopes	^{48}SO, ^{101}Ru, ^{102}Ru	^{34}S, ^{72}Ge, ^{101}Ru, ^{102}Ru
Scan mode	Peak hopping	-
Sampler	Ni (0.1 mm orifice)	
Skimmer	Ni (0.4 mm orifice)	

NCI/DPT cytotoxicity tests and COMPARE analysis

The protocol for the determination of cytotoxicity on the 60 cell line panel can be found at http://dtp.nci.nih.gov/branches/btb/ivclsp.html. The cell line panel comprises subpanels of leukemia, melanoma, and cancers of lung, colon, brain, ovary, renal, breast and prostate. The Developmental Therapeutics Program (DTP) homepage can be accessed at http://dtp.cancer.gov/.

A COMPARE analysis was performed using KP1019 as a seed, and the analysis was carried out as described at the Developmental Therapeutics Program webpage (http://www.dtp.nci.nih.gov/docs/compare/compare.html).

Results and Discussion

The pharmacokinetics and tissue distribution of drug compounds have a major influence on their therapeutic efficacy and adverse effects. In order to study the accumulation and biodistribution for the drug candidate KP1339, the Ru content was determined in nude BALB/c mice after *i.v.* administration of a single dose of 40 mg/kg. The *i.v.* route was chosen in order to allow the compounds to experience conditions similar to those observed in humans and to provide cleaner pharmacokinetic profiles without the complication of the absorption phase [24]. The mice were sacrificed 0.1, 1, 3, 6, 12 and 24 h after injection. Blood, liver, spleen, kidneys, stomach, colon, muscle, bone, lung, thymus and brain were collected from each mouse and stored at –80 °C until microwave digestion and analysis for the Ru content. In addition, the blood was centrifuged to separate plasma which was analyzed for the Ru distribution among the blood plasma components.

Analysis of mouse blood samples
The total Ru content in plasma and in blood cells was determined by flow injection ICP-MS (Figure 2). The Ru concentration in both compartments was found to increase slightly within the first hours of analysis. In plasma the Ru concentration is 3-times higher than in the blood cells. After approximately 2.5 h the Ru content reaches a maximum and starts to decrease slowly to reach 50% of the peak concentration after *circa* 24 h. Similar pharmacokinetics were found for the parent compound KP1019 in humans during a clinical trial in which the Ru peak concentration in the plasma was reached approximately 2.5 h after drug administration [8]. The pharmacokinetics of the Ru compounds KP1019 and KP1339 in plasma differ significantly from the classical picture obtained after *i.v.* administration but are conform with a two-compartment pharmacokinetic model.
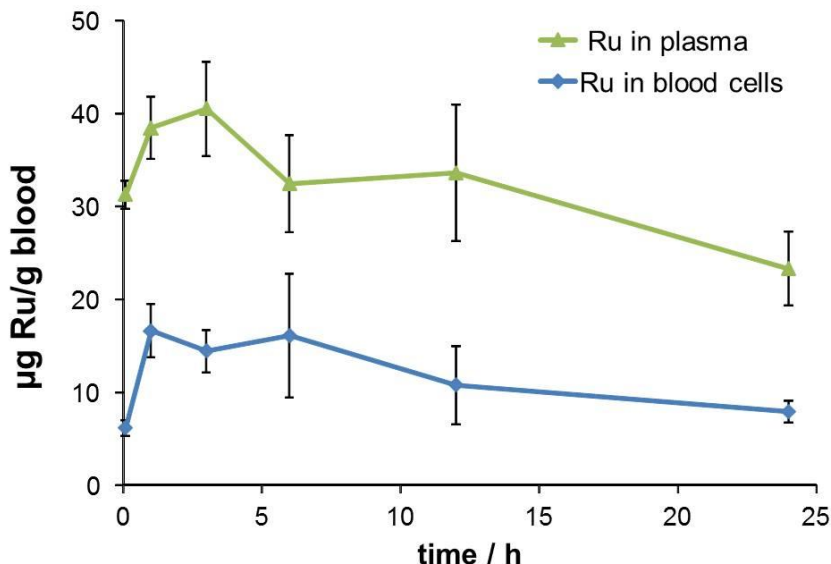
Figure 2. Ruthenium concentration in plasma and blood cells after administration of a single dose of 40 mg/kg KP1339.

Serum proteins including albumin and Tf are thought to play a crucial role in the transport, delivery and storage of certain anticancer metallodrugs, including KP1019 and KP1339 [3,26,27]. For determining the distribution of KP1339 between serum proteins in the mouse plasma samples, both capillary electrophoretic and chromatographic methods were coupled to ICP-MS. The electropherograms of the mouse plasma measured by CZE-ICP-MS contain two peaks in the Ru traces after treatment with KP1339. The peak with the higher migration time corresponds to the KP1339-MSA adduct, whereas the first peak is assumed to stem from MSA aggregates (Figure 3). In all plasma samples approximately 70% of the total content was detected attached to MSA. The high Ru load of MSA is probably also responsible for the long half-life of the drug. Similar results were obtained in a SEC–ICP-MS study with the majority of KP1339 bound to MSA and higher molecular weight species stemming from MSA conjugates. The presences of MSA conjugate was confirmed by collecting the SEC fractions off-line and performing orthogonal reversed phase separations in combination with ESI-TOF-MS determination [21].
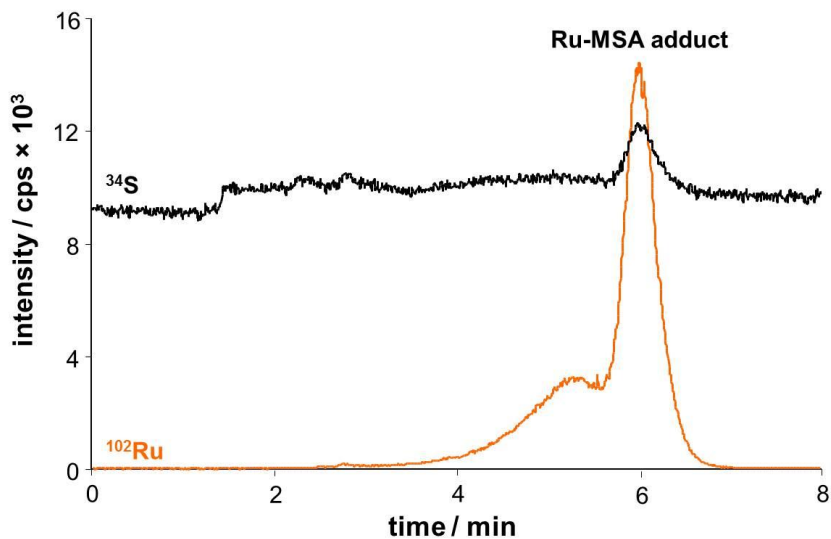
Figure 3. Ru traces recorded for a mouse plasma sample collected 24 h after injection. Shown are the traces of ^{102}Ru and ^{34}S (the latter for MSA detection).

The molar ratios of Ru/S for the KP1339-MSA adducts were determined by both CZE–ICP-MS and SEC–ICP-MS. For calibration, a set of standards containing KP1339 and human serum albumin at molar ratios of 0.5, 1, 2 and 3 were used and the concentration of the protein was kept constant (50 µM). Both methods delivered high linearity for the standard set and good agreement with calibration using inorganic standards was achieved. Analysis of the mouse plasma samples with both methods delivered essentially the same results within the standard errors (Figure 4). In general, the Ru/S ratios measured with the CZE setup are slightly higher than those obtained by SEC-IC–ICP-MS, but are still in good accordance to those determined with the LC method. The shape of the curves resembles widely the one obtained for the total Ru levels in plasma (Figure 2), with an increased level of ruthenation found after 1 h in comparison to the sample taken after 5 min. The peak ratio measured after 1 h was at approximately 1.2–1.5 Ru per albumin molecule and started to decline to about 1 after 24 h.
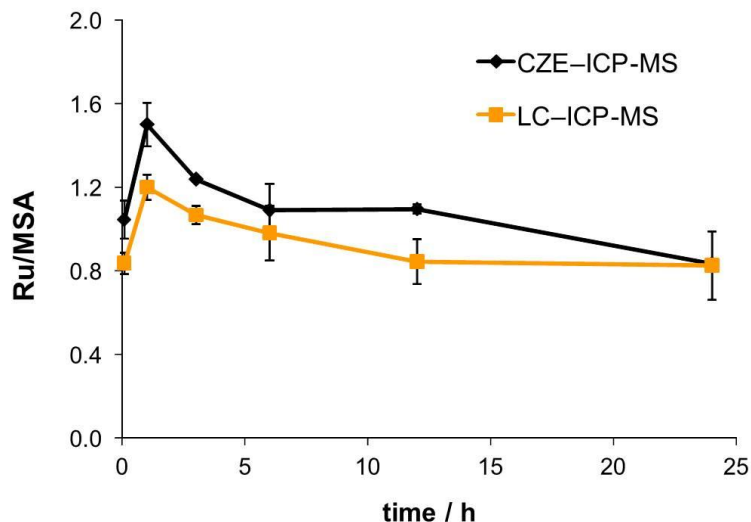
Figure 4. Comparison of the molar ratios of Ru per MSA molecule measured by SEC–ICP-MS and CZE–ICP-MS.

Tissue distribution of KP1339

The *in vivo* tissue distribution of KP1339 in non-tumor-bearing mice was determined by measuring the Ru content in bone, brain, colon, kidney, liver, lung, muscle, spleen, stomach and thymus by ICP-MS. Before analysis 10–50 mg of the organ samples were digested with nitric acid (34%) in a microwave digestion system.

Several trends are extractable from the data set: the highest Ru levels were found in colon, lung, liver, kidney and thymus (Figure 5). As expected, the organ samples taken from the animals sacrificed within 5 min after administration contained low levels of Ru (Table 2). Over time Ru concentration increased in all tissues analyzed with the exception of the brain, which might be related to the low potential of the drug compound to cross the blood brain barrier. In case of bone, colon, liver, lung, kidney, muscle, stomach and thymus samples, the peak Ru concentration were reached 1–6 h after administration (paralleling the total Ru levels in blood plasma) and declined slowly over time whereas in the spleen the concentrations increased slightly (from about 9.5 to 14.6 µg/g Ru after 1 and 24 h, respectively).

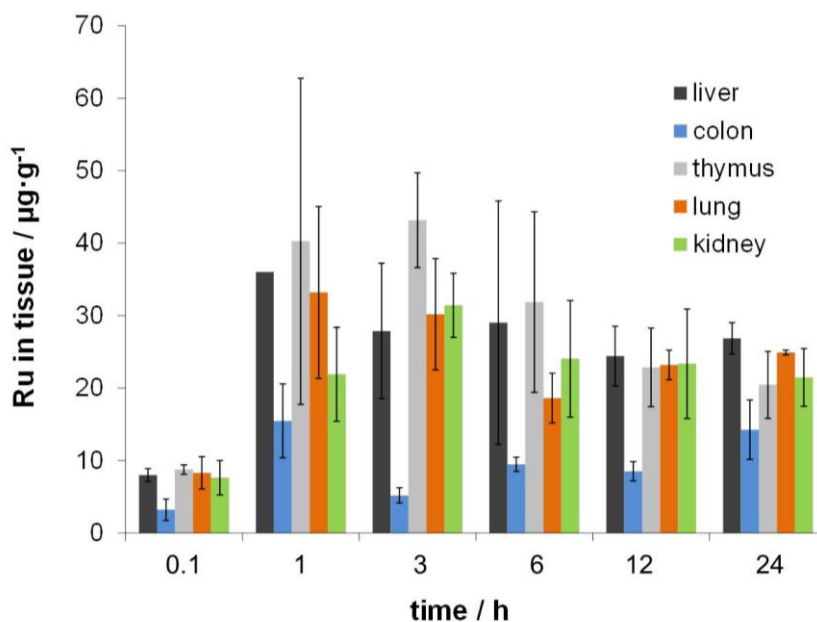**Figure 5.** Ru content in liver, colon, thymus, lung and kidney *ca.* 0.1, 1, 3, 6, 12 and 24 h after intravenous administration of KP1339. The values are the average of data collected from samples taken from three animals at each time point, and the bars indicate the standard deviations.

Table 2. Organ distribution of Ru in non-tumor bearing mice treated with KP1339.

	µg Ru / g tissue					
Time / h	0.1	1	3	6	12	24
bone	4.99 [a]	9.17 ± 1.17	8.03 ± 1.09	9.46 ± 2.39	5.40 ± 2.43	7.77 ± 0.87
brain	0.58 ± 0.31	0.61 ± 0.28	0.44 ± 0.11	0.48 ± 0.08	0.37 ± 0.02	0.61 ± 0.08
colon	3.21 ± 1.47	15.48 ± 5.08	5.19 ± 1.06	9.48 ± 0.97	8.53 ± 1.32	14.26 ± 4.09
lung	8.31 ± 2.21	33.19 ± 11.84	30.17 ± 7.66	18.62 ± 3.42	23.20 ± 2.04	24.92 ± 0.33
liver	7.99 ± 0.9	36.02 ± 19.24	27.87 ± 9.34	29.02 ± 16.80	24.42 ± 4.11	26.86 ± 2.17
kidney	7.65 ± 2.38	21.90 ± 6.49	31.41 ± 4.42	24.03 ± 8.03	23.35 ± 7.56	21.47 ± 3.97
muscle	0.99 [a]	7.94 ± 2.72	13.60 ± 2.70	5.40 ± 2.47	3.86 ± 0.83	5.67 ± 1.31
spleen	2.87 ± 0.13	9.54 ± 2.08	10.30 ± 5.54	11.09 ± 4.69	10.13 ± 2.77	14.63 ± 4.41
stomach	7.07 ± 5.20	7.66 ± 1.59	9.99 ± 0.31	5.85 ± 1.59	5.85 ± 0.98	7.38 ± 3.53
thymus	8.77 ± 0.65	40.24 ± 22.50	43.14 ± 6.53	31.86 ± 12.45	22.85 ± 5.41	20.44 ± 4.61

[a] only a single sample was available.

The high Ru levels measured in the liver and the kidneys were expected due to the role of these organs in clearance and excretion. Furthermore, relatively high Ru concentrations were found in the lungs, which is most probably related to the high blood flow through this tissue. Similar observations were made in *in* vivo biodistribution experiments with the anticancer complexes imidazolium *trans*-[tetrachloride(1*H*-imidazole)(dimethylsulfoxide-κS)ruthenate(III)] (NAMI-A) and imidazolium *trans*-[tetrachloridebis(1*H*-imidazole)ruthenate(III)] (KP418) and were explained by the high affinity of these compounds to collagen [27,28]. Furthermore, the colon is among the five organs with the highest Ru level which appears promising considering its potential in the treatment of colorectal cancer [2].

A point of particular note is the surprising high Ru concentrations found in the thymus. The thymus gland is a specialized organ in the immune system and its main function is the processing and maturation of T-lymphocytes or T-cells. T-lymphocytes are the body's immune system and protect the body by producing antibodies that stop the invasion of foreign agents, bacteria and viruses. In this experiments nude BALB/c mice were used, which differ from normal mice by a genetic mutation in the Foxn1 gene that causes a very small thymus with abnormal architecture lacking cortical and medullary domains, resulting in an inhibited immune system due to T-cell deficiency. There is no intrinsic defect of thymocytes (T-cell precursors) in nude mice, but the thymocytes are specifically blocked at both the DN1 and DP differentiation stages, express constitutively low TCR, and just very few SP thymocytes develop and immigrate into the periphery [28]. Literature data indicate that Ru(III) complexes with *N*-donor ligands can act as immunosuppressants and inhibit the antigen-independent phase of T-cell proliferation at nanomolar concentrations [29-31]. Based on these data, it appears as KP1339 could have potential in the treatment of lymphoblastic leukemia.

Moreover, for the parent compound KP1019 (NSC-666158) particular activity against leukemia was observed in an NCI screening against a 60 cell line panel in the concentration range of 10^{-4}–10^{-8} M (Figure 6). Especially CCRF-CEM and MOLT-4 cells were sensitive to the compound and both stem from T-lymphoblasts of patients with acute lymphoblastic leukemia. In a mean graph derived from the GI_{50} values (50% growth inhibition; Figure 6), the vertical line represents the mean GI_{50} value of the compound against all cell lines and bars extending to the right or left represent relative cellular sensitivity or insensitivity, respectively. From that representation it is obvious that the leukemia cell line panel is most sensitive to the treatment with the Ru drug candidate, whereas in other subpanels cell lines are included that are not sensitive to KP1019.

The NCI 60 cell line panel screening data was further subjected to a COMPARE analysis, in order to get further insight into the mode of action of KP1019 as compared to other anticancer

drugs. Therefore, KP1019 was used as a seed in the COMPARE analysis and related to the activity pattern of established anticancer agents and developmental drugs (for details see the standard agent database with 170 compounds including compounds with established modes of action at http://www.dtp.nci.nih.gov/docs/cancer/searches/standard_agent_table.html). Analysis of the Pearson correlation coefficients (P) obtained for a series of compounds revealed no correlation better than 0.627 (Table 3). Correlation coefficient values <0.6 are not considered to be significant. Therefore, the mode of action of the Ru complex appears to be different from those of established drugs, including those of other metal-based anticancer agents.
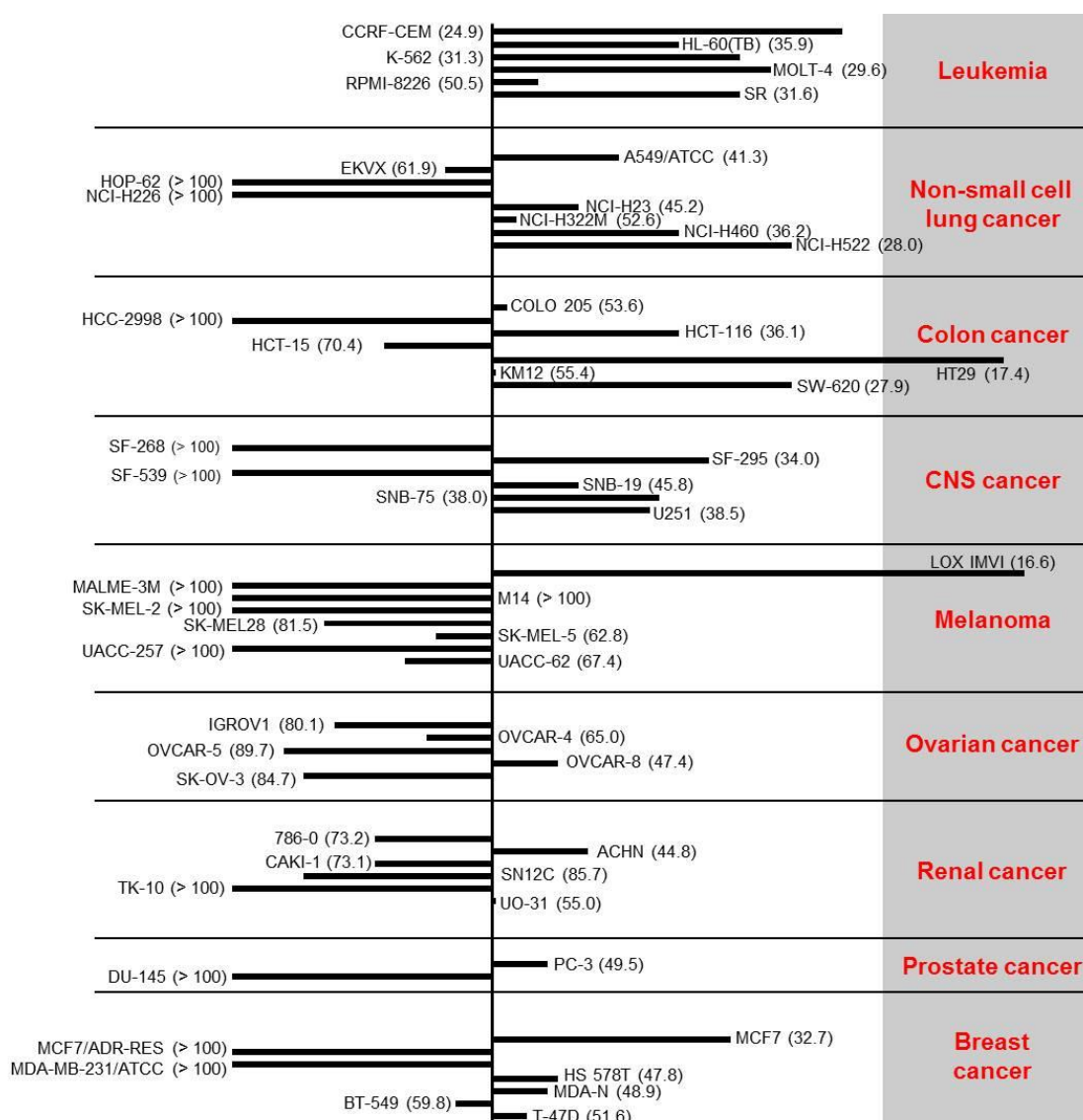

Figure 6. GI_{50} mean graph derived of the data obtained from the NCI screening program for KP1019 against a 60 cell line panel; the numbers in parenthesis are the GI_{50} values in the respective cell line (µM).

Table 3. Results obtained using KP1019 as the seed compound in a COMPARE analysis based on the NCI Anticancer Drug Screen database.

Rank	Correlation *	Name	NSC.NO.
1	0.627 **	AT-125 (acivicin)	163501
2	0.606 **	aclacinomycin A	208734
3	0.576	*N,N*-dibenzyldaunomycin	268242
4	0.534	hydrazine sulfate	150014
5	0.533	actinomycin D	3053
6	0.525	anguidine	141537
7	0.524	*N,N*-dibenzyldaunomycin	268242
8	0.506	DUP785 (brequinar)	368390
9	0.501	*S*-trityl-L-cysteine	83265

* Pearson correlation coefficients.
** Values > 0.6 are significant.

Conclusions

The accumulation and biodistribution are important factors for drugs to exhibit their activity in the desired tissue and also cause unwanted side effects. Adverse effects are a major issue in cancer chemotherapy, in particular in case of treatment with low specificity small molecule drugs. In the case of KP1019 and KP1339, drug candidates based on the $Ru(indazole)_2$, clinical trials demonstrated minor drug-related toxicity which is often attributed to the mode of action, which involves binding to proteins and activation in the tumor. The high affinity of KP1339 to proteins was confirmed in an *in vivo* study in mice and a large portion of the Ru was found attached to albumin and albumin aggregates. With regard to tissue distribution, the highest concentrations were found in colon, lung, liver, kidney and thymus. In particular the high amounts of Ru in the thymus are interesting in the light that the parent compound KP1019 showed high activity in the leukemia cell subpanel of the NCI 60 cell line panel. Especially, the marked activity of KP1019 in T-lymphoblasts and the high accumulation of KP1339 in the thymus make such Ru drugs interesting candidates against lymphoblastic leukemia.

References

1.   Rademaker-Lakhai JM, Van Den Bongard D, Pluim D, Beijnen JH, Schellens JHM (2004) A Phase I and Pharmacological Study with Imidazolium-*trans*-DMSO-imidazole-tetrachlororuthenate, a Novel Ruthenium Anticancer Agent. Clin Cancer Res 10:3717-3727.

2.   Hartinger CG, Zorbas-Seifried S, Jakupec MA, Kynast B, Zorbas H, Keppler BK (2006) From bench to bedside - preclinical and early clinical development of the anticancer agent indazolium *trans*-[tetrachlorobis(1*H*-indazole)ruthenate(III)] (KP1019 or FFC14A). J Inorg Biochem 100:891-904.

3.   Hartinger CG, Jakupec MA, Zorbas-Seifried S, Groessl M, Egger A, Berger W, Zorbas H, Dyson PJ, Keppler BK (2008) KP1019, a New Redox-Active Anticancer Agent – Preclinical Development and Results of a Clinical Phase I Study in Tumor Patients. Chem Biodiversity 5:2140-2155.

4.   Bergamo A, Gagliardi R, Scarcia V, Furlani A, Alessio E, Mestroni G, Sava G (1999) In Vitro Cell Cycle Arrest, In Vivo Action on Solid Metastasizing Tumors, and Host Toxicity of the Antimetastatic Drug NAMI-A and Cisplatin. J Pharmacol Exp Ther 289:559-564.

5.   Depenbrock H, Schmelcher S, Peter R, Keppler BK, Weirich G, Block T, Rastetter J, Hanauske AR (1997) Preclinical activity of *trans*-indazolium[tetrachlorobis(indazole)ruthenate(III)] (NSC 666158; IndCR; KP1019) against tumor colony-forming units and hematopoietic progenitor cells. Eur J Cancer 33:2404-2410.

6.   Kapitza S, Pongratz M, Jakupec MA, Heffeter P, Berger W, Lackinger L, Keppler BK, Marian B (2005) Heterocyclic complexes of ruthenium(III) induce apoptosis in colorectal carcinoma cells. J Cancer Res Clin Oncol 131:101-110.

7.   Polec-Pawlak K, Abramski JK, Ferenc J, Foteeva LS, Timerbaev AR, Keppler BK, Jarosz M (2008) Application of capillary electrophoresis-inductively coupled plasma mass spectrometry to comparative studying of the reactivity of antitumor ruthenium(III) complexes differing in the nature of counter-ion toward human serum proteins. J Chromatogr A 1192:323-326.

8.   Lentz F, Drescher A, Lindauer A, Henke M, Hilger RA, Hartinger CG, Scheulen ME, Dittrich C, Keppler BK, Jaehde U (2009) Pharmacokinetics of a novel anticancer ruthenium complex (KP1019, FFC14A) in a phase I dose-escalation study. Anti-Cancer Drugs 20:97-103.

9.   Heffeter P, Bock K, Atil B, Hoda MAR, Korner W, Bartel C, Jungwirth U, Keppler BK, Micksche M, Berger W, Koellensperger G (2010) Intracellular protein binding patterns of the anticancer ruthenium drugs KP1019 and KP1339. J Biol Inorg Chem 15:737-748.

10.   Kratz F, Hartmann M, Keppler B, Messori L (1994) The binding properties of two antitumor ruthenium(III) complexes to apotransferrin. J Biol Chem 269:2581-2588.

11.   Smith CA, Sutherland-Smith AJ, Keppler BK, Kratz F, Baker EN (1996) Binding of ruthenium(III) anti-tumor drugs to human lactoferrin probed by high resolution X-ray crystallographic structure analyses. J Biol Inorg Chem 1:424-431.

12.   Kratz F, Keppler BK, Messori L, Smith C, Baker EN (1994) Protein-binding properties of two antitumor Ru(III) complexes to human apotransferrin and apolactoferrin. Metal-Based Drugs 1:169-173.

13.   Pongratz M, Schluga P, Jakupec MA, Arion VB, Hartinger CG, Allmaier G, Keppler BK (2004) Transferrin binding and transferrin-mediated cellular uptake of the ruthenium coordination compound KP1019, studied by means of AAS, ESI-MS and CD spectroscopy. J Anal At Spectrom 19:46-51.

14.   Polec-Pawlak K, Abramski JK, Semenova O, Hartinger CG, Timerbaev AR, Keppler BK, Jarosz M (2006) Platinum group metallodrug-protein binding studies by capillary electrophoresis - inductively coupled plasma-mass spectrometry: A further insight into the reactivity of a novel antitumor ruthenium(III) complex toward human serum proteins. Electrophoresis 27:1128-1135.

15.   Sulyok M, Hann S, Hartinger CG, Keppler BK, Stingeder G, Koellensperger G (2005) Two dimensional separation schemes for investigation of the interaction of an anticancer ruthenium(III) compound with plasma proteins. J Anal At Spectrom 20:856-863.

16.   Timerbaev AR, Rudnev AV, Semenova O, Hartinger CG, Keppler BK (2005) Comparative binding of antitumor indazolium [*trans*-tetrachlorobis(1*H*-indazole)ruthenate(III)] to serum transport proteins assayed by capillary zone electrophoresis. Anal Biochem 341:326-333.

17.   Trynda-Lemiesz L, Keppler BK, Kozlowski H (1999) Studies on the interactions between human serum albumin and imidazolium [*trans*-tetrachlorobis(imidazol)ruthenate(III)]. J Inorg Biochem 73:123-128.

18.   Hartinger CG, Hann S, Koellensperger G, Sulyok M, Grössl M, Timerbaev AR, Rudnev AV, Stingeder G, Keppler BK (2005) Interactions of a novel ruthenium-based anticancer drug (KP1019 or FFC14a) with serum proteins - significance for the patient. Int J Clin Pharmacol Ther 43:583-585.

19.   Szpunar J, Makarov A, Pieper T, Keppler BK, Lobinski R (1999) Investigation of metallodrug-protein interactions by size-exclusion chromatography coupled with inductively coupled plasma mass spectrometry (ICP-MS). Anal Chim Acta 387:135-144.

20.   Cetinbas N, Webb MI, Dubland JA, Walsby CJ (2010) Serum-protein interactions with anticancer Ru(III) complexes KP1019 and KP418 characterized by EPR. J Biol Inorg Chem 15:131-145.

21.   Bytzek AK, Boeck K, Hann S, Keppler BK, Hartinger CG, Koellensperger G (2011) LC– and CZE–ICP-MS approaches for the in vivo analysis of the anticancer drug candidate sodium

trans-[tetrachloridobis(1H-indazole)ruthenate(III)] (KP1339) in mouse plasma. Metallomics:submitted.

22. Aleksenko SS, Hartinger CG, Semenova O, Meelich K, Timerbaev AR, Keppler BK (2007) Characterization of interactions between human serum albumin and tumor-inhibiting amino alcohol platinum(II) complexes using capillary electrophoresis. J Chromatogr A 1155:218-221.

23. Bytzek AK, Enyedy EA, Kiss T, Keppler BK, Hartinger CG (2009) Biodistribution of anti-diabetic Zn(II) complexes in human serum and in vitro protein-binding studies by means of CZE-ICP-MS. Electrophoresis 30:4075-4082.

24. Birner A (2003) Pharmacology of oral chemotherapy agents. Clin J Oncol Nurs 7:11-19.

25. Delord J-P, Umlil A, Guimbaud R, Gregoire N, Lafont T, Canal P, Bugat R, Chatelut E (2003) Population pharmacokinetics of oxaliplatin. Cancer Chemother Pharmacol 51:127-131.

26. Kratz F (2008) Albumin as a drug carrier: Design of prodrugs, drug conjugates and nanoparticles. J Controlled Release 132:171-183.

27. Qian ZM, Li H, Sun H, Ho K (2002) Targeted drug delivery via the transferrin receptor-mediated endocytosis pathway. Pharmacol Rev 54:561-587.

28. Xiao SY, Manley NR (2010) Impaired Thymic Selection and Abnormal Antigen-Specific T Cell Responses in Foxn1(Delta/Delta) Mutant Mice. Plos One 5:-.

29. Allardyce CS, Dyson PJ (2001) Ruthenium in medicine: Current clinical uses and future prospects. Platinum Met Rev 45:62-69.

30. Dwyer DS, Gordon K, Jones B (1995) Ruthenium red potently inhibits immune responses both in vitro and in vivo. Int J Immunopharmacol 17:931-940.

31. Clarke MJ, Bailey V, Doan P, Hiller C, LaChance-Galang KJ, Daghlian H, Mandal S, Bastos CM, Lang D (1996) 1H NMR, EPR, UV-Vis, and Electrochemical Studies of Imidazole Complexes of Ru(III). Crystal Structures of cis-[(Im)2(NH3)4RuIII]Br3 and [(1MeIm)6RuII]Cl2.2H2O. Inorg Chem 35:4896-4903.

3.6. Biodistribution of anti-diabetic Zn(II) complexes in human serum and *in vitro* protein-binding studies by means of CZE-ICP-MS

Bytzek A.K., Enyedy E.A., Kiss T., Keppler B.K., Hartinger C.G.

Anna K. Bytzek[1]
Éva A. Enyedy[2]*
Tamás Kiss[2]
Bernhard K. Keppler[1]
Christian G. Hartinger[1]

[1]Institute of Inorganic Chemistry, University of Vienna, Vienna, Austria
[2]Department of Inorganic and Analytical Chemistry, University of Szeged, Szeged, Hungary

Research Article

Biodistribution of anti-diabetic Zn(II) complexes in human serum and *in vitro* protein-binding studies by means of CZE–ICP-MS

Application of modern analytical technology for studying the fate of metallodrugs after administration to the blood is of utmost importance for drug development. Zn(II) compounds are under development as insulin-enhancing drugs with potential use in the treatment of diabetes. In comparison to the well-established vanadium compounds, especially the lower risk of adverse effects due to the essentiality of the element in biological processes is advantageous. Herein, CZE–ICP-MS studies on the interaction of Zn(II)-maltolato, -2-picolinato and -2,6-dipicolinato complexes with human serum proteins are discussed and modeling calculations were confirmed by experimental results. Studies with human serum reveal preference for HSA over other less abundant proteins and serum components.

1 Introduction

Diabetes mellitus (DM) is a disease from which people suffer all over the world, and with a continuously increasing number of patients, especially in the industrialized world. It is considered as a syndrome of disordered metabolism resulting in abnormal high blood glucose level (hyperglycemia) due to defects in either insulin secretion or insulin action. There are three forms of DM: the insulin-dependent type 1, the non-insulin-dependent or adult-onset type 2 and the gestational DM. Type 1 is an autoimmune disease caused by a lack of the insulin hormone due to the destruction of insulin-producing β-cells, and it is therefore treated by insulin replacement administered as daily injection. Type 2 DM is characterized by insulin resistance, *i.e.* lack of proper answer of the cells to the presence of insulin. This kind of DM can be usually treated by a well-controlled use of drugs, which are able to increase the

quantity of secreted insulin or the sensitivity of target organs to insulin, or to decrease the rate of glucose absorption from the gastrointestinal (GI) tract. The available drugs for DM type 2 are mostly oral hypoglycemic agents such as biguanide, sulfonylurea, thiazolidinediones and α-glucosidase inhibitors. Since these anti-hyperglycemic chemicals do not yield satisfactory results for all patients, there are efforts on the development of new anti-diabetic drugs with high efficacy and with no or minor adverse effects [1, 2].

In recent years, metal complexes and organometallic compounds have gained considerable interest for medicinal applications [3–5]. Cu, Cr, Mo, V, Zn, Mn, *etc.* species were found to exhibit insulin-enhancing activity [2, 6–8] and vanadium compounds in the oxidation states IV and V are among the most effective representatives [6–8]. More than 100 vanadium complexes have been developed and tested both *in vitro* and *in vivo* [7–10], out of which bis(ethylmaltolato)oxovanadium(IV) (Fig. 1) has completed phase I clinical trials and has advanced to phase II studies [11].

In addition to the V compounds, anti-diabetic Zn(II) complexes have gained considerable interest for the treatment of DM in the last few years [7]. They were found less effective than the vanadium complexes [7, 10], but may be introduced more easily into the medical treatment due to the fact that Zn(II) is an essential metal ion, less toxic and better bioavailable. Zn is a cofactor for more than 200 biologically important enzymes (which are particularly involved in protein synthesis) and plays a key role in the

Correspondence: Dr. Christian G. Hartinger, Institute of Inorganic Chemistry, University of Vienna, Waehringer Str. 42, A-1090 Vienna, Austria
E-mail: christian.hartinger@univie.ac.at
Fax: +43-1-4277-9526

Abbreviations: α2M, α$_2$-macroglobulin; **apoTf,** apotransferrin; **cit,** citric acid; **Cys,** cysteine; **dipic,** 2,6-dipicolinic acid; **DM,** diabetes mellitus; **GI,** gastrointestinal; **His,** histidine; **HMM,** high molecular mass; **HSA,** human serum albumin; **LMM,** low molecular mass; **mal,** maltol; **pic,** 2-picolinic acid; **Tf,** human serum transferrin

*Additional corresponding author: Dr. Éva A. Enyedy,
E-mail: enyedy@chem.u-szeged.hu

WILEY InterScience®
DISCOVER SOMETHING GREAT

www.electrophoresis-journal.com

synthesis and action of insulin. Moreover, Zn supplementation has also demonstrated a protective effect in DM type 2 animal models [12].

Fugono *et al.* have developed numerous Zn(II) complexes and some of the complexes bearing, *e.g.* maltol (mal) or 6-methyl-picolinic acid ligands were found to be active in KK-A^y mice when administered orally [13]. The effective Zn(II) complexes have a favorable effect not merely on the blood glucose level, but on the concentrations of adipocytokines such as free fatty acids, resistin, leptin, adiponectin, *etc.* and also on obesity and the systolic blood pressure [14]. The mode of action of anti-diabetic Zn(II) complexes is still not completely understood: Most probably they act at different sites of insulin signaling due to the activation of tyrosine kinase (of the insulin receptor), phosphatidyl inositol-3 kinase, phosphodiesterase enzymes and glucose transporters, and due to the inhibition of the protein tyrosine phosphatase [14]. Furthermore, these drug candidates are regarded as prodrugs. Hence the active forms are assumed to differ from the administered species as a consequence of biotransformation processes in different biological environments such as the GI tract, blood serum or the cytosol. According to recent studies, the carrier ligand determines mainly the absorption from the GI tract and it may be partly or completely displaced by suitable endogenous metal ion binders in the human serum [15, 16].

Improved knowledge about the Zn(II) speciation in serum might contribute to a better understanding of the transport processes *in vivo*. Previous results obtained *in vitro* using ultrafiltration–ICP-atomic emission spectroscopy and modeling calculations on artificial serum showed that Zn(II) is mostly bound to the high molecular mass (HMM) fraction of the serum, and the binding toward HSA is predominant [16, 17]. However, analysis of *real* blood serum should provide more detailed information about the Zn(II) distribution in the case of insulin-enhancing metal complexes. Among the different separation techniques, CZE exhibits high resolution, fast and efficient separation of metal-containing species of biomolecules [18]. CZE hyphenated to an ICP-MS provides a powerful tool to detect metal ions with high sensitivity and is perfectly suited for analyzing biological samples [19–21].

Herein, the biodistribution of Zn(II) complexes of mal, 2-picolinic acid (pic) and 2,6-dipicolinic acid (dipic), which exhibit anti-diabetic effects [14, 22], in human serum

samples is described. A CZE–ICP-MS method was developed for analyzing such samples under conditions maintaining metal-protein bonds.

2 Materials and methods

2.1 Instrumentation

CZE experiments were performed with an HP^{3D} CZE system (Agilent Technologies, Waldbronn, Germany) interfaced to an Agilent 7500ce ICP-MS with a CETAC CEI-100 microconcentric nebulizer. For all experiments capillaries of 60 cm total length (75-µm id) were used (Polymicro Technologies, Phoenix, AZ, USA). Injections were performed by applying a pressure of 25 mbar for 4 s, and constant voltages of 15 or 30 kV were used for Tris or carbonate buffer as BGE, respectively. Prior to the first use, the capillary was flushed at 1 bar with 0.1 M HCl, water, 0.1 M NaOH and again with water (10 min each). Before each injection, the capillary was purged for 2 min both with water and the BGE followed by applying a voltage of 30 kV for 30 s and flushed for 1 min with BGE again. The cleaning procedure included purging with 0.1 M HCl, water and 0.1 M NaOH (each for 2 min). The operational values for the CZE–ICP-MS interface are shown in Table 1. The nebulizer was employed in self-aspiration mode with the sheath liquid closing the electrical circuit and spraying a fine aerosol. Analyses were only started if a sufficiently stable signal (RSD ^{72}Ge < 5%) was attained.

2.2 Reagents and solutions

A 0.1M ZnCl$_2$ stock solution was prepared by the dissolution of ZnCl$_2$ (Reanal) in a defined amount of HCl (0.007 M) and its Zn concentration was determined by complexometry *via* the EDTA complex. NaOH, HCl and NH$_4$HCO$_3$ were obtained from Fluka; mal, pic and dipic (*puriss*) were from Sigma Aldrich, as were HSA (approximately 99%, fraction V), apotransferrin (apoTf; approximately ≥ 98%) and human serum. The concentrations of the protein solutions were estimated from their UV absorption: $\varepsilon_{280\,nm}$(apoTf) = 92300 M^{-1}cm^{-1} and $\varepsilon_{280\,nm}$(HSA) = 36850 M^{-1}cm^{-1} [23, 24]. The ICP-MS tuning solution
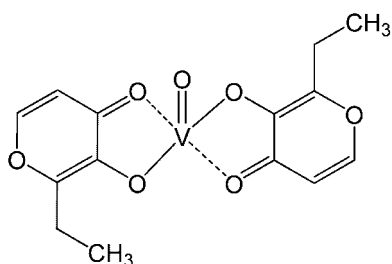
Figure 1. Structure of the vanadium compound BEOV (AKP-020), undergoing in clinical trials [11].

Table 1. ICP-MS conditions

Sampler	Ni (0.1 mm orifice)
Skimmer	Ni (0.4 mm orifice)
Plasma RF power, W	1500
Isotopes recorded	^{34}S, ^{72}Ge, ^{64}Zn, ^{66}Zn
Nebulizer gas flow rate, L/min	1.14
Sheath liquid	20 mM Tris with 20 ppb Ge or 10 mM ammonium bicarbonate with 20 ppb Ge
BGE	20 mM Tris or 10 mM ammonium carbonate

containing Li, Y, Ce, Tl and Co in 2% HNO_3 (each 10 mg/L) as well as the Ge standard were obtained from Agilent Technologies. High purity water used throughout this work was obtained from a Millipore Synergy 185 UV Ultrapure Water system (Molsheim, France).

2.3 Sample preparation

The Zn(II) complexes were synthesized *in situ*: A $ZnCl_2$ solution was added to the ligand in 1 mM Tris buffer or in 20 mM carbonate buffer (both pH 7.4). Depending on the denticity of the ligand (bidentate or tridentate) and the conditional stability constants of the formed complexes (at pH 7.4), the ratio $ZnCl_2$ ligand was varied (for dipic 1:2, for mal and pic from 1:2 to 1:6). For *in vitro* studies on the binding of the Zn compounds toward HSA and apoTf, samples containing 0.1 mM of $ZnCl_2$, 0.2 mM of the ligand and 0.1 mM of the serum proteins were prepared in 1 mM Tris buffer or 20 mM carbonate buffer. For the HSA–Zn-dipic titration, 100 µM HSA was mixed with 50–300 µM $[Zn(dipic)_2]^{2-}$ in carbonate buffer for 24 h. The samples for the competitive binding studies contained 100 µM of HSA, apoTf and Zn(II) and 200 µM dipic in carbonate buffer and were kept for 24 h at 25°C. The human serum was diluted 1:4 with the incubation buffer and the mixtures were incubated at 25°C for 24 h prior to the analysis. The experiments were repeated at least three times.

2.4 Data processing and calculations

Modeling calculations on the speciation of the Zn(II)-complexes in an artificial serum containing HSA, human serum transferrin (Tf), α_2-macroglobulin (α_2M) as HMM and L-cysteine (Cys), L-histidine (His), citric acid (cit) as low molecular mass (LMM) serum components were performed using the computer program PSEQUAD [25] based on the stability constants taken from Refs. [16, 17, 26–29] at physiological pH and at 25°C in the presence of HCO_3^-. The other LMM components of the serum were omitted from the modeling calculations because of their negligible Zn(II)-binding abilities [30]. The concentrations of the serum components used for the calculations were equivalent to those in the diluted blood serum [31].

The CZE–ICP-MS data was recorded using the Chem-Station software bundle (Agilent Technologies), data analysis was performed using Microsoft Excel 2003.

3 Results and discussion

Zn(II) is present at relatively low concentration in the human blood serum (the normal level is *appr.* 10–15 µM [31, 32]). When anti-diabetic Zn(II)-complexes are administered in animal DM type 2 models, the Zn(II) level was increased significantly to 100–200 µM [13]. HSA, α_2M and Tf as HMM

components, and Cys and His as LMM components are considered as the most efficient Zn(II) binders according to their blood concentrations and Zn(II)-binding abilities [16, 17, 26–29, 31, 32]. HSA is the most abundant serum protein (630 µM) with a molecular weight of *appr.* 67 kDa; it is negatively charged at physiological pH and has a key role in transport and/or storage processes of fatty acids, Cu(II), Ni(II), toxic metabolites (*e.g.* bilirubin) or drugs [18, 33, 34]. HSA is able to bind Zn(II) with conditional binding constants in the range of logK' = 7.1–7.9. The binding site is situated at the interface of domains I and II, which consists of two His-nitrogen atoms (His-67, His-247), two carboxylate-oxygen donor atoms (Asn-99, Asp-249) and a water molecule in the coordination sphere, and the Zn center adopts a distorted trigonal bipyramidal geometry [26, 34]. α_2M is a fairly large protein with 720 kDa, but found at much lower concentration in the blood than albumin (2–6 µM), and with conditional formation constants of $logK_1' = 7.49$ and $logK_2' = 5.12$ it has also considerable Zn(II)-binding properties [29, 35–37]. Another possible Zn(II) binder is the 79 kDa iron transport protein Tf (37 µM in serum), but 30% of the binding sites are occupied by Fe(III) ions in the serum [27, 33]. The Zn(II)-binding constants are $logK_1' = 7.8$ and $logK_2' = 6.4$ (15 mM $NaHCO_3$) [27] and the presence of the synergistic HCO_3^- is also considered important.

Literature data show that most of the total serum Zn(II) is bound to the serum proteins (*appr.* 98%) and HSA is the primary target (80–90%) [32, 35, 37], followed by α_2M (5-15%) [35–37]. However, the role of Tf is under discussion [36, 38] and also a minority of Zn(II) is circulating unbound or attached to LMM components (considered as the mobile portion of the metal ion).

In the case of anti-diabetic VO(IV) complexes the knowledge of the binding constants, characterizing their interactions with the HMM and LMM components of the blood serum, allows to calculate the distribution of VO(IV) among the various serum constituents. It was found that under physiological conditions in serum, Tf is the primary VO(IV) transporter and the binding ability of HSA is practically negligible, as confirmed by HPLC–ICP-MS analyses [39].

Zn(II) complex formation with mal, pic and dipic results predominantly in *bis* species in aqueous solution at physiological pH (see Fig. 2 for the structures) [22, 40], as demonstrated by the concentration distribution curves (for the Zn(II)-dipic system see Fig. 3). The bidentate mal and pic coordinate *via* (*O,O*) and (*N,O*) donor sets, respectively, to form $[ZnA(H_2O)_4]^+$, $[ZnA_2(H_2O)_2]$, $[ZnA_3]^-$ and $[ZnA_2(H_2O)(OH)]^-$ octahedral complexes ("A" stands for the fully deprotonated form of the ligands). Dipic is able to coordinate in a tridentate mode through the (*N,O,N*) donor atoms and forms the *bis* complex $[ZnA_2]^{2-}$, which is predominant in a wide pH range [22]. Conditional constants of the *bis* complexes of mal, pic and dipic are 8.13, 9.52 and 12.77, respectively, at physiological pH. The tridentate dipic forms a significantly more stable complex with Zn(II) as compared to the bidentate ligands mal and pic [22].
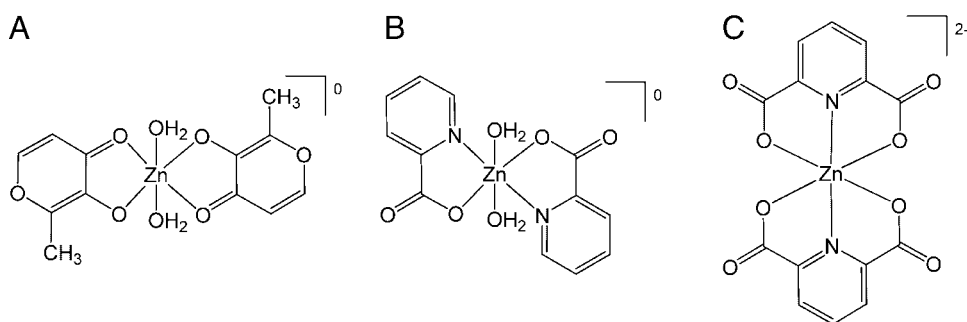
Figure 2. Structural formulae of the predominant species in aqueous solution at physiological pH: (A) $[Zn(mal)_2(H_2O)_2]$, (B) $[Zn(pic)_2(H_2O)_2]$, and (C) $[Zn(dipic)_2]^{2-}$.
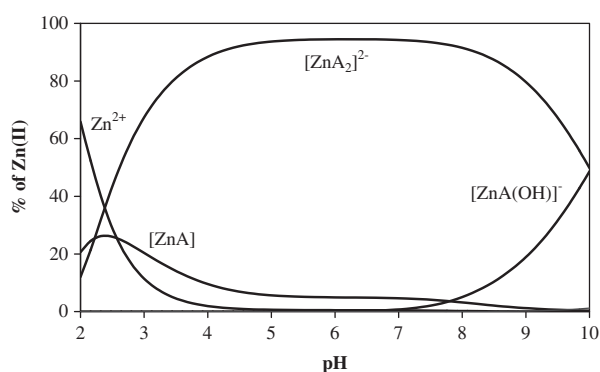

Figure 3. Concentration distribution curves for complexes formed in the Zn(II)–dipic system at 1:2 metal ion to ligand ratio; $c_{Zn(II)} = 0.1$ mM.

The migration behavior of the Zn(II) complexes was determined by CZE–ICP-MS with 1,2-dibromoethane as a neutral EOF marker. The species distribution of Zn(II)–ligand systems is highly dependent on the pH (see Fig. 3): At physiological pH the octahedral complex $[Zn(dipic)_2]^{2-}$ is the dominant species at a metal ion-to-ligand ratio of 1:2 and according to the expectations, a negatively charged species was observed in the electropherogram (Fig. 4). In the case of the bidentate ligands (mal and pic), the octahedral coordination sphere of the neutral *bis* complexes is not saturated, hence coordinated water molecules can be substituted by, *e.g.* separation buffer components. To shift the equilibrium to *tris* complexes, migrating then in the CZE mode slower than the EOF, the metal to ligand ratio was increased from 1:2 to 1:6 in the incubation solutions, since the extent of the formation of the negatively charged $[ZnA_3]^-$ species is higher at elevated ligand concentrations. In the case of the Zn(II)-mal system at a metal-to-ligand ratio of 1:2, no clear peaks were identified. When raising the ratio to 1:6, the neutral *bis* complex $[Zn(mal)_2(H_2O)_2]$ was detected in addition to a negatively charged *tris* species. Incubation of Zn(II) with an excess of pic resulted exclusively in a negatively charged complex, most probably $[Zn(pic)_3]^-$.

3.1 Interaction with HSA

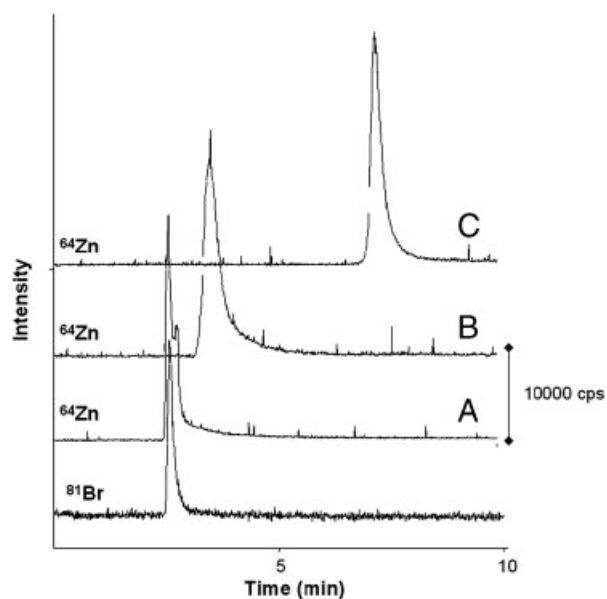To characterize the interaction between HSA and the Zn(II)-complexes with mal or dipic as ligands, samples containing

Figure 4. Comparison of the electropherograms of the Zn(II)-mal-system (1:6) (A), Zn(II)-pic system (1:6) (B) and Zn(II)-dipic-system (1:2) (C) after 24 h in carbonate buffer at pH 7.4. Shown are the traces of ^{64}Zn and ^{81}Br (EOF marker; 100 μM).

100 μM HSA, 100 μM ZnCl$_2$ and 200 μM of the ligand were prepared in 20 mM carbonate buffer (BGE: 10 mM carbonate solution at pH 7.4) or 1 mM Tris buffer (BGE: 20 mM Tris) and analyzed after an incubation time of 24 h at 25°C to ensure equilibrium conditions. Quantification of non-metal-containing proteins by ICP-MS is only accessible *via* analysis of the sulfur content. Polyatomic isotope interference from atmospheric gas and biological material can, however, cause serious errors in detection of sulfur. The most abundant ^{32}S isotope (94.93%) suffers from polyatomic interferences, such as ^{16}O^{16}O, which cannot be resolved by conventional quadrupole instruments. The second most abundant isotope ^{34}S (4.29%) is interfered mainly by ^{16}O^{18}O and ^{16}O^{17}O^{1}H, but quantification is still possible to a certain extent [41].

Figure 5 shows an electropherogram for the Zn(II)-dipic system in carbonate buffer, and approximately 60% of the total observed Zn content are bound to HSA. The second peak in the ^{64}Zn trace of the electropherogram was assigned to the parent complex $[Zn(dipic)_2]^{2-}$, based on the migration time and the absence of a sulfur peak. Switching
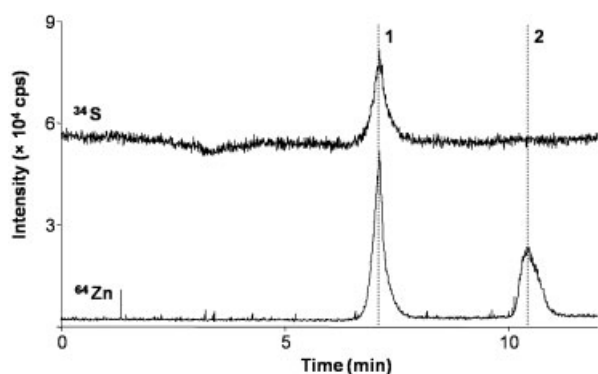
Figure 5. Electropherogram of $[Zn(dipic)_2]^{2-}$ incubated for 24 h with HSA in carbonate buffer. Shown are the traces of ^{64}Zn and ^{34}S (for HSA detection). Peak identification: 1 – HSA adduct, 2 – $[Zn(dipic)_2]^{2-}$; Conditions: see Section 2.

Figure 6. Titration of HSA with $[Zn(dipic)_2]^{2-}$ (incubated for 24 h). Legend: ■ $[Zn-dipic]_{exp}$, □ $[Zn-dipic]_{calc}$, ● $\Sigma[Zn-HSA]_{exp}$, ○ $\Sigma[Zn-HSA]_{calc}$; $\Sigma[Zn-HSA]$ stands for the summed concentrations of the binary and ternary species $[Zn-HSA]$ and $[Zn-HSA-dipic]$, respectively. Conditions: see Section 2.

the incubation/separation system to Tris buffer causes no significant changes. Under these conditions, *appr.* 55% of the total observed Zn content was found bound to HSA, whereas for Zn(II)-mal almost quantitative binding was observed. Modeling calculations on the Zn(II) distribution in the Zn(II)-ligand-HSA system were performed using equivalent conditions as for the CZE–ICP-MS measurements and based on the stability constants of the Zn(II)-ligand complexes, Zn(II)-binding ability of HSA and the HSA-ligand interactions [16, 17, 26] at equimolar ratio of the metal complex and HSA. Calculations show that in the case of dipic equimolar amounts of Zn are bound to the carrier ligand dipic and in a Zn(II)-HSA-ligand ternary complex. In contrast, the weak ligand mal is able to maintain merely *appr.* 6% of Zn(II) in a binary complex and the large majority of the Zn was found attached to HSA. These calculations are in good agreement to the experimental data.

Titration experiments with a constant amount of HSA (100 μM) with $[Zn(dipic)_2]^{2-}$ (from 50–300 μM; incubation time: 24 h) were performed. These studies show at low Zn(II)-dipic to HSA ratios that the majority of the Zn(II) is bound to albumin, whereas at increasing concentrations, $[Zn(dipic)_2]^{2-}$ becomes the predominant species in solution. The experimentally obtained results were compared with the calculated distribution and relatively good agreement was obtained (Fig. 6).

To characterize the binding kinetics for the reaction of $[Zn(dipic)_2]^{2-}$ with HSA, samples containing 100 μM HSA, 100 μM ZnCl₂ and 200 μM dipic were prepared in carbonate buffer and again analyzed by CZE–ICP-MS. Time resolved studies monitoring the peak area for the HSA adduct demonstrate that the binding of Zn(II) to HSA is very quick and already completed when the first data point was recorded (approximately 5 min after the start of the incubation).

3.2 Interaction with Tf

The same method as described for the analysis of the Zn-HSA system was transferred to the Zn-apoTf system
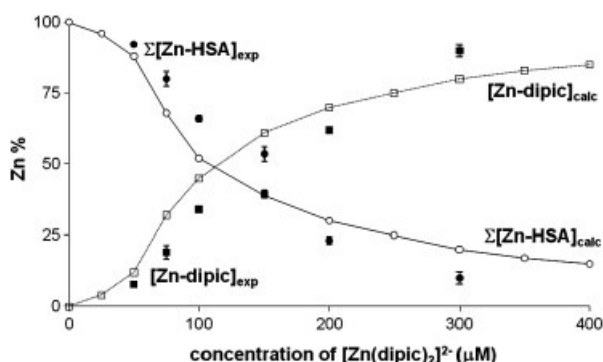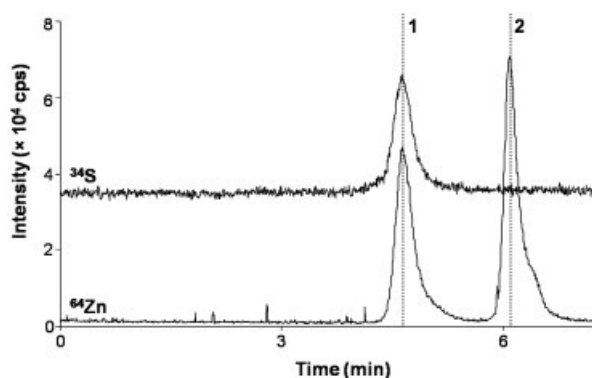

Figure 7. Electropherogram of $[Zn(dipic)_2]^{2-}$ incubated for 24 h with apoTf in carbonate buffer. Shown are the traces of ^{64}Zn and ^{34}S (for apoTf detection). Peak identification: 1 – apoTf adduct; 2 – $[Zn(dipic)_2]^{2-}$; Conditions: see Section 2.

(100 μM apoTf, 100 μM ZnCl₂, 200 μM dipic) and the Zn(II)-binding ability of apoTf was characterized. Incubation of apoTf with $[Zn(dipic)_2]^{2-}$ causes a partial carrier ligand displacement. In the presence of apoTf in carbonate buffer as incubation medium approximately 46% of the total observed Zn content is bound to apoTf (Fig. 7). The binding of Zn(II) to apoTf is strongly influenced by the incubation buffer: In Tris buffer nearly no interaction of Zn(II) with apoTf was observed and only 4% of the total Zn(II) content was found attached to apoTf after an incubation time of 24 h.

Hydrogencarbonate appears to act as a synergistic ion necessary for Zn(II) binding [42]. To study the role of hydrogen carbonate, the same set of samples was prepared in 1 mM Tris buffer containing 500 μM NaHCO₃ (incubation for 24 h) and the sample was analyzed using 20 mM Tris buffer or 10 mM carbonate buffer as BGE. When using Tris buffer as BGE, 20% of the total Zn(II) content was bound to apoTf, whereas with the carbonate buffer 50% of the Zn content was found attached to apoTf. These results demonstrate the importance of the choice of the BGE and

furthermore when using Tris as BGE, in addition to the adduct peak, broad peaks and an unstable baseline were visible in the electropherogram, most probably indicating the presence of mixed ligand species.

3.3 Competitive serum protein binding

Selective binding to a single protein after intravenous administration might be an option for exploiting a transport mechanism, *e.g.* known for Tf, causing enrichment of drugs in the desired tissue [43]. Therefore, competitive binding between HSA and apoTf was studied and it was found that, in contrast to VO(IV)-based insulin-enhancing complexes, HSA is the preferred binding partner at equimolar ratio of HSA to apoTf (42 *versus* 50 sulfur atoms (http://www.expasy.org/, ExPASy Proteomics Server, Swiss Institute for Bioinformatics): ~64% of Zn(II) is bound to HSA, ~25% to apoTf peak and the rest to the carrier ligand (Fig. 8); however, the peaks of the proteins are slightly overlapping and therefore no exact quantification is possible.

3.4 Interaction with proteins in human serum

To study the binding behavior of the Zn(II) complexes to serum proteins under more realistic conditions, serum samples were incubated with the Zn(II) compounds (0.1 mM; serum diluted with buffer; 1:4; 24 h; at 25°C; see caption of Fig. 10 for exact concentrations of the serum components). CZE–ICP-MS analysis revealed for the complexes with the dipic ligand that most of the Zn(II) was bound to HSA (approximately 70%), as identified *via* the ^{34}S trace. A minor amount of Zn(II) was still coordinated to dipic or other buffer components; however, no Zn(II) was detected at Tf (Fig. 9). This result might be explained by the low concentration of Tf in serum and also the iron-binding sites of transferrin are partly occupied by Fe(III), competing for the same binding site as Zn(II) [27].
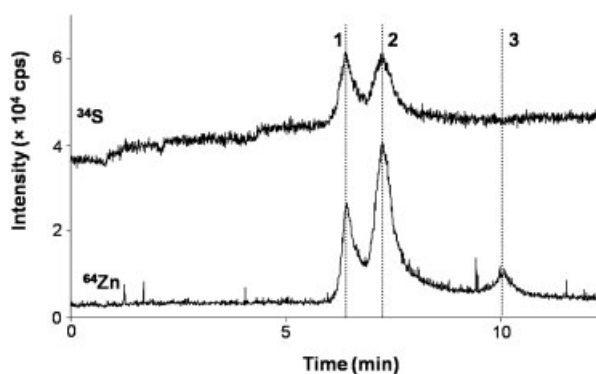
Serum incubation with $[Zn(mal)_2(H_2O)_2]$ and $[Zn(pic)_2(H_2O)_2]$ gives similar electropherograms, however nearly quantitative binding to HSA was observed.

Modeling calculations on the Zn(II) distribution in serum samples containing 100 μM of anti-diabetic *bis* complex were performed according to the conditions of the CZE–ICP-MS measurements. Formation of binary complexes [Zn(II)+carrier ligands; Zn(II)+LMM components], mixed-ligand species [Zn(II)+carrier ligands+LMM compounds] and the interactions between serum proteins and Zn(II) and between HSA and the carrier ligands were considered [16, 17, 26–29]. The modeling calculations for the Zn(II) distribution in artificial serum and with the most important HMM and LMM components (HSA, Tf, Cys, His, cit) showed that most of the Zn(II) is bound to the HMM fraction, mostly to HSA (Fig. 10) [16, 17]. At equimolar concentration of the *bis* complex and HSA, dipic is able to maintain Zn(II) at higher concentration in the LMM fraction compared to the binary ligands owing to its high potency to bind Zn(II). It was also revealed that HSA-ligand interaction affects the metal ion distribution. The results of the modeling calculation were also confirmed
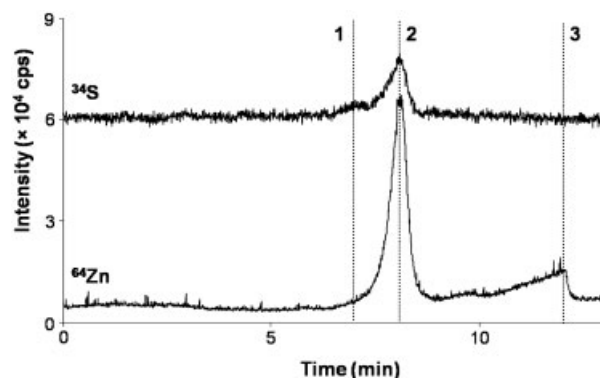
Figure 9. Electropherogram of $[Zn(dipic)_2]^{2-}$ incubated for 24 h with serum in carbonate buffer. Shown are the traces of ^{64}Zn and ^{34}S (for HSA and Tf detection). Peak identification: 1 – Tf; 2 – HSA adduct and 3 – $[Zn(dipic)_2]^{2-}$; Conditions: see Section 2.

Figure 8. Electropherogram of $[Zn(dipic)_2]^{2-}$ incubated for 24 h with apoTf and HSA at a ratio of 1:1:1 in carbonate buffer. Shown are the traces of ^{64}Zn and ^{34}S (for HSA and apoTf detection). Peak identification: 1 – apoTf adduct; 2 – HSA adduct and 3 – $[Zn(dipic)_2]^{2-}$; Conditions: see Section 2.
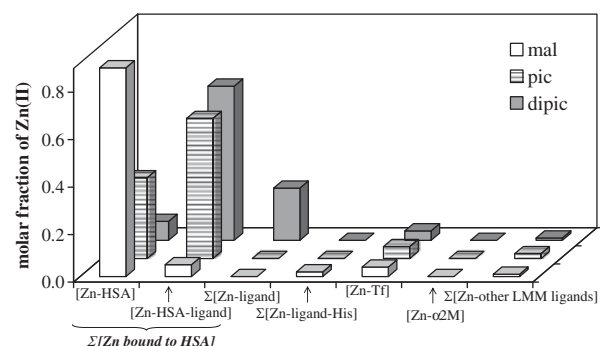
Figure 10. Calculated Zn(II) speciation in the blood serum. Sample concentration of the anti-diabetic complex: c([Zn(ligand)$_2$]) 100 μM; of the relevant serum components: c(HSA) 158 μM; c(Tf) 6.3 μM; c(α2M) 1.5 μM; c(cit) 25 μM; c(His) 19 μM; c(Cys) 8 μM (pH = 7.40; T = 25°C).

Table 2. Conditional stability constants of Zn-protein, HSA-ligand and Zn-HSA-ligand complexes (pH = 7.40; $T = 25°C$)

	dipic[a]	maltol[a]	pic[a]
Log β' (HSA-L)[b]	6.0	3.47	4.33
Log β' (HSA-(L)$_2$)[b]	8.9	–	–
Log β' (Zn-HSA-L)[b]	13.3	10.77	11.63
Log β' (Zn-HSA-(L)$_2$)[b]	16.2	–	–
Log β' (Zn-HSA)[c]		7.30	
Log β' (Zn-Tf)[d]		7.80	
Log β' (Zn$_2$-Tf)[d]		14.20	
Log β' (Zn-α2 M)[e]		7.49	
Log β' (Zn$_2$-α2 M)[e]		12.61	

a) Constants for the (Zn-L); (binary Zn-LMM serum components) and (ternary Zn-L-LMM serum components) complexes are taken from Refs. [16, 17].
b) Constants taken from Ref. [16].
c) Constants taken from Ref. [26].
d) Constants taken from Refs. [27, 28].
e) Constants taken from Ref. [29].

experimentally by ultrafiltration–ICP-atomic emission spectroscopy studies [16]. HSA has a higher capacity to bind Zn(II) than α2M at elevated Zn(II) concentration, due to its much higher concentration and accordingly a higher number of available binding sites.

4 Concluding remarks

Zn(II) complexes are promising candidates as insulin-enhancing drugs for the treatment of diabetes. Zn(II) complexes with mal, pic and dipic ligands were prepared *in situ* and their reaction with human serum proteins was studied by means of CZE hyphenated to ICP-MS. As compared to the tridentate ligand dipic, the bidentate metal binders mal and pic form less stable complexes with Zn(II) and accordingly higher amounts of Zn were detected at both HSA and apoTf. Competitive experiments with HSA and apoTf revealed significant preference for HSA over apoTf at equimolar incubation ratios. However, under serum conditions, HSA is by far the preferred binding partner for all three Zn(II)-ligand systems. Modeling calculations based on solution speciation studies and stability constants of binary and ternary Zn-ligand (-biomolecule) systems can give a good estimation of the distribution of such bioelements in biological fluids, with kinetic factors and the time course of these metal transport processes potentially having a significant influence on this picture. Attempts to correlate the experimental data for the distribution of Zn(II) in the serum with calculated results demonstrated overall good agreement of data obtained by calculations and experiments. Such metal ion distribution results can be used for designing carrier compounds with the desired chemical characteristics for obtaining ideal transport properties and mobility features.

5 References

[1] WHO, Reports of a WHO Study Group, WHO Technical Report Series 1985, pp. 727–876.

[2] Meyer, J. A., Spence, D. M., *Metallomics* 2009, *1*, 32–41.

[3] Guo, Z., Sadler, P. J., *Adv. Inorg. Chem.* 2000, *49*, 183–306.

[4] Hartinger, C. G., Dyson, P. J., *Chem. Soc. Rev.* 2009, *38*, 391–401.

[5] Jakupec, M. A., Galanski, M., Arion, V. B., Hartinger, C. G., Keppler, B. K., *Dalton Trans.* 2008, 183–194.

[6] Thompson, K. H., Chiles, J., Yuen, V. G., Tse, J., McNeill, J. H., Orvig, C., *J. Inorg. Biochem.* 2004, *98*, 683–690.

[7] Sakurai, H., Katoh, A., Yoshikawa, Y., *Bull. Chem. Soc. Jpn.* 2006, *79*, 1645–1664.

[8] Thompson, K. H., Orvig, C., *J. Inorg. Biochem.* 2006, *100*, 1925–1935.

[9] Rehder, D., Pessoa, J. C., Geraldes, C. F. G. C., Castro, M. M. C. A., Kabanos, T., Kiss, T., Meier, B. *et al.*, *J. Biol. Inorg. Chem.* 2002, *7*, 384–396.

[10] Sakurai, H., Kojima, Y., Yoshikawa, Y., Kawabe, K., Yasui, H., *Coord. Chem. Rev.* 2002, *226*, 187–198.

[11] Thompson, K. H., Lichter, J., LeBel, C., Scaife, M. C., McNeill, J. H., Orvig, C., *J. Inorg. Biochem.* 2009, *103*, 554–558.

[12] Taylor, C. G., *BioMetals* 2005, *18*, 305–312.

[13] Fugono, J., Fujimoto, K., Yasui, H., Kawabe, K., Yoshikawa, Y., Kojima, Y., Sakurai, H., *Drug Metab. Pharmacokinet.* 2002, *17*, 340–347.

[14] Yoshikawa, Y., Ueda, E., Kojima, Y., Sakurai, H., *Life Sci.* 2004, *75*, 741–751.

[15] Kiss, T., Jakusch, T., Hollender, D., Doernyei, A., Enyedy, E. A., Pessoa, J. C., Sakurai, H., Sanz-Medel, A., *Coord. Chem. Rev.* 2008, *252*, 1153–1162.

[16] Kiss, T., Jakusch, T., Hollender, D., Enyedy, É. A., Horváth, L., *J. Inorg. Biochem.* 2009, *103*, 527–535.

[17] Enyedy, E. A., Horvath, L., Gajda-Schrantz, K., Galbacs, G., Kiss, T., *J. Inorg. Biochem.* 2006, *100*, 1936–1945.

[18] Timerbaev, A. R., Hartinger, C. G., Keppler, B. K., *Trends Anal. Chem.* 2006, *25*, 868–875.

[19] Hartinger, C. G., Keppler, B. K., *Electrophoresis* 2007, *28*, 3436–3446.

[20] Hartinger, C. G., Timerbaev, A. R., Keppler, B. K., *Electrophoresis* 2003, *24*, 2023–2037.

[21] Yin, X.-B., Li, Y., Yan, X.-P., *Trends Anal. Chem.* 2008, *27*, 554–565.

[22] Enyedy, E. A., Lakatos, A., Horvath, L., Kiss, T., *J. Inorg. Biochem.* 2008, *102*, 1473–1485.

[23] Beaven, G. H., Chen, S.-H., D'Albis, A., Gratzer, W. B., *Eur. J. Biochem.* 1974, *41*, 539–546.

[24] Chasteen, N. D., Grady, J. K., Holloway, C. E., *Inorg. Chem.* 1986, *25*, 2754–2760.

[25] Zékány, L., Nagypál, I., in: Leggett, D. L. (Ed.), *Computational Methods for the Determination of Stability Constants*, Plenum Press, New York 1985, pp. 291–353.

[26] Masuoka, J., Saltman, P., *J. Biol. Chem.* 1994, *269*, 25557–25561.

[27] Harris, W. R., *Biochemistry* 1983, *22*, 3920–3926.

[28] Sun, H., Cox, M. C., Li, H., Sadler, P. J., *Struct. Bonding* 1997, *88*, 71–102.

[29] Adham, N. F., Song, M. K., Rinderknecht, H., *Biochim. Biophys. Acta Protein Struct.* 1977, *495*, 212–219.

[30] Pettit, L. D., Powell, H. K. J., *IUPAC Stability Constants Database*, ver. 5.5, Otley, Academic Software, 2000.

[31] Harris, W. R., *Clin. Chem.* 1992, *38*, 1809–1818.

[32] Lu, J., Stewart, A. J., Sadler, P. J., Pinheiro, T. J. T., Blindauer, C. A., *Biochem. Soc. Trans.* 2008, *36*, 1317–1321.

[33] Timerbaev, A. R., Hartinger, C. G., Aleksenko, S. S., Keppler, B. K., *Chem. Rev.* 2006, *106*, 2224–2248.

[34] Stewart, A. J., Blindauer, C. A., Berezenko, S., Sleep, D., Sadler, P. J., *Proc. Natl. Acad. Sci. USA* 2003, *100*, 3701–3706.

[35] Kiilerich, S., Christiansen, C., *Clin. Chim. Acta* 1986, *154*, 1–6.

[36] Boyett, J. D., Sullivan, J. F., *Metab. Clin. Exp.* 1970, *19*, 148–157.

[37] Foote, J. W., Delves, H. T., *J. Clin. Pathol.* 1984, *37*, 1050–1054.

[38] Charlwood, P. A., *Biochim. Biophys. Acta Protein Struct.* 1979, *581*, 260–265.

[39] Jakusch, T., Hollender, D., Enyedy, E. A., Gonzalez, C. S., Montes-Bayon, M., Sanz-Medel, A., Costa Pessoa, J. *et al.*, *Dalton Trans.* 2009, 2428–2437.

[40] Jakusch, T., Gajda-Schrantz, K., Adachi, Y., Sakurai, H., Kiss, T., Horvath, L., *J. Inorg. Biochem.* 2006, *100*, 1521–1526.

[41] Groessl, M., Hartinger, C. G., Polec-Pawlak, K., Jarosz, M., Keppler, B. K., *Electrophoresis* 2008, *29*, 2224–2232.

[42] Harris, W. R., Stenback, J. Z., *J. Inorg. Biochem.* 1988, *33*, 211–223.

[43] Hartinger, C. G., Jakupec, M. A., Zorbas-Seifried, S., Groessl, M., Egger, A., Berger, W., Zorbas, H. *et al.*, *Chem. Biodiversity* 2008, *5*, 2140–2155.

105

4. Conclusions and Outlook

10.9 million people are worldwide diagnosed with cancer every year [1]. By the time cancer is diagnosed most of the patients have already infected lymph nodes and metastases. In these cases complete eradication by surgery is nearly impossible and chemotherapy is necessary. The three approved Pt drugs, cisplatin, carboplatin and oxaliplatin, are among the few metal-based compounds in contemporary medical oncology [18, 19]. They have improved chemotherapy significantly [49, 132, 133] but their administration is accompanied by severe side effects as well as intrinsic and acquired resistance. The resistance is explained by enhanced repair of Pt-DNA adducts or enhanced tolerance to these adducts [32-36], detoxification by reaction with intracellular thiols [38-40] and by lower intracellular drug concentration due to reduced drug uptake and enhanced efflux [29-31]. All three compounds are administrated intravenously and therefore serum proteins are the first possible binding partners for these complexes. It was found that 65% to 98% of cisplatin in the blood plasma is bound to proteins within a day after administration [44, 134]. The literature about the binding of Pt-antitumor agents to serum proteins is contradictory and it seems that this interaction is important for both drug activity and toxicity. Through the irreversible binding of cisplatin to plasma proteins it is believed that the formation of Pt-protein adducts competes with formation of cyctotoxic Pt-DNA lesions, and results in a reduction of the efficacy of Pt antitumor agents [135-138]. On the other side there are also reports that indicated the effectiveness of cisplatin-HSA complexes in the treatment of patients with various types of tumors [139]. These studies demonstrated that the tumor Pt concentration was considerably higher after cisplatin-HSA administration than after conventional cisplatin therapy. Furthermore, it was shown that the response of hypo-albuminemic patients to cisplatin therapy is poor [140, 141]. Pt anticancer drugs are used in the clinic for more than 30 years and despite the controversy about the interaction of cisplatin, carboplatin and oxaliplatin with plasma proteins clinical trials concerning this issue just started in 2005 [142].

Due to the resistance and severe side effects of the anticancer drugs used nowadays in the clinics there is an intensive search for new and better tolerated drugs. Based on the pathophysiology of cancer cells it is important to design new, targeted anticancer drugs and investigate their modes of action for further optimization. In this thesis, CE and ICP-MS as well as a hyphenated approach of both have been used to study the influence of the lipophilicity on the anticancer activity of Pt complexes and for the characterization of the interaction of metal-based drugs with serum proteins.

One way to improve contemporary chemotherapy is to enhance the intracellular drug concentration in tumor cells [143-145]. Therefore the relationship between lipophilicity, accumulation of anticancer drugs in tumor cells and cytotoxicity was investigated closer. The lipophilicity of a compound is a useful parameter for an efficient screening of new drug candidates and was determined for various anticancer Pt complexes by the shake-flask method as well as indirectly by MEEKC. A linear correlation between the log P and log k values obtained by the shake-flask method and MEEKC, respectively, was only observable as long the Pt complexes varied only slightly in their structure. Due to the simplicity and automation of MEEKC as compared to the shake-flask method further studies on the correlation of log P and log k appear attractive. Moreover, in order to establish a more general rule, a broader series of compounds is required. Because of the limitation of conventional MEEKC technique to UV/vis active compounds, the hyphenation of MEEKC to ICP-MS was established. Log k values obtained by ICP-MS detection were very similar to the values obtained with UV/vis detection. Initial performance tests revealed slightly higher sensitivity for the ICP-MS system as compared to UV/vis. However, MEEKC-UV/vis was more stable in terms of operation, and high linearity of the calibration curve was obtained without addition of an internal standard. Further improvements of the MEEKC-ICP-MS system are necessary, especially with regard to peak shape and this could broaden the area of application of the method. With the aim of gaining a deeper insight into the mechanism of action of anticancer Pt complexes and in order to understand the structure-activity relationships, the lipophilicity was correlated to the redox potentials, *in vitro* antiproliferative activity and cellular accumulation. The cytotoxic properties of the studied Pt compounds correlate well with the lipophilicity as well as the accumulation of the compounds in tumor cells, but are not caused by differences in the reduction potentials.

The relationship between lipophilicity and cellular uptake of Pt compounds was also investigated by analysis of *in vivo* samples. In contrast to cisplatin and carboplatin, the cellular uptake of oxaliplatin is mainly based on passive diffusion and less dependent on facilitated transport by the copper influx transporter CTR1 [19, 56]. Therefore, oxaliplatin and its methyl derivatives KP1691 and KP1537 were chosen for the in vivo studies. Organ samples from tumor-bearing mice, collected 1 and 6 h post-injection, were analyzed for biodistribution and accumulation in the tumor. The complex KP1691 had the fastest accumulation rate in all analyzed tissue samples but also a fast efflux was observed. In contrast, the Pt tumor content in the KP1537 group was similar to that of oxaliplatin 6 h after administration. A closer look at Pt tumor levels indicates that for KP1537 no changes were found between the samples taken 1 and 6 h post-injection, whereas in the oxaliplatin group an increase was seen. It would be interesting to perform the same experiments but over a longer time and see if the Pt content further increases for oxaliplatin. Considering that

neurotoxicity is a central problem of clinical oxaliplatin applications [50], the lower accumulation of KP1537 in the sciatic nerve makes it a promising oxaliplatin follower.

A further focus of my PhD thesis was the interaction of metal complexes with serum proteins as well as their biodistribution. For metal-based drugs the interaction with serum proteins is thought to be important for their activity and better accumulation in cells [84-86]. For that reason a better understanding of the formation and reactivity of metal-protein adducts could help in defining the therapeutic profile of these drugs and improve treatment strategies. A CZE-ICP-MS technique was optimized to study the *in vitro* binding of diverse anticancer Ru complexes and antidiabetic Zn compounds with the serum proteins HSA and Tf. Both classes of metal complexes showed a high affinity toward HSA. The experimental data for the Zn compounds were confirmed by theoretical calculations. The findings for the Ru complexes are interesting considering the accumulation of HSA in malignant tissue due to anatomical pathophysiology of tumor blood vessels that facilitates the transport of macromolecules into tumor tissue combined with an absent or defective lymphatic drainage system. In the case of the Ru complex KP1339, the *in vitro* results were verified by *in vivo* experiments in non-tumor bearing nude BALB/c mice. Additionally, to the serum protein interaction also the accumulation of KP1339 in different tissues was investigated. The highest Ru levels were found in colon, lung, liver, kidney and thymus. Until now KP1339 was considered a promising drug candidate against colon cancer [73] but the high accumulation in lung and thymus makes this compound also interesting for the treatment of lung cancer and lymphoblastic leukemia. Further investigations in this direction are desirable.

In conclusions, this thesis indicates how important preclinical studies are and how they can aid in the prediction of the activity of a compound. Simple parameters like *e.g.* lipophilicity can help in the screening of drug candidates but there is a need for better techniques. Furthermore, *in vitro* experiments can only give limited information and animal tests are required to consider important factors such as bioavailability, -distribution and pharmacokinetics. All these joint efforts have potential to enhance drug development in future.

5. References

1. Cancer Research UK, *Mortality from cancer worldwide.* www.info.cancerresearchuk.org, last update 25/09/2009.
2. German Cancer Research Center, *Atlas of cancer mortality; comparison with other causes of death.* www.dkfz.de, last update 26/10/2010.
3. German Cancer Research Center, *Atlas of cancer mortality; leading causes of cancer deaths.* www.dkfz.de, last update 23/05/2007.
4. Cancer Research UK, *Trends in cancer mortality-UK statistics.* www.info.cancerresearchuk.org, last update 01/04/2010.
5. American Cancer Society, *What is cancer.* www.cancer.org, last update 22/03/2010.
6. American Cancer Society, *Cancer causes: theories throughout history.* www.cancer.org, last update 22/03/2010.
7. M. J. Atkinson and S. Tapio, *Tumorgenesis.* The impact of tumor biology on cancer treatment and multidisciplinary strategies 2009: p. 2-15.
8. B. Alberts, Lehrbuch der molekularen Zellbiologie, 2002: p. 1317.
9. T. Sjöblom, et al., *The Consenous Coding Sequences of Human Breast and Colorectal Cancers.* Science, 2006. **314**: p. 268-274.
10. R. C. Smart, *Chemical Cancerogenesis.* A Textbook of Modern Toxicology, 2004.
11. P. Hainaut and M. Hollstein, *p53 and human cancer: The first ten thousand mutations.* Advances in Cancer Research, Vol 77, 2000. **77**: p. 81-137.
12. A. Hamai, et al., *Immune surveilance of human cancer: if the cytotoxic T-lymphocytes play the music, does the tumoral system call the tune?* Tissue Antigens, 2010. **75**: p. 1-8.
13. D. Hanahan and R. A. Weinberg, *The Hallmarks of Cancer.* Cell, 2000. **100**: p. 57-70.
14. J. H. Mao, et al., *Stochastic modelling of tumorgenesis in p53 deficient mice.* British Journal of Cancer, 1998. **77**(2): p. 243-252.
15. German Cancer Research Center, *Atlas of Cancer Mortality; Trends by age range.* www.dkfz.de, last update 06/11/2007.
16. V. T. DeVita and E. Chu, *A history of cancer chemotherapy.* Cancer Res, 2008. **68**(21): p. 8643-53.
17. J. F. Kelvin and L. B. Tyson, *What is cheotherapy and how is it given?* One hundred questions and answers about cancer treatment side effects, 2005: p. 8.
18. M. Galanski, et al., *Recent developments in the field of tumor-inhibiting metal complexes.* Curr Pharm Des, 2003. **9**(25): p. 2078-89.
19. L. Kelland, *The resurgence of platinum-based cancer chemotherapy.* Nature Reviews Cancer, 2007. **7**(8): p. 573-584.
20. B. Rosenberg, L. Vancamp, and T. Krigas, *Inhibition of Cell Division in Escherichia Coli by Electrolysis Products from a Platinum Electrode.* Nature, 1965. **205**: p. 698-9.
21. B. Rosenberg, et al., *Platinum-induced filamentous growth in Escherichia coli.* J Bacteriol, 1967. **93**(2): p. 716-21.
22. M. Peyrone, *Über die Einwirkung des Ammoniaks auf Platinchlorid.* Annalen der Chemie und Pharmacie, 1844. **51**: p. 1-29.
23. G. B. Kauffman, et al., *Michele Peyrone (1813-1883), Discoverer of Cisplatin.* Platinum Metals Rev., 2010. **54**(4): p. 250-256.
24. T. Boulikas and M. Vougiouka, *Recent clinical trials using cisplatin, carboplatin and their combination chemotherapy drugs (Review).* Oncology Reports, 2004. **11**(3): p. 559-595.
25. L. H. Einhorn, *Curing metastatic testicular cancer.* Proc Natl Acad Sci U S A, 2002. **99**(7): p. 4592-5.

26. A. M. Fichtinger-Schepman, et al., *cis-Diamminedichloroplatinum(II)-induced DNA adducts in peripheral leukocytes from seven cancer patients: quantitative immunochemical detection of the adduct induction and removal after a single dose of cis-diamminedichloroplatinum(II).* Cancer Res, 1987. **47**(11): p. 3000-4.

27. F. P. T. Hamers, W. H. Gispen, and J. P. Neijt, *Neurotoxic Side-Effects of Cisplatin.* European Journal of Cancer, 1991. **27**(3): p. 372-376.

28. Drug Information online, *Cisplatin Side Effects.* www.drugs.com.

29. D. J. Stewart, et al., *Platinum Concentrations in Human Autopsy Tumor Samples.* American Journal of Clinical Oncology-Cancer Clinical Trials, 1988. **11**(2): p. 152-158.

30. D. P. Gately and S. B. Howell, *Cellular accumulation of the anticancer agent cisplatin: a review.* Br. J. Cancer, 1993. **67**: p. 1171-1176.

31. K. Katano, et al., *Acquisition of resistace to cisplatin is accompanied by changes in the cellular pharmacology of copper.* Cancer Res., 2002. **62**: p. 6559-6565.

32. D. Fink, *The role of DNA mismatch repair in platinum drug resistance.* Cancer Res., 1996. **56**: p. 4881-4886.

33. S. Johnson, et al., *Relationship between platinum-DNA adduct formation and removal and cisplatin cytotoxicity in cisplatin-sensitive and-resistant human ovarian cancer cells.* Cancer Res., 1994. **54**: p. 5911-5916.

34. K. V. Ferry, T. C. Hamilton, and S. W. Johnson, *Increased nucleotide excision repair in cisplatin-resistant ovarian cancer cells: role of ERCC1-XPF.* Biochem. Pharmacol., 2000. **60**: p. 1305-1313.

35. I. Y. Chang, et al., *Small interfering RNA-induced suppresion of ERCC1, enhances sensitivity of human cancer cells to cisplatin.* Biochem.Biophys.Res.Commun., 2005. **327**: p. 225-233.

36. E. Reed, *ERCC1 and clinical resistance to platinum-based therapy.* Clin. Cancer Res., 2005. **11**: p. 6100-6102.

37. E. R. Jamieson and S. J. Lippard, *Structure, recognition, and processing of cisplatin-DNA adducts.* Chemical Reviews, 1999. **99**(9): p. 2467-2498.

38. P. Mistry, et al., *The relationships between glutathione, glutathione-S-transferase and cytotoxicity of platinum drugs and melphalan in eight human ovarian carcinoma cell lines.* Br. J. Cancer, 1991. **64**: p. 215-220.

39. A. D. Lewis, J. D. Hayes, and C. R. Wolf, *Glutathione and glutathione-dependent enzymes in ovarian adenocarcinoma cell lines derived from a patient before and after the onset of drug resistance: intrisic differences and cell cycle effects.* Carcinogenesis, 1988. **9**: p. 183-1287.

40. S. L. Kelland, et al., *Overexpression of metallothionein confers resistance to anticancer drugs.* Science, 1988. **241**: p. 1813-1815.

41. D. Lebwohl and R. Canetta, *Clinical development of platinum complexes in cancer therapy: an historical perspective and an update.* European Journal of Cancer, 1998. **34**(10): p. 1522-1534.

42. M. Galanski, M. A. Jakupec, and B. K. Keppler, *Update of the preclinical situation of anticancer platinum complexes: Novel design strategies and innovative analytical approaches.* Current Medicinal Chemistry, 2005. **12**(18): p. 2075-2094.

43. F. M. Muggia, *Overview of Carboplatin - Replacing, Complementing, and Extending the Therapeutic Horizons of Cisplatin.* Seminars in Oncology, 1989. **16**(2): p. 7-13.

44. L. Pendyala and P. J. Creaven, *In Vitro Cytotoxicity, Protein Binding, Red Blood Cell Partitioning, and Biotransformation of Oxaliplatin.* Cancer Research, 1993. **53**: p. 5970-5976.

45.   A. K. Holzer, G. H. Manorek, and S. B. Howell, *Contribution of the major copper influx transporter CTR1to the cellular accumulation of cisplatin, carboplatin and oxaliplatin.* Molec. Pharmacol., 2006. **70**: p. 1390-1394.

46.   H. Bing, et al., *Oxaliplatin, fluorouracil and leucovorin (FOLFOX) as first-line chemotherapy for metastatic or recurrent colorectal cancer patients.* Chinese Journal of Clinical Oncology, 2007. **4**(6): p. 397-400.

47.   S. Giachetti, et al., *Phase III multicenter randomized trial of oxaliplatin added to chronomodulated fluorouracil-leucovorin as first-line treatment of metastatic colorectal cancer.* J. Clin. Oncol., 2000. **18**: p. 136-147.

48.   A. de Gramont, et al., *Leucovorin and fluorouracil with or without oxaliplatin as first-line treatment in advanced colorectal cancer.* J. Clin. Oncol., 2000. **18**: p. 2938-2947.

49.   R. M. Goldberg, et al., *A key clincial phase III study showing significantly improved survival with oxaliplatin, fluorouracil/leucovorin (FOLFOX regimen) in patients with previously untreated metastatic colorectal canccer.* J. Clin. Oncol., 2004. **22**: p. 23-29.

50.   M. W. Saif and J. Reardon, *management of oxaliplatin-induced peripheral neutropathy.* Therapeutics and Clinical Risk Management, 2005. **1**(4): p. 249-258.

51.   M. D. Hall, et al., *Basis for design and development of Platinum(IV) anticancer complexes.* J. Med. Chem., 2007. **50**(15): p. 3403-3411.

52.   C. N. Sternberg, et al., *Phase III trial of satraplatin, an oral platinum plus prednisone vs. prednisone alone in patients with hormone-refractory prostate cancer.* Oncology, 2005. **68**(1): p. 2-9.

53.   M. R. Reithofer, et al., *Tuning of lipophilicity and cytotoxic potency by structural variation of anticacer platinum(IV)complexes.* Journal of Inorganic Bichemistry, 2011. **105**(1): p. 46-51.

54.   L. R. Kelland, *An update on satraplatin: the first orally available platinum anticancer drug.* Exp.Opin. Invest. Drugs, 2000. **9**: p. 1373-1382.

55.   A. P. Silverman, et al., *2.4-A crystal structure of the asymmetric platinum complex [Pt(ammine)(cyclohexylamine)] bound to a dodecamer DNA duplex.* J. Biol.Chem., 2002. **277**: p. 49743-49749

56.   G. Samimi and S. B. Howell, *Modulation of the cellular pharmacology of JM118, the major metabolite of satraplatin, by copper influx and efflux transporters.* Cancer Chemother. Pharmacol., 2006. **57**: p. 781-788.

57.   S. Y. Sharp, P. M. Rogers, and L. R. Kelland, *Transport of cisplatin and Bis-acetato-ammine-dichlorocyclohexylamine-platinum(IV) (JM216) in human ovarian carcinoma cell lines: identification of a plasma membrane protein associated with cisplatin resistance.* Clin.Cancer Res., 1995. **1**: p. 981-989.

58.   A. Kozubik, et al., *High effectiveness of platinum(IV) complex with adamantylamine in overcoming resistance to cisplatin and suppressing proliferation of ovarian cancer cells in vitro.* Biochem. Pharmacol., 2005. **69**(3): p. 373-383.

59.   J. Turanek, et al., *New platinum(IV) complex with adamantylamine ligand as a promising anti-cancer drug: comparison of in vitro cytotoxic potential towards A2780/cisR cisplatin-resistant cell line within homologous series of platinum(IV) complexes.* Anti-Cancer Drugs, 2004. **15**(5): p. 537-543.

60.   Y. K. Yan, et al., *Organometallic chemistry, biology and medicine: ruthenium arene anticancer complexes.* Chemical Communications, 2005(38): p. 4764-4776.

61.   N. Katsaros and A. Anagnostopoulou, *Rhodium and its compounds as potential agents in cancer treatment.* Critical Reviews in Oncology Hematology, 2002. **42**(3): p. 297-308.

62.   G. A. Woldemariam and S. S. Mandal, *Iron(III)-salen damages DNA and induces apoptosis in human cell via mitochondrial pathway.* J. Inorg. Biochem., 2008. **102**(4): p. 740-747.

63.   D. S. Dwyer, K. Gordon, and B. Jones, *Ruthenium Red potently inhibits immune responses both in vitro and in vivo.* Int J Immunopharmacol, 1995. **17**(11): p. 931-40.

64.   R. A. Sanchez-Delgado, et al., *Toward a novel metal-based chemotherapy against tropical diseases. 2. Synthesis and antimalarial activity in vitro and in vivo of new ruthenium- and rhodium-chloroquine complexes.* J Med Chem, 1996. **39**(5): p. 1095-99.

65.   C. S. Allardyce and P. J. Dyson, *Ruthenium in medicine:Current clinical uses and future prospects.* Platinum Metals Review, 2001. **45**(2): p. 62-69.

66.   M. J. Clarke, *The Potential of Ruthenium in anticancer pharmaceuticals.* Inorganic Chemistry in Biology and Medicine, 1980: p. 157-180.

67.   M. Gielen and E.R.T. Tiekink, *Perspectives of Ruthenium complexes in Cancer Therapy* Metallotherapeutic Drugs and Metal-Based Diagnostic Agents: The Use of Metals in Medicine, 2005.

68.   J. M. Rademaker-Lakhai, et al., *A Phase I and pharmacological study of the platinum polymer AP5280 given as an intravenous infusion once every 3 weeks in patients with solid tumors.* Clin Cancer Res, 2004. **10**(10): p. 3386-95.

69.   E. S. Antonarakis and A. Emadi, *Ruthenium-based chemotherpeutics: are they ready for prime time?* Cancer Chemotherapy and Pharmacology, 2010. **66**(1): p. 1-9.

70.   M. Cocchietto, et al., *Primary tumor, lung and kidney retention and antimetastasis effect of NAMI-A following different routes of administration.* Investigational New Drugs, 2003. **21**(1): p. 55-62.

71.   P. J. Dyson and G. Sava, *Metal-based antitumour drugs in the post genomic era.* Dalton Trans., 2006(16): p. 1929-1933.

72.   P. Heffeter, et al., *Intracellular protein binding patterns of the anticancer ruthenium drugs KP1019 and KP1339.* JBIC, J. Biol. Inorg. Chem., 2010. **15**(5): p. 737-748.

73.   C. G. Hartinger, et al., *From bench to bedside - preclinical and early clinical development of the anticancer agent indazolium trans-[tetrachlorobis(1H-indazole)ruthenate(III)] (KP1019 or FFC14A).* J. Inorg. Biochem., 2006. **100**(5-6): p. 891-904.

74.   C. Scolaro, et al., *In vitro and in vivo evaluation of ruthenium(II)-arene PTA complexes.* J. Med. Chem., 2005. **48**(12): p. 4161-4171.

75.   W. Forth, et al., *Allgemeine und Spezielle Pharmakologie und Toxikologie.* 6. Auflage Mannheim; Leipzig; Wien; Zürich BI-Wiss.-Verlag, 1992: p. 3.

76.   E. Oberdisse, E. Hackenthal, and K. Kuschinsky, *Pharmakologie und Toxikologie.* 3. Auflage Springer-Verlag, 2002: p. 4.

77.   Institut für Biochemische Pharmakologie Universität Innsbruck, *Pharmakokinetik.* 1994: p. 1-18.

78.   Merck, *Clinical Pharmacology, Introduction.* http://www.merckmanuals.com/professional/sec20/ch303/ch303a.html, last update 11/2007.

79.   Merck, *Clinical Pharmacology, Absorption.* http://www.merckmanuals.com/professional/sec20/ch303/ch303b.html, last update 11/2007.

80.   S. Chillistone and J. Hardman, *Factors affecting drug absorption and distribution.* Anaesthesia and Intensive Care Medicine, 2008. **9**(4): p. 167-171.

81.   H. P. Rang, M. M. Dale, and J. M. Ritter, *Absorption and distribution of drugs.* Pharmacology & Therapeutics, 1999: p. 68.

82.   M. J. Banker and T. H. Clark, *Plasma/serum protein binding determinations.* Curr. Drug. Metab., 2008. **9**(9): p. 854-9.

83.   J.J.H.M. Lohman, F.W.H.M. Merkus, and K.H. Rahn, *Plasma protein binding of drugs. Implications for therapeutic drug monitoring.* Pharmacy world & science, 1986. **8**(6): p. 302-304.

84.   L. Hongyan, S. Hongzhe, and M. Q. Zhong, *The role of the transferrin-transferrin-receptor system in drug delivery and targeting.* Trends in Pharmacological Sciences, 2002. **23**(5): p. 206-209.

85.   F. Kratz, *Albumin, a versatile carrier in oncology.* International Journal of Clinical Pharmacology and Therapeutics, 2010. **48**(7): p. 453-455.

86.   G.Stehle, et al., *Plasma protein (albumin) catabolism by the tumor itself-implications for tumor metabolism and the genesis of catechexia.* Crit. Rev. Oncol., 1997. **26**: p. 77-100.

87.   Merck, *Clinical Pharmacology, Metabolism.* http://www.merckmanuals.com/professional/sec20/ch303/ch303e.html, last update 09.2007.

88.   J. A. DiMasi, R. W. Hansen, and H. G. Grabowski, *The price of innovation: new estimates of drug development costs.* Journal of Health Economics, 2003. **22**(2): p. 151-185.

89.   P. M. Lorosso, *Phase 0 clinical trials:an answerto drug development stagnation?* J. Clin.Oncol., 2009. **27**: p. 2586-2588.

90.   US Department of Health and Human Services Food and Drug Administration, *Clinical trials of medical treatment.* http://www.fda.gov, last update 01/04/2010.

91.   aCCeSSCR, www.aCCeSSCr.com.au/upload/Image/Drugdeveolpment, 2007.

92.   US Department of Health and Human Services Food and Drug Administration, *The critical path:making medical products better, faster and cheaper.* http://www.fda.gov/ForConsumers/ConsumerUpdates/ucm061234.htm, last accessed:29/07/2010.

93.   A. McNaught and A. Wilksinson, IUPAC Compendium of Chemical Terminology, Royal Society of Chemistry, Cambridge, UK, 1997.

94.   H. H. Lauer and G. P. Rozing, *High Performance Capillary Electrophoresis.* 2010, 2nd. ed.

95.   J. W. Jorgenson and K. D. Lukacs, *Capillary Zone Electrophoresis.* Science, 1983. **222**(4621): p. 266-272.

96.   J. W. Jorgenson and K. D. Lukacs, *Zone Electrophoresis in Open-Tubular Glass-Capillaries.* Analytical Chemistry, 1981. **53**(8): p. 1298-1302.

97.   A. Shafaati, *Capillary Electrophoresis.* mnpc.congress.sums.ac.ir:8080/mnpc/ppt/Dr.shafaati.ppt, 01.05.2005.

98.   P. Camilleri, *Capillary Electrophoresis, Theory and Practice.* 1998, . **2nd. ed.**

99.   Capillary electrophoresis, www.answers.com/topic/capillary-electrophoresis.

100.   K. D. Altria, *Background theory and applications of microemulsion electrokinetic chromatography.* Journal of Chromatography A, 2000. **892**(1-2): p. 171-186.

101.   R. Ryan, et al., *Advances in the theory and application of MEEKC.* Electrophoresis, 2010. **31**(5): p. 755-767.

102.   Y. Henchoz, et al., *High-throughput log P determination by MEEKC coupled with UV and MS detections.* Electrophoresis, 2010. **31**(5): p. 952-964.

103.   H. Wan, M. Ahman, and A. G. Holmen, *Relationship between Brain Tissue Partitioning and Microemulsion Retention Factors of CNS Drugs.* J. Med. Chem., 2009. **52**(6): p. 1693-1700.

104.   C. N. Yin, et al., *Rapid determination of water- and fat-soluble vitamins with microemulsion electrokinetic chromatography.* Journal of Chromatography A, 2008. **1193**(1-2): p. 172-177.

105. S. Lucangioli, et al., *A capillary electrophoretic system based on a novel microemulsion for the analysis of coenzyme Q10 in human plasma by electrokinetic chromatography.* Electrophoresis, 2009. **30**(11): p. 1899-1905.

106. Y. H. Cao, et al., *Comparison of microemulsion electrokinetic chromatography with high-performance liquid chromatography for fingerprint analysis of resina draconis.* Analytical and Bioanalytical Chemistry, 2008. **392**(5): p. 1003-1010.

107. T. F. Jiang, et al., *Separation and Determination of Nitrofuran Antibiotics in Turbot Fish by Microemulsion Electrokinetic Chromatography.* Analytical Sciences, 2009. **25**(7): p. 861-864.

108. R. Thomas, *A Beginner's Guide to ICP-MS Part I.* Spectroscopy Tutorial, 2001. **16**(4): p. 38-42.

109. K. Cottingham, *ICPMS: It's Elemental.* Analytical Chemistry, 2004: p. 35-38.

110. Agilent Technologies, *The Principles of ICP-MS.* http://www.chem.agilent.com/en-US/Products/Instruments/atomicspectroscopy/icp-ms/pages/gp455.aspx.

111. Perkin Elmer SCIEX, *The 30-Minute Guide to ICP-MS.*

112. R. Thomas, p.-. *A Beginner's Guide to ICP-MS. Part III: The Plasma Source.* Spectroscopy Tutorial, 2001. **16**(6): p. 26-30.

113. R. Thomas, *A Beginner's Guide to ICP-MS Part IV: The Interface Region.* Spectroscopy Tutorial, 2001. **16**(7): p. 26-34.

114. R. Thomas, *A Beginner's Guide to ICP-MS Part V: The Ion Focusing System.* Spectroscopy Tutorial, 2001. **16**(9): p. 38-44.

115. R. Thomas, *A Beginner's Guide to ICP-MS Part VI: The Mass Analyzer.* Spectroscopy Tutorial, 2001. **16**(10): p. 44-48.

116. Georg-August-Universität Göttingen, *Massenspektrometrie und Ionenbeschleuniger.* https://lp.uni-goettingen.de/get/text/5338.

117. J. W. Olesik, J. A. Kinzer, and S. V. Olesik, *Capillary Electrophoresis Inductively-Coupled Plasma Spectrometry for Rapid Elemental Speciation.* Analytical Chemistry, 1995. **67**(1): p. 1-12.

118. X. B. Yin, Y. Li, and X. P. Yan, *CE-ICP-MS for studying interactions between metals and biomolecules.* Trac-Trends in Analytical Chemistry, 2008. **27**(6): p. 554-565.

119. G. Alvarez-Llamas, et al., *Comparison of two CE-ICP-MS interfaces based on microflow nebulizers: application to cadmium speciation in metallothioneins using quadrupole and double focusing mass analyzers.* J. Anal. At. Spectrom., 2002. **17**(7): p. 655-661.

120. D. Schaumloffel and A. Prange, *A new interface for combining capillary electrophoresis with inductively coupled plasma-mass spectrometry.* Fresenius Journal of Analytical Chemistry, 1999. **364**(5): p. 452-456.

121. C. Moller, et al., *Comparison of two CE-ICP-MS interfaces and quantitative measurements of carboplatin in plasma samples using an internal standard.* J. Anal. At. Spectrom., 2009. **24**(9): p. 1208-1212.

122. S.Y. Lin, et al., *Speciation of selenium compounds by open tubular capillary electrochromatography-inductively coupled plasma mass spectrometry.* Electrophoresis, 2006. **27**: p. 4257-4265.

123. B. Michalke and P. Schramel, *Application of capillary zone electrophoresis-inductively coupled plasma mass spectrometry and capillary isoelectric focusing-inductively coupled plasma mass spectrometry for selenium speciation.* Journal of Chromatography A, 1998. **807**(1): p. 71-80.

124. A. K. Bytzek, et al., *The first example of MEEKC-ICP-MS coupling and its application for the analysis of anticancer platinum complexes.* Electrophoresis, 2010. **31**(7): p. 1144-1150.

125.   M. Dole, L.L. Mack, and R.L. Hines, *Molecular Beams of Macroions.* Journal of Chemical Physics, 1968. **49**(5): p. 2240.

126.   M. Yamashita and J. B. Fenn, *Electrospray Ion-Source - Another Variation on the Free-Jet Theme.* Journal of Physical Chemistry, 1984. **88**(20): p. 4451-4459.

127.   M. Yamashita, M. and J. B. Fenn, *Negative-Ion Production with the Electrospray Ion-Source.* Journal of Physical Chemistry, 1984. **88**(20): p. 4671-4675.

128.   C. M. Whitehouse, et al., *Electrospray Interface for Liquid Chromatographs and Mass Spectrometers.* Analytical Chemistry, 1985. **57**(3): p. 675-679.

129.   J. B. Fenn, et al., *Electrospray Ionization for Mass-Spectrometry of Large Biomolecules.* Science, 1989. **246**(4926): p. 64-71.

130.   E. Hoffmann and V. Stroobant, *Mass spectrometry, Principles and Applications.* Wiley VCH, Weinheim, 2002.

131.   The University of Bristol School of Chemistry, *Electrospray Ionisation.* http://www.chm.bris.ac.uk/ms/theory/esi-ionisation.html,, last update 20.01.2004.

132.   D. Machover, et al., *Two consecutive phase II studies of oxaliplatin (L-OHP) for treatment of patients with advanced colorectal carcinoma who were resistant to previous treatment with fluoropyrimidines.* Ann. Oncol., 1996. **7**: p. 95-98.

133.   F. Levi, et al., *A chronopharmacologic phase II clinical trial with 5-fluorouracil, folinic acid, and oxaliplatin using an ambulatory multichannel programmable pump. High antitumour effectiveness against metastatic colorectal cancer.* Cancer 1992. **69**: p. 893-900.

134.   J. Will, A. Dirk, and W. S. Sheldrick, *Characterisation of Cisplatin Binding Sites in Human Serum Proteins Using Hyphenated Multidimensional Liquid Chromatography and ESI Tandem Mass Spectrometry.* Chem. Med. Chem, 2008. **3**: p. 1696-1707.

135.   S. Urien and F. Lokiec, *Population pharmacokinetics of total and unbound plasma cisplatin in adult patients.* Br. J. Clin. Pharmacol., 2004. **57**(6): p. 756-763.

136.   T. Peleg-Shulman, Y. Najajreh, and D. Gibson, *Interaction of cisplatin and transplatin with proteins. Comparison of binding kinetics, binding sites and reactivity of the Pt-protein adducts of cisplatin and transplatin towards biological nucleophils.* J. Inorg. Biochem., 2002. **91**: p. 306-311.

137.   K. Takahashi, et al., *Antitumor activity and toxicity of serum protein-bound platinum formed from cisplatin.* Jpn. J. Cancer Res., 1985. **2**: p. 68-74.

138.   W. C. Cole and W. Wolf, *Preparation and metabolism of a cisplatin/serum protein complex.* Chem. Biol. Interactions, 1980. **30**: p. 223-235.

139.   J. D. Holding, et al., *Phase I trial of a cisplatin-albumin complex for the treatment of cancer of the head and neck.* Br. J. Clin. Pharmacol., 1992. **33**(1): p. 75-81.

140.   J. D. Holding, et al., *Disposition and tumour concentrations of platinum in hypoalbuminaemic patients after treatment with cisplatin for cancer of the head and neck.* Br. J. Clin. Pharmacol., 1991. **32**: p. 173-179.

141.   E. Espinosa, et al., *Serum albumin and other prognostic factors to response and survival in patients with advanced non-small cell lung cancer.* Lung Cancer, 1995. **12**(3): p. 67.

142.   Alberta Health Services, *Cisplatin, Carboplatin, and Oxaliplatin interactions with plasma proteins.* http://clinicaltrials.gov/ct2/show/NCT00131586?term=NCT00131586&rank=1, last update 22.09.2008.

143.   D. J. Stewart, et al., *Platinum Concentrations in Human Autopsy Tumor Samples.* American Journal of Clinical Oncology-Cancer Clinical Trials, 1988. **11**(2): p. 152-158.

144.   L.Yang, E. B. Douple, and H. Wang, *Irradiation enhances cellular uptake of carboplatin.* Int. J. Radiation Oncology Biol. Phys., 1995. **33**(3): p. 641-646.

145.   S. A. Abramkin, et al., *{(1R,2R,4R)-4-Methyl-1,2-cyclohexanediamine}oxalatoplatinum(II): A Novel Enantiomerically Pure Oxaliplatin Derivative Showing Improved Anticancer Activity in Vivo.* J. Med.Chem., 2010.

Ich habe mich bemüht, sämtliche Inhaber der Bildrechte ausfindig zu machen und ihre Zustimmung zur Verwendung der Bilder in dieser Arbeit eingeholt. Sollte dennoch eine Urheberrechtsverletzung bekannt werden, ersuche ich um Meldung bei mir.

6. Curriculum Vitae

Dipl.-Chem. Anna Katharina Bytzek

PERSONAL DATA

Date of Birth	April 1, 1982
Place of Birth	Beuthen (Poland)
Nationality	German
Civil status	unmarried
Tel	+43-1-4277-52666
E-mail	anna.bytzek@univie.ac.at
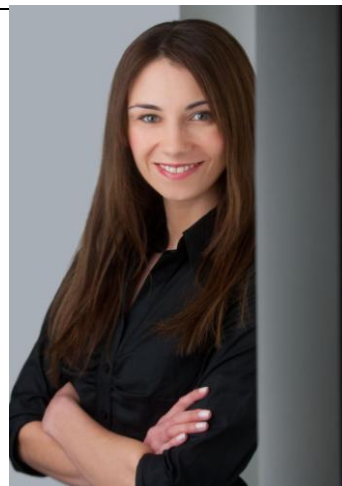
EDUCATION

11.2007-now	PhD Study of Chemistry at the University of Vienna, Austria Specialization: Bioinorganic Chemistry "Studies on the biophysical properties and biotransformation of metal-based drugs"
02.-10.2007	Diploma-Thesis at the University of Kaiserslautern, Germany Specialization: Bioinorganic Chemistry "Untersuchungen der elektronischen und strukturellen Eigenschaften sowie der Reaktivität von Catecholat-, Semichinonat-und Benzo-chinonant-komplexen"
04.-08.2006	Studies at the University of Barcelona, Spain Specialization: Molecular Magnetism
08.2004	Intermediate Diploma in Chemistry (Bachelor degree equivalent) at the University of Kaiserslautern, Germany
10.2002	Begin of studies at the University of Kaiserslautern, Germany Field of study: Chemistry
1989 – 2002	Elementary and Grammar school, Germany

PROFESSIONAL SKILLS AND RESEARCH INTERESTS

Biological Inorganic Chemistry, Molecular Magnetism, Coordination and Organometallic Chemistry, Medicinal Chemistry, Biodistribution of Anticancer Compounds, Bioanalytical Chemistry (Mass Spectrometry, Capillary Electrophoresis)

AWARDS AND FELLOWSHIPS

2004	Award of the GdCh for Intermediate Degree
12.3.2008	Forschungsstipendium der Universität Wien „Wechselwirkung von Metallkomplexen mit Biomolekülen"

LANGUAGE SKILLS

German	native language
English	fluently
Polish	fluently
Spanish	mediocre
French	high school level

PUBLICATIONS IN SCIENTIFIC JOURNALS

Biodistribution of the anticancer drug candidate sodium *trans*-[tetrachloridobis(1*H*-indazole)ruthenate(III)] (KP1339)

Bytzek A.K., Koellensperger G., Keppler B.K., Hartinger C.G.
Status: in preparation

LC- and CZE-ICP-MS approaches for the *in vivo* analysis of the anticancer drug candidate sodium *trans*-[tetrachloridobis(1*H*-indazole)ruthenate(III)] (KP1339) in mouse plasma

Bytzek A.K., Boeck K., Hann S., Keppler B.K., Hartinger C.G., Koellensperger G.
Status: in preparation

The first example of MEEKC-ICP-MS coupling and its application for the analysis of anticancer platinum complexes

Bytzek A.K., Reithofer M.R., Galanski M., Groessl M., Keppler B.K., Hartinger C.G.

Status: published in **Electrophoresis**, 2010, *31*, 1-7. (Cover article)

Tuning of lipophilicity and cytotoxic potency by structural variation of anticancer platinum(IV) complexes

Reithofer M.R., Bytzek A.K., Valiahdi S.M., Kowol C.R., Groessl M., Hartinger C.G., Jakupec M.A., Galanski M., Keppler B.K.

Status: published in **Journal of Inorganic Biochemistry**, 2010, *105*, 46-51.

Improved in vitro and in vivo activity of novel methyl-substituted oxaliplatin analogs: impact of stereoisomerism

Jungwirth U., Gojo J., Bytzek A.K., Koerner W., Heffeter P., Jakupec M.A., Galanski M., Hartinger C.G., Keppler B.K., Berger W.

Status: in preparation

KP1537- an oxaliplatin analog with reduced side effects

Jungwirth U., Xanthos D., Bytzek A.K., Heffeter P., Hartinger C.G., Keppler B.K., Sandkühler J., Berger W.

Status: in preparation.

Biodistribution of anti-diabetic Zn(II) complexes in human serum and *in vitro* protein-binding studies by means of CZE-ICP-MS

Bytzek A.K., Enyedy E.A., Kiss T., Keppler B.K., Hartinger C.G.

Status: published in **Electrophoresis**, 2009, *30*, 4075-4082.

The serum protein binding of pharmacologically active gallium(III) compounds assessed by hyphenated CE-MS techniques

Groessl M., Bytzek A., Hartinger C.G

Status: published in **Electrophoresis**, 2009, *30*, 2720-2727.

Physiochemical studies and anticancer potency of ruthenium(η^6-*p*-cymene) complexes containing antibacterial quinolones

Kljun J., Bytzek A.K., Kandioller W., Bartel C., Jakupec M.A., Hartinger C.G., Keppler B.K., Turel I.

Status: accepted in **Organometallics**

Cellular uptake, DNA interaction and protein binding studies of active *trans*-platinum anticancer compounds

Bartel C., Bytzek A., Scaffidi-Domianello Y.Y., Hartinger C.G., Jakupec M.A., Kukushkin V. Y., Galanski M., Keppler B.K.

Status: in preparation

Mechanistic insights into the unexpected rearrangement of tosylated flavones to aminoaurones.

Kandioller W., Kubanik M., Bytzek A., Jakupec M.A., Arion V.B., Keppler B.K., Hartinger C.G.

Status: submitted to **Tetrahedron**

From hydrolytically labile to hydrolytically stable Ru^{II}-arene anticancer complexes with carbohydrate-derived co-ligands

Hanif M., Meier S.M., Kandioller W., Bytzek A., Hejl M., Hartinger C.G., Nazarov A.A., Arion V.B., Jakupec M.A., Dyson P.J., Keppler B.K.

Status: published in **Journal of Inorganic Biochemistry**, 2011, *105*, 224-231.

Strategies for the covalent conjugation of a bifunctional chelating agent to albumin: Synthesis and characterization of potential MRI contrast agents

Kundu A., Peterlik H., Krssak M., Bytzek A.K., Pashkunova-Martic I., Arion V.B., Helbich T.H., Keppler B.K.

Status: published in **Journal of Inorganic Biochemistry**, 2011, 105, 250-255.

POSTER PRESENTATIONS

The application of MEEKC-ICP-MS for the determination of octanol-water partition coefficients of anticancer platinum complexes

Bytzek A.K., Galanski M., Hartinger C.G., Keppler B.K.

Winter Conference on Plasma Spectrochemistry. Fort Myers, Florida, USA 2010.

Metabolism of organometallic Ru compounds with antimetastatic activity

Bytzek A.K., Hartinger C.G., Dyson P., Keppler B.K.

European Winter Conference on Plasma Spectrochemistry. Graz, Austria 2009.

ORAL PRESENTATIONS

The first example of MEEKC-ICP-MS coupling and its application for the analysis of anticancer platinum complexes

Bytzek A.K., Galanski M., Keppler B.K., Hartinger C.G.

MassSpec-Forum-Vienna-2010, Vienna, Austria 2010.

Further studies of bis(carboxylate)platinum(IV) compounds: Correlation between lipophilicity, reduction potential, cellular accumulation and cytotoxicity

Reithofer M R., Bytzek A.K., Valiahdi S.M, Kowol Ch.R., Groessl M., Galanski, M., Hartinger C. G., Jakupec M.A., Keppler, B.K.,

240th ACS National Meeting, Boston, MA, USA 2010.